Title
Fine-Tuning Catechol Reactivity in Synthetic Polymeric Materials

Permalink
https://escholarship.org/uc/item/81n7232w

Author
Menyo, Matthew Stephen

Publication Date
2015

Peer reviewed|Thesis/dissertation

UNIVERSITY OF CALIFORNIA

Santa Barbara

Fine-Tuning Catechol Reactivity in Synthetic Polymeric Materials

A dissertation submitted in partial satisfaction of the
requirements for the degree Doctor of Philosophy
in Biochemistry and Molecular Biology

by

Matthew Stephen Menyo

Committee in charge:

Professor J. Herbert Waite, Chair

Professor Craig Hawker

Professor Alison Butler

Professor Cyrus Safinya

June 2015

The dissertation of Matthew Stephen Menyo is approved.

Craig Hawker

Alison Butler

Cyrus Safinya

Herbert Waite, Committee Chair

June 2015

Fine-Tuning Catechol Reactivity in Synthetic Polymeric Materials

ACKNOWLEDGEMENTS

The past five years in Santa Barbara have made for a truly incredible ride. The road has been smooth and it's been rough, with unexpected twists and beautiful vistas; the sections pockmarked with potholes only serving to accentuate the sweetness of the destination. Like any great journey though, the real thrill has not been the places, but the people with whom I've been able to share this experience.

I owe a tremendous amount of gratitude to my family, for more reasons that I can possibly list. Thank you to my parents, Laurie and Stephen, for raising me to be the person I am today. Mom, you have been incredibly strong and supportive my entire life. I admire your dedication, your work ethic, and your selflessness. Dad, your perseverance and strength amazes and inspires me on a daily basis. You taught me the value of doing things the right way and finishing what you start and for that I am forever grateful. Andrew, you've been my partner in crime since our days building snow forts in the front yard and playing tackle football in the basement. You have pushed and motivated me my entire life, and I am constantly impressed by your fearlessness, your energy, your generosity, and your intelligence. Thank you to my extended family on the Menyo and Dromgold sides for your support and encouragement throughout my life.

I cannot imagine a more engaging and supportive scientific community than I have seen at UCSB. Thank you Herb for teaching me the importance of rigor and curiosity, of integrity and balance, and of finding and pursuing my own path to becoming an independent researcher. Thank you to the members of the Waite lab, past and present, for being such a friendly, supportive, and welcoming group of talented, multidisciplinary scientists. Thank you to Craig for the opportunity to work alongside your group, and to the members of that group for the camaraderie, company, and collaboration that helped shape my scientific career. Thank you to the members of the IRG-1 team. It has been a pleasure to tackle big problems with an incredible group of interdisciplinary experts.

Thank you to the many friends in Santa Barbara that have made this an unforgettable experience both on-campus and off. I'm going to miss the cookouts, the "high-level" beach volleyball matches, the excessively adventurous hikes, the kickball costumes, the FIBDs, the brunches, the late night bike rides and Mammoth drives, the deep conversations, the swing dance flips, the successful homebrew batches, the nights spent in tents, and the memories formed from State Street to the Funk Zone. It’s been such a treat to be a part of this community and I look forward to coming back again and again.

Last but not least, thank you to my friends, educators, music instructors, coaches, and neighbors from Philadelphia and Penn State that have inspired wonderment, cultivated determination, and provided support all throughout my life. I couldn’t have done this without you.

VITA OF MATTHEW STEPHEN MENYO

March 2015

EDUCATION

Bachelor of Science in Materials Science and Engineering, Concentration in Polymers Science and Engineering, The Pennsylvania State University, June 2005 (summa cum laude)
Doctor of Philosophy in Biochemistry and Molecular Biology, University of California, Santa Barbara, March 2015 (expected)

AWARDS

Presidential Academic Excellence Scholarship, Penn State, 2005-2008
College of Earth and Mineral Sciences Scholarship, Penn State, 2006 & 2007
Coleman Award in Polymer Science, Penn State, 2009
Dean's Fellowship for Graduate Studies, UCSB, 2009
ICMR International Travel Fellowship, UCSB, 2012
Best Presentation, BMSE/MCDB Seminar Series, 2012 & 2013
Dow Materials Institute Travel Fellowship, 2013

PUBLICATIONS

Yu, J., Wei, W., Menyo, M.S., Waite, J.H., and Israelachvili. (2013). Adhesion of Mussel Foot Protein-3 to TiO_2 Surfaces: the Effect of pH. Biomacromolecules. 14 (4), 1072-1077.

Menyo, M.S., Hawker, C.J. and Waite, J.H. (2013). Versatile tuning of supramolecular hydrogels through metal complexation of oxidation-resistant catechol-inspired ligands. Soft Matter. 9, 10314-10323.

Fors, B.P., Poelma, J.E., Menyo, M.S., Robb, M.J., Spokoyny, D.M., Waite, J.H., and Hawker, C.J. (2013). Fabrication of Unique Chemical Patterns and Concentration Gradients with Visible Light. J. Am. Chem. Soc. 135 (38), 14106-14109.

Bubel S., Menyo M.S., Mates T.E., Waite J.H., Chabinyc M.L. (2015) Schmitt trigger using a self-healing ionic liquid transistor. Advanced Materials, accepted.

*Wang C.X., Brändle A., Menyo M.S., Klinger D., Hawker C.J. (2015) Bio-inspired nanocomposites from catechol-based layer-by-layer assembly. In preparation.

*Menyo M.S., Hawker C.J., Waite J.H. Strong, sacrificial metal coordination bonds enhance toughness and recovery in interpenetrating network hydrogels. In preparation.

ABSTRACT

Fine-Tuning Catechol Reactivity in Synthetic Polymeric Materials

by

Matthew Stephen Menyo

The robust, versatile attachment of mussels in the intertidal zone has motivated a large effort to create adhesives, coatings and energy dispersive materials based on the design principles of these marine organisms. Much progress has been made, but these materials frequently run up against two challenges related to the promiscuous reactivity of the catechol moiety. The first is the inability of reductionist constructs to incorporate the chemical nuances which modulate and optimize the performance of catechols. The second is the great propensity of catechols to oxidize and oligomerize under relatively benign conditions. Addressing these challenges will allow broader control and enhanced performance of catecholic moieties in synthetic systems. Two different strategies were employed to address these challenges: modulating the chemical nature of catechols, and utilizing stimuli-responsive protection chemistries.

First, the effect of local environment on the adhesive, adsorptive, and metal binding behavior of catechols was investigated for both native proteins and synthetic polymeric analogues. The presence of charged cofunctionality is able to modulate the binding properties of catechols by tuning their proton affinity. This effect can be re-created by chemically modifying catechols to create electron-deficient analogues with greater acidity and a lower susceptibility to oxidation. A simple metal coordination crosslinked hydrogel model system and an interpenetrating network hydrogel were used to demonstrate that these analogues possessed clear advantages in the construction of mechanically active structures. Finally, photo-mediated patterning and deprotection strategies were used to exert spatiotemporal control over the reactivity of catechols. By selectively activating catechols, binding can be controlled and catechols protected from premature oxidation. Taken together, these strategies show that controlled catecholic reactivity can be achieved by fusing biological design principles with designed materials engineering. Furthermore, this work identifies the 3-hydroxy-4-pyridinone moiety as an especially promising functionality for metal coordination bonding in supramolecular materials.

TABLE OF CONTENTS

LIST OF FIGURES

LIST OF TABLES

LIST OF SCHEMES

1 Introduction

I. The philosophical underpinnings of biologically inspired design

Life is resilient. Across the planet, living organisms adapt and evolve to their local environment to better harvest energy, elude predators, and regulate internal function. Not the biggest, fastest, or strongest, *Homo sapiens* have relied largely on intelligence and ingenuity to create the tools required to carve out habitats ranging from the scorching deserts of the Middle East to the frozen tundra of Siberia. It’s no coincidence that the development of advanced civilizations is commonly tracked by the advancement of tool-making materials: the Stone, Bronze and Iron Ages. Traditional engineering methods take a “top down” approach, in which the final, functional products frequently require intensive processing methods to shape monolithic starting materials.

At the same time, humans have never been hesitant to draw on the superior adaptive features of shared inhabitants of the planet. Across the globe, we have utilized the superior warmth of beaver pelts, harnessed the navigational ability of passenger pigeons, and repurposed the paralyzing venom of poison dart frogs. We are intelligent to enough to recognize that over thousands of years, selection pressures have cultivated the development of remarkably tuned biological structures, skills, capabilities, and behaviors. By fusing inspiration from the nature world with traditional engineering methods, we can continue to drive technology forward to meet the demands of an ever-growing world.

The structural materials produced by biological organisms are an especially ripe and diverse source of inspiration. These materials play important roles in support, defense, attachment, prey capture, and many other uses. Some biomaterials are already widely utilized. Wood[1] and bamboo[2] are used as construction materials across the globe. The nacre of pearls has long been prized for its luster and its longevity.[3] Others, such as the "stronger-than-steel" silk of spiders[4], and the sticky feet of geckos[5] are the subject of much research development and the stuff of comic book legend. Not only are these materials capable of durable, responsive performance in various environments, they are synthesized under benign, physiological conditions, with minimal waste, and limited starting materials.

II. Adhesion in the intertidal zone

The intertidal zone is a particularly demanding place to live. The organisms that populate this environment are exposed to waves reaching speeds of greater than 20 m/s and loaded with abrasive suspended sand, but also to periods of desiccation.[6,7] Predators such as starfish abound. Inhabitants utilize a variety of adhesive strategies to remain affixed, to dissipate wave energy, and to create protective defenses. The marine environment is a challenging environment for many synthetic adhesives, as the high dielectric and high ionic strength of ocean water greater mitigate the dispersion and electrostatic interactions that play important roles in attachment.

The sandcastle worm (*Phragmatopoma californica*) draws its colloquial moniker from to its proclivity to create expansive reef-like colonies.[8] These honeycombed constructs consist of individual tubes of sand, built in a manner analogous to stone masonry. Passing sand grains are collected from the water column, treated with a dab of an adhesive protein cocktail, and added to a cylindrical arrangement around the worm. When given the opportunity, sandcastle worms will build tubes from substrates ranging from glass and zirconium oxide beads, to egg shell, red sand, bone and silicon.[9]

Marine mussels of the species *Mytilus* create a bundle of collagenous threads known as a byssus to hold fast against the crashing waves.[10,11] These threads are tipped in adhesive plaques which provide robust and versatile attachment to a wide variety of hard organic and inorganic surfaces. Threads are formed in a process uncannily similar to injection-molding. The extensible foot of the mussel scouts and identifies a substrate for plaque deposition. A suite of proteins stored in the foot is then secreted into the ventral groove of this foot.[12] These proteins self-assemble and the foot is retracted in a process that takes less than 5 minutes in adults and 30 seconds in juveniles.[13]

Attachment requires cooperative mechanical behavior to provide versatile interfacial adhesion, cohesion and energy dissipation during repeated wave episodes. The thread itself must bridge from the byssal retractor muscles (0.2 MPa) to hard external surfaces like rocks (25 GPa), a modulus mismatch of 5 orders of magnitude.[14] In natural conditions, the thread is exposed to repeated strains of up to 40%[15,16] and capable of remaining in use for up to nine weeks.[17]

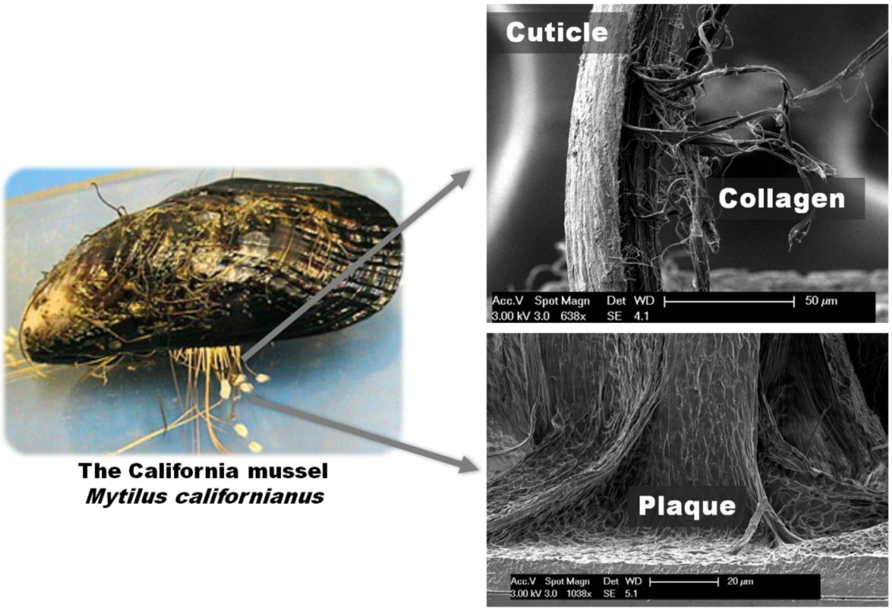

Figure 1. *Mytilus californianus* creates a bundle of adhesive threads known as the byssus. These threads consist of collagen cores wrapped in a hard cuticle and tipped with an adhesive plaque. (SEM images courtesy of Eric Danner)

The plaque connects the distal portion of the thread to a diverse array of substrates, in an underwater environment.[18] (Figure 1) Each point represents an impressive accomplishment. Young and Crisp showed that mussel plaques attach to Teflon, paraffin, acetal, glass and slate.[19] The tensile strength of the plaques was shown to be dependent on the surface energy of the substrate as well as the season, with stronger plaques produced during the more turbulent winter months.

The thread contains a graded distribution of collagens, and has been found to exhibit both chemically and mechanically different properties in the distal and proximal regions.[11,20] The distal region has a stiffness greater than that of Achilles tendon, an extensibility of up to 100%, a notable yield point, and a large, recoverable hysteresis.[16,21] The proximal region has a lower stiffness and lacks mechanical yielding behavior, but is extensible out to 200%

strain.[11] Treatment of the distal regions of the thread with the broad-spectrum metal chelator ethylenediaminetetraacetic acid (EDTA) lead to a dramatic decrease in the initial modulus, yield and hysteresis, as shown in Figure 2.[22] These mechanical properties of the thread also change with pH,[23] supporting a model in which metal coordination crosslinks impart substantial mechanical strength.[20]

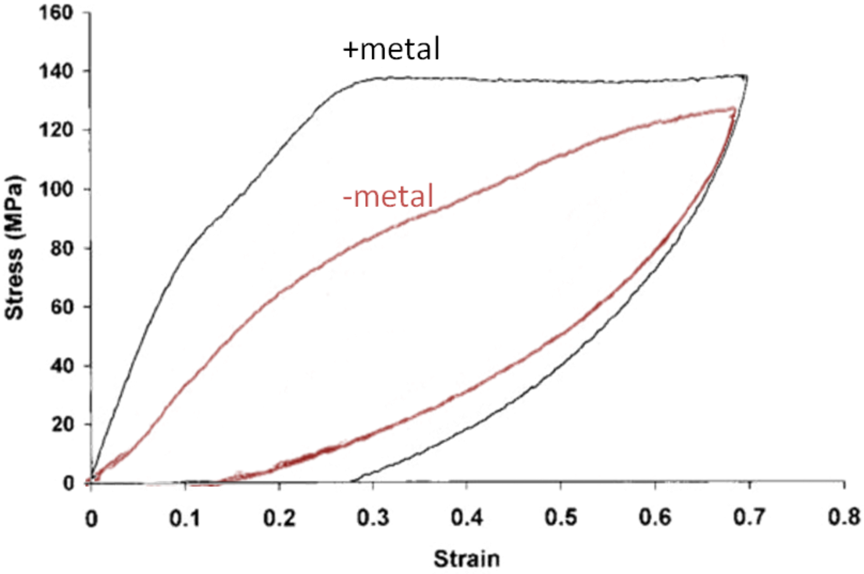

Figure 2: The mechanial performance of the distal portion of byssal threads treated with EDTA and exposed to artificial sea water (black) and deionized water (red). Figure adapted from Vaccaro and Waite.[22]

The collagenous cores of the proximal and distal regions of the threads are not exposed to the marine environment, rather, they are encased in a protective layer known as the cuticle. This cuticle is 4-5 times stiffer and harder than the underlying collagen core, but, remarkably, is able to withstand the strains faced by the thread without fracture.[24] The thickness, mechanical properties and morphology of the cuticle vary from species to species.

A groundbreaking study of the cuticle of two mussel species, *Perna canaliculus* and *Mytilus galloprovinicalis,* identified several key differences in structure and mechanical properties.[24] The cross-section of each thread shows the clear presence of granular inclusions in the cuticle of *M. galloprovincialis*, but no such features in *P. canaliculus*. (Figure 3).[24]

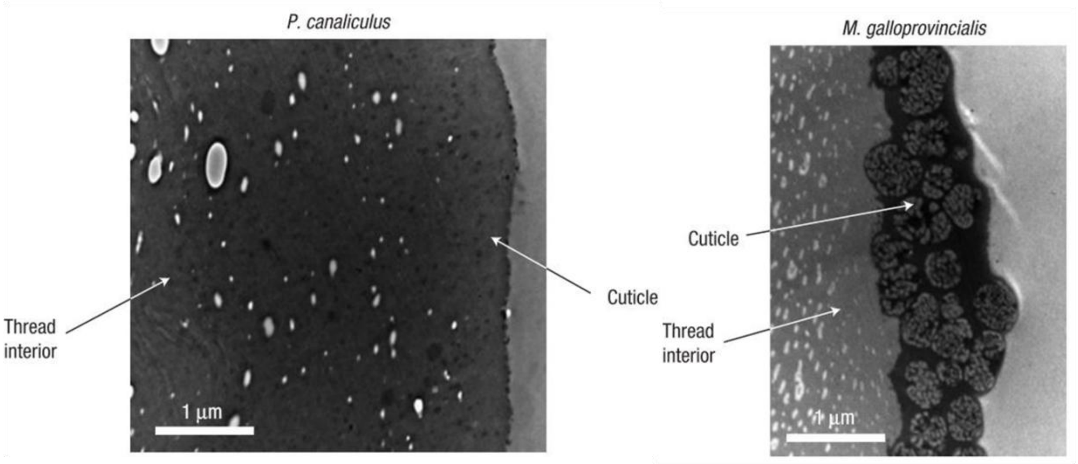

Figure 3: Transmission electron micrographs of transverse cross-sections of the distal portion of byssal threads from *Perna canaliculus* and *Mytilus galloprovinicalis*. Figure adapted from Holten-Andersen *et al.*[24]

Although the stiffness and hardness are similar between species, the cuticle of *P. canaliculus* began to fracture at 30% strain, while than of *M. galloprovincialis* is extensible to 70% before failure. The current model for this system is that these inclusions serve to blunt crack propagation in a manner analogous to the polybutadiene inclusions in high-impact polystyrene.[25]

III. Catecholic adhesive proteins

The versatile adhesive properties of mussels and sandcastle worms have motivated a large amount of research into the components which make up these glues. Eight proteins have been identified from the byssal threads of the *Mytilus* species. These proteins are summarized in table 1. PreCOL-D and pCOLNG are localized to the collagenous core of the threads. The other six carry the prefix Mfp, for mussel foot protein, and are numbered in their order of characterization. Mfp-1 is the primary isolatable component of the mussel cuticle.[26] Mfp-2 through 6 are located in various locations throughout the plaque. mfp-3[27] and mfp-5[28] are distributed at the plaque/substrate interface and have been found to be powerful adhesion primers to biologically relevant silicates.[29,30] Despite differences in sequence and length, mfp-1, 3 and 5 share several similarities. The most notable is the high incorporation of the post-translationally modified amino acid 3,4-dihydroxyphenylalanine (Dopa). Dopa has been found to play an essential role in much of the mechanical behavior of the byssal thread. This is due in part to the rich and robust chemistry of the catechol functionality, as described in the following section. Furthermore, all three proteins contain a large amount of cationic cofunctionality and have highly basic isoelectric points. Several adhesive proteins that make up the cement of the sandcastle worm have also been shown to contain high amounts of both Dopa and positively charged residues.[31,32]

Table 1. Biochemical features of the proteins of the mussel byssus. Adapted from Yu.[33]

Protein	Mass (kDa)	pI	Dopa (mol%)	Location
Mfp-1	110	10	18	Cuticle
Mfp-2	45	10	5	Foam
Mfp-3	5-7	8-10	20	Interface
Mfp-4	80	8.4	3	Foam
Mfp-5	9	9.8	30	Interface
Mfp-6	11	9.3	4	Interface
preCOL-D	240	9.5	0.5	Thread/plaque
preCOLNG	240	8.8	0.5	Thread/plaque

IV. The rich, versatile chemistry of catechols

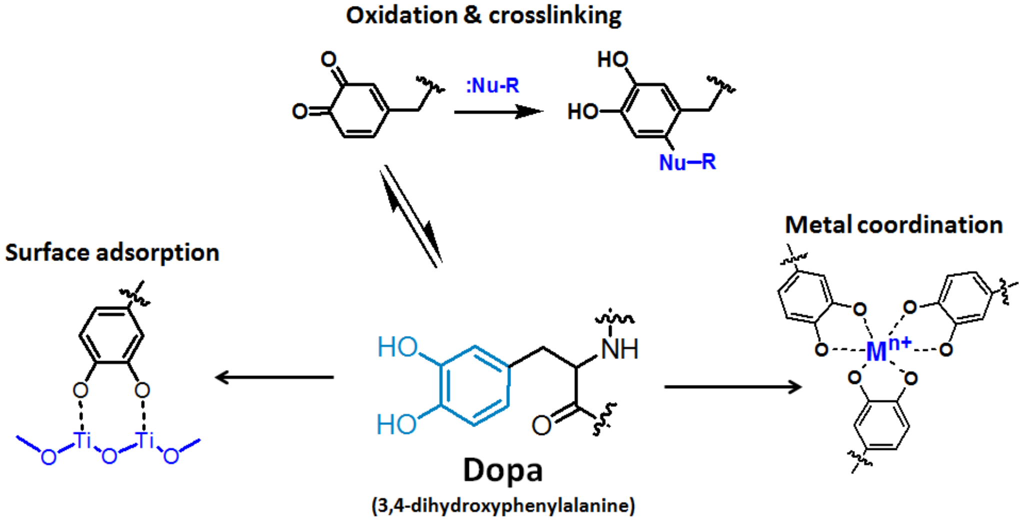

Figure 4. The modified amino acid Dopa is responsible in part for surface adsorption, oxidation and crosslinking, and metal coordination within the mussel byssus.

Dopa has been found to be an important part of the adhesion of mfp-3 and 5 not only to inorganic substrates, [29,34,35] but also to hydrophobic substrates.[36,37] This has been attributed to the ability of catechols to employ a wide variety of surface binding modes. In addition to non-specific dispersion and hydrophobic interactions, the two vicinal hydroxyl groups allow catechols to form powerful bidentate hydrogen and coordination bonds, and the aromatic nature promotes π-π and π-cation interactions.[38,39] The coordination bonds formed by catechols are especially strong. Messersmith *et al*. measured pull-off forces of 800 pN and energies of 22 kcal/mol in single-molecule atomic force microscope (AFM) experiments to TiO_2 surfaces.[40]

Another important arm of Dopa reactivity stems from its susceptibility to undergo a two electron, two proton oxidation to form a Dopaquinone species. This reaction proceeds rapidly in the presence of mild oxidizing agents such as sodium periodate, Fe^{3+}, and Ag^{+}, as well as rapid auto-oxidation at neutral and alkaline pH in the presence of oxygen.[41–45] Quinones are especially reactive with a variety of nucleophiles, forming covalent crosslinks with amines, thiols, and catechols.[46–49] It is reasonable to presume that this arm of reactivity has important implications in the rapid curing and internal cohesion within the plaque, though this has not been conclusively proven.

A final avenue of interaction in which catechols are capable of providing mechanical support is through the chelation of free metal ions. The vicinal hydroxyls appended to the aryl ring provide two hard catecholate ligands which are able to donate non-bonding electron pairs to bind metal ions in a strong, bidentate geometry. These complexes bind with remarkably high affinities to hard trivalent metal ions such as Fe^{3+}, Al^{3+}, In^{3+}, Ga^{3+}, Cr^{3+}, V^{3+} and divalent metal ions such as Zn^{2+}, Cu^{2+}, and Mn^{2+}.[50] Holten-Andersen *et al*. first demonstrated that Ca^{2+}, Fe^{3+} and Dopa are localized to the granules in the cuticle,[51] and that the hardness of the cuticle decreased by half upon treatment with EDTA. Using resonance Raman spectroscopy, Harrington *et al.* found spectroscopic evidence for the formation of Dopa-Fe^{3+} complexes in the cuticles, and proposed that these coordination crosslinks serve to prevent crack formation through the cuticle at high strains.[52] Furthermore, the addition of $FeCl_3$ solutions has been found to promote bridging adhesion between layers of adsorbed mfp-1 and 2.[53,54]

V. Synthetic catecholic materials

Byssal threads are capable of adhesion to a diverse milieu of substrates in aqueous and high ionic strength conditions which present difficulties for traditional synthetic adhesives. The threads exhibit impressive mechanical properties, including high stiffness, yield behavior, and recoverable hysteresis. Byssal threads are non-mineralized, highly proteinaceous and completely extracellular. As such, these threads are inherently light and biodegradable, and do not require cellular processes for the repair and continued function of these materials once deployed. Furthermore, these structures self-assemble, and are created in a manner analogous to the conventional polymer processing technique injection molding. Combined, these characteristics make byssal threads an attractive subject of research in materials science, with potential implications in fields such as synthetic adhesives and coatings, anti-fouling and tissue engineering.

As a result, a substantial amount of research over the past 10 years has focused on creating synthetic materials which employ the design principles of mussel adhesive proteins. The general motivation for synthetic attempts at biomimicry is to address the high effort and low yield of extraction of the native proteins. Synthetic constructs strive to replice the key materials properties of the mussel byssus in systems of reduced complexity and synthetic difficulty.

Dopa is an intriguing target for translation into synthetic constructs, as it is found to be instrumental to the surface adsorption, cohesive crosslinking, and energy dissipation properties of the mussel byssus. The earliest examples of these attempts used solid-phase peptide chemistry to create Dopa-containing polypeptides.[55] While effective, this strategy is also low-yield and is costly in both time and resources. [56,57] To combat this, efforts have been carried out to incorporate catechols into synthetic polymer architectures. Various studies have reported the free radical polymerization of Dopa-containing acrylic[58–60] and styrenic monomers, [61] as well as post-polymerization functionalization strategies including active ester[62] and thiol-ene chemistries.[63] The true scope of catechol incorporation is quite vast, and is the subject of a variety of recent reviews.[48,64,65]

VI. Challenges of synthetic constructs

By their nature, these constructs fail to completely reproduce the chemical nuances of the native proteins. As a result, the performance of these materials exhibits varying degrees of success depending on the desired application and the specific system. Two major challenges that frequently limit the performance of synthetic catecholic materials are: (1) a lack of control over the modes of catecholic reactivity, and (2) suboptimal binding, adhesion and adsorption.

The first challenge manifests most notably in the undesired oxidation of catechols to quinones. While quinones are very effective at crosslinking with a variety of nucleophiles, they lack the adhesive and coordinative prowess of catechols.[34,59,66] Synthetic adhesives commonly employ catechols as both interfacial binding moieties as well as oxidative crosslinking functionalities.[67,68] This approach requires careful control of the degree of oxidation in order to balance the ratio of binding and cohesive character of the system.

The chemical versatility of Dopa residues in the mussel byssus is carefully controlled by several mechanisms. The proteins are secreted in acidic conditions, slowing auto-oxidation processes.[13,66,69] In addition, interfacial binding proteins are co-secreted along with a thiol-rich antioxidant protein, mfp-6.[35]

The second challenge is a result of an inability to adequately recreate the local environment of catechols in the mussel adhesive proteins in the byssus. This is evident most notably in the coordination complexes formed by catechols and metal ions. In the cuticle of the mussel byssus (ca. pH 8.2), 3:1 Dopa-Fe^{3+} (*tris*) coordination is the primary binding stoichiometry.[52] The *tris* complex is both more stable and confers a higher degree of crosslinking as compared to *mono* and *bis* complexes. In synthetic constructs such as poly(ethylene glycol) with terminal catechol functionality, achieving complete *tris* complex formation requires pHs greater than 10.[43,70,71]

VII. Strategies for controlling the reactivity of catechols

The overarching goal of this work has been to create synthetic catecholic constructs in which reactivity is better tuned, controlled, and optimized. This requires a focused effort to bridge the gap between biology and materials science, by cultivating a deeper understanding of the mechanisms which govern catechol chemistry in the native system and using materials engineering principles to build upon this knowledge. By doing so, I have made strides to address the challenges of promiscuous reactivity and chemical context outlined above, to create materials which are able to highlight the remarkable properties of the catecholic functionality in a well-behaved, externally modulated fashion.

Chapter 2 describes work to understand the effect of the local environment on the adsorptive, adhesive and coordinative properties of catecholic macromolecules. To probe this question, I carried out a comparative characterization of a native mussel foot protein, mfp-3fast, with a library of synthetic polyacrylamides. Mfp-3fast is known to be localized to the interface of byssal plaques, and has a relatively simple chemical composition, consisting primarily of 4 amino acids (Dopa, lysine, arginine, and glycine), with no detectable secondary structure (Figure 5). I investigated the binding of this protein to TiO_2 surfaces, measuring the adhesion using the Surface Forces Apparatus (SFA), and the degree of coordinative binding using confocal resonance Raman spectroscopy. This protein was found to exhibit strong adhesion and coordinative binding to TiO_2 surfaces in a manner that was dependent on the pH.

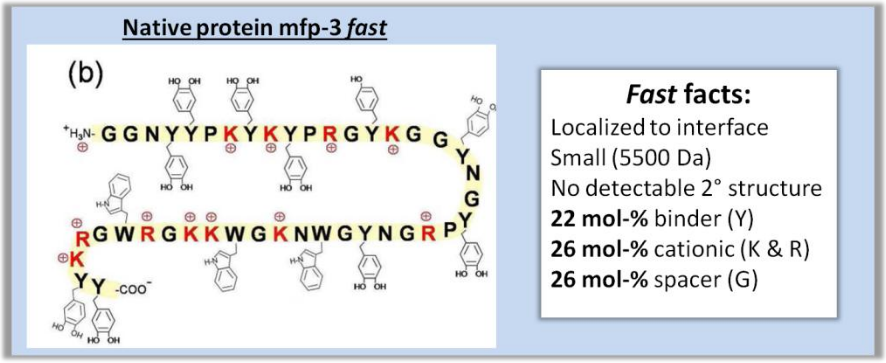

Figure 5. Amino acid sequence of mfp-3fast. Figure adapted from Wei *et al.*[37]

As a comparison, I synthesized a series of catecholic polymer starting from a common poly(pentafluorophenyl) acrylate precursor. These polymers were co-functionalized with a variety of charged residues, to probe the effect of localized positive and negative charges on the binding capability of the catecholic moiety. Positive charges were found to have a substantial effect on binding, increasing the amount of coordinatively bound catechols to TiO_2 surfaces under optimal binding conditions, and shifting the speciation of metal ion binding.

The experimental results led to a deeper understanding of the importance of local environment on the adsorption and binding capabilities of both native and synthetic catecholic polymers. The presence of positively charged residues is purported to create a locally basic milieu, favoring deprotonation and binding, but also oxidation. The results of this study highlight a promising approach to tuning the reactivity of catechols.

Chapter 3 describes the use of catechol analogues for the creation of hydrogels employing dynamic metal-ligand coordination crosslinking. The high-affinity metal complexes formed by catechols and hard metal ions have been demonstrated to play an important structural role in the cuticle of the byssal thread. These coordination bonds are a unique supramolecular interaction due to a their strength, dynamic exchangeability, and stimuli responsiveness. However, catechol-metal interactions show incomplete crosslinking at physiological pH and are susceptible to oxidation and crosslinking.

To solve these challenges, I drew on the key finding from Chapter 2: that a locally basic environment modulates the binding of catechols. In this work, I identified and investigated the metal coordination of two acidic catechol analogues. Chemical modification of the aryl ring results in comparatively electron-deficient ligands which maintain the robust metal coordination of catechols, but shift the binding speciation to realize strong crosslinking under physiological conditions. Furthermore, these analogues are less susceptible to oxidation. I used rheological measurements to relate the coordination chemistry to the bulk mechanical properties of the hydrogels. The mechanical properties of the hydrogel can be tuned by chelation, metal ions, and pH. Gelation can be triggered by injection into physiological buffer. The dynamic nature of the crosslinks allows these hydrogels to dissolve over the course of several days and the hydrogels are capable of encapsulating and releasing a model payload. The chelating functionality 3-hydroxy-4-pyridinone (HOPO) is identified as a particularly promising catechol surrogate, as it is capable of robust coordination crosslinks under physiological conditions, with minimal oxidation and crosslinking.

Chapter 4 expands on the HOPO metal binding functionality identified in the previous chapter. I use rheological frequency sweep experiments of hydrogels made with a series of metal ions and at various temperatures to elucidate the thermodynamic and kinetic properties of HOPO-M^{n+} structural crosslinks. The activation energy of viscoelasticity in this system is comparable to strong non-covalent interactions like biotin-avidin, gold-thiol and Upy quadruple H-bonding interactions. The bond lifetime is determined by the complex exchange kinetics of the hydrogel and is tuned by high-affinity metal ions with different characteristic water exchange rates.

The dynamic coordination network is capable of re-healing, but lacks toughness and is confined to perform at small strain amplitudes due to its chain architecture. To address this, I combined this coordination network with a loosely crosslinked covalent scaffold to form an interpenetrating network (IPN) hydrogel. This construct combines the dynamic, self-healing capabilities of coordination crosslinks with the shape stability and elastic restoring force of the covalent network to create a material in which the coordination crosslinks serve as sacrificial, energy dispersive components.

Chapter 5 details two photo-mediated methods for the spatiotemporal control and activation of catechols at surfaces. These catechols are non-reactive until activated with an external stimuli. In this way, catechols can be used to create complex surface patterns with a wide variety of reacting components.

In the first example, triethylsilyl-protected eugenol is patterned using an iridium photoredox catalyst. The short excited state lifetime allows excellent pattern fidelity. The low energy absorbance allows non-destructive patterning. The finding that reactivity is dependent on light dosage allows the creation of complex gradients and features. This chemistry is used to selectively bind iron oxide nanoparticles to regions patterned with activated catecholic moieties.

In the second example, *ortho*-nitrobenzyl alcohol (*o*-NB) protecting groups are used to create photodecaged catechol species. These *o*-NB molecules are immobilized on silica and silicon substrates and activated by controlled exposure to long wavelength ultraviolet radiation. Activation is monitored by the disappearance of characteristic features of the *o*-nitrobenzyl functionality. Substrates are selectively irradiated through a binary photomask. This local activation allows the rich chemistry of the catechols to be used for surface patterning. This strategy is utilized to pattern inorganic species such as TiO_2 nanoparticles and CdSe@ZnS quantum dots, metallic components such as silver nanoparticles and copper layers, and both hydrophobic and hydrophilic organic nucleophiles.

Finally, Chapter 6 provides a summary of the work described in the preceding chapters, and takes a look at the broader impact of the research described within. From this perspective, the key insights and important questions and challenges facing this work are identified and addressed.

VIII. References

(1) Hoadley, R. *Understanding wood: a craftsman's guide to wood technology*; 2nd ed.; Taunton Press: Newtown, CT, 2000; pp. 1–280.

(2) Amada, S.; Ichikawa, Y.; Munekata, T. *Compos. Part B …* **1997**, *8368*, 13–20.

(3) Rousseau, M.; Lopez, E.; Stempflé, P.; Brendlé, M.; Franke, L.; Guette, A.; Naslain, R.; Bourrat, X. *Biomaterials* **2005**, *26*, 6254–6262.

(4) Altman, G.; Diaz, F.; Jakuba, C.; Calabro, T. *Biomaterials* **2003**, *24*, 401–416.

(5) Autumn, K.; Sitti, M.; YA, L.; Peattie, A.; Hansen, W.; Sponberg, S.; Kenny, T.; Fearing, R.; Israelachvili, J. N.; Full, R. *Proc. …* **2002**, *99*, 12252.

(6) Hunt, H.; Scheibling, R. *Mar. Ecol. Prog. Ser.* **2001**, *213*, 157–164.

(7) Denny, M.; Gaylord, B. *J. Exp. Biol.* **2002**, *1362*, 1355–1362.

(8) Sisson, R. *Natl. Geogr.* **1986**, *169*, 252–259.

(9) Wang, C.; Svendsen, K.; Stewart, R. In *Biological Adhesive Systems*; 2010; pp. 169–179.

(10) Gosline, J.; Lillie, M.; Carrington, E.; Guerette, P.; Ortlepp, C.; Savage, K. *Philos. Trans. R. Soc. Lond. B. Biol. Sci.* **2002**, *357*, 121–132.

(11) Bell, E.; Gosline, J. *J. Exp. Biol.* **1996**, *1017*, 1005–1017.

(12) Waite, J. *Results Probl. Cell. Differ* **1992**, *19*, 27–54.

(13) Martinez Rodriguez, N. R.; Das, S.; Kaufman, Y.; Waite, J.; Israelachvili, J. *Biofouling* **2015**.

(14) Waite, J. H.; Andersen, N. H.; Jewhurst, S.; Sun, C. *J. Adhes.* **2005**, *81*, 297–317.

(15) Bell, E.; Gosline, J. *Mar. Ecol. Prog. Ser.* **1997**, *159*, 197–208.

(16) Smeathers, J.; Vincent, J. *J. Molluscan …* **1979**, 219–230.

(17) Moeser, G. M.; Carrington, E. *J. Exp. Biol.* **2006**, *209*, 1996–2003.

(18) Waite, J. H. *Integr. Comp. Biol.* **2002**, *42*, 1172–1180.

(19) GA, Y.; DJ, C. *Marine animals and adhesion*; 1982; pp. 19–39.

(20) Coyne, K. J.; Qin, X.; Waite, J. H. **1997**, *1*, 1995–1998.

(21) Carrington, E.; Gosline, J. *Am. Malacol. Bull.* **2004**, *18*, 135.

(22) Vaccaro, E.; Waite, J. *Biomacromolecules* **2001**, 906–911.

(23) Harrington, M. J.; Waite, J. H. *J. Exp. Biol.* **2007**, *210*, 4307–4318.

(24) Holten-Andersen, N.; Fantner, G. E.; Hohlbauch, S.; Waite, J. H.; Zok, F. W. *Nat. Mater.* **2007**, *6*, 669–672.

(25) Unnikrishnan, K.; Thachil, E. *Des. Monomers Polym.* **2006**, *9*, 129–152.

(26) JH, W.; TJ, H.; ML, T. *Biochemistry* **1985**, *10*, 5010–5014.

(27) VV, P.; TV, D.; K, B.; JH, W. *Biol. Chem.* **1995**, *270*, 20183.

(28) Waite, J. H.; Qin, X. *Biochemistry* **2001**, *40*, 2887–2893.

(29) Lin, Q.; Gourdon, D.; Sun, C.; Holten-Andersen, N.; Anderson, T. H.; Waite, J. H.; Israelachvili, J. N. *Proc. Natl. Acad. Sci.* **2007**, *104*, 3782.

(30) Danner, E.; Kan, Y.; Hammer, M. *Biochemistry* **2012**, *51*, 6511–6518.

(31) Zhao, H.; Sun, C.; Stewart, R. J.; Waite, J. H. *J. Biol. Chem.* **2005**, *280*, 42938–42944.

(32) Waite, J.; Jensen, R.; Morse, D. *Biochemistry* **1992**, 583–585.

(33) Yu, J. Adhesive Interactions of Mussel Foot Proteins, 2011.

(34) Anderson, T. H.; Yu, J.; Estrada, A.; Hammer, M. U.; Waite, J. H.; Israelachvili, J. N. *Adv. Funct. Mater.* **2010**, *20*, 4196–4205.

(35) Yu, J.; Wei, W.; Danner, E.; Ashley, R. K.; Israelachvili, J. N.; Waite, J. H. *Nat. Chem. Biol.* **2011**, *7*, 586–588.

(36) Wei, W.; Yu, J.; Broomell, C.; Israelachvili, J. N.; Waite, J. H. **2013**.

(37) Yu, J.; Kan, Y.; Rapp, M.; Danner, E.; Wei, W.; Das, S.; Miller, D. R.; Chen, Y. **2013**, *110*.

(38) Yu, J.; Wei, W.; Menyo, M. S.; Masic, A.; Waite, J. H.; Israelachvili, J. N. *Biomacromolecules* **2013**, *14*, 1072–1077.

(39) Hwang, D.; Harrington, M.; Lu, Q.; Masic, A.; Zeng, H.; Waite, J. *J. Mater. Chem.* **2012**, *22*, 15530–15533.

(40) Lee, H.; Scherer, N. F.; Messersmith, P. B. *Proc. Natl. Acad. Sci.* **2006**, *103*, 12999.

(41) Mentasti, E.; Pelittetti, E.; Saini, G. *J. Chem. Soc., Dalt. Trans.* **1973**, 2609–2614.

(42) Mentasti, E.; Pelizzetti, E. *J. Chem. Soc., Dalt. Trans.* **1973**, 2605–2608.

(43) Barrett, D. G.; Fullenkamp, D. E.; He, L.; Holten-Andersen, N.; Lee, K. Y. C.; Messersmith, P. B. *Adv. Funct. Mater.* **2012**, 1111–1119.

(44) Weidman, S.; Kaiser, E. *J. Am. Chem. ...* **1966**, *4575*, 5820–5827.

(45) Schweigert, N.; Zehnder, A. J. B.; Eggen, R. I. L. **2001**, *3*.

(46) Yu, M.; Hwang, J.; Deming, T. J. *J. Am. Chem. Soc.* **1999**, *121*, 5825–5826.

(47) Burzio, L.; Waite, J. *Biochemistry* **2000**, 11147–11153.

(48) Yang, J.; Stuart, M.; Kamperman, M. *Chem. Soc. Rev.* **2014**, *43*, 8271–8298.

(49) Waite, J. *Int. J. Adhes. Adhes.* **1987**, *7*, 9–14.

(50) Martell, A.; Smith, R. *Critical Stability Constants*; Plenum Press: New York, 1977.

(51) Holten-Andersen, N.; Mates, T. E.; Toprak, M. S.; Stucky, G. D.; Zok, F. W.; Waite, J. H. *Langmuir* **2009**, *25*, 3323–3326.

(52) Harrington, M. J.; Masic, A.; Holten-Andersen, N.; Waite, J. H.; Fratzl, P. *Science* **2010**, *328*, 216–220.

(53) Zeng, H.; Hwang, D. S.; Israelachvili, J. N.; Waite, J. H. *Proc. Natl. Acad. Sci.* **2010**, *107*, 12850.

(54) Hwang, D. S.; Zeng, H.; Masic, A.; Harrington, M. J.; Israelachvili, J. N.; Waite, J. H. *J. Biol. Chem.* **2010**, *285*, 25850–25858.

(55) Tatehata, H.; Mochizuki, A. *J. Appl. ...* **2000**, 929–937.

(56) Cha, H. J.; Hwang, D. S.; Lim, S. *Biotechnol. J.* **2008**, *3*, 631–638.

(57) Deming, T. J. **1999**, 100–105.

(58) Glass, P.; Chung, H.; Washburn, N. R.; Sitti, M. *Langmuir* **2009**, *25*, 6607–6612.

(59) Lee, B. P.; Dalsin, J. L.; Messersmith, P. B. *Biomacromolecules* **2002**, *3*, 1038–1047.

(60) Lee, H.; Lee, B. P.; Messersmith, P. B. *Nature* **2007**, *448*, 338–341.

(61) Westwood, G.; Horton, T.; Wilker, J. *Macromolecules* **2007**, 3960–3964.

(62) Wang, J.; Tahir, M. N.; Kappl, M.; Tremel, W.; Metz, N.; Barz, M.; Theato, P.; Butt, H.-J. *Adv. Mater.* **2008**, *20*, 3872–3876.

(63) Heo, J.; Kang, T.; Jang, S. G.; Hwang, D. S.; Spruell, J. M.; Killops, K. L.; Waite, J. H.; Hawker, C. J. *J. Am. Chem. Soc.* **2012**, *134*, 20139–20145.

(64) Sedó, J.; Saiz-Poseu, J.; Busqué, F.; Ruiz-Molina, D. *Adv. Mater.* **2013**, *25*, 653–701.

(65) Ye, Q.; Zhou, F.; Liu, W. *Chem. Soc. Rev.* **2011**, *40*, 4244–4258.

(66) Yu, J.; Wei, W.; Danner, E.; Israelachvili, J. N.; Waite, J. H. *Adv. Mater.* **2011**, *23*, 2362–2366.

(67) Yu, M.; Deming, T. *Macromolecules* **1998**, *31*, 4739–4745.

(68) Chung, H.; Glass, P.; Pothen, J. M.; Sitti, M. **2011**, 342–347.

(69) Wei, W.; Yu, J.; Gebbie, M. a; Tan, Y.; Martinez Rodriguez, N. R.; Israelachvili, J. N.; Waite, J. H. *Langmuir* **2015**.

(70) Holten-Andersen, N.; Harrington, M. J.; Birkedal, H.; Lee, B. P.; Messersmith, P. B.; Lee, K. Y. C.; Waite, J. H. *Proc. Natl. Acad. Sci. U. S. A.* **2011**, *108*, 2651–2655.

(71) Holten-Andersen, N.; Jaishankar, A.; Harrington, M. J.; Fullenkamp, D. E.; DiMarco, G.; He, L.; McKinley, G. H.; Messersmith, P. B.; Lee, K. Y. C. *J. Mater. Chem. B* **2014**, *2*, 2467.

2 The effect of global and local chemical environment on the binding and adhesion of catecholic proteins, polymers and peptides

Reproduced in part with permission from: Yu, J., Wei, W., Menyo, M.S., Waite, J.H., and Israelachvili. (2013). Adhesion of Mussel Foot Protein-3 to TiO_2 Surfaces: the Effect of pH. Biomacromolecules. 14 (4), 1072-1077. Copyright (2013) American Chemical Society.

I. Introduction

Achieving robust adhesion to surfaces underwater remains a grand challenge in materials science. Many recent research efforts have drawn inspiration to address this challenge from the adhesive proteins of the inhabitants of the intertidal zone.[1] An important question that remains to be fully understood is the role that the local and global chemical environment play in the behavior of mussel-inspired constructs. This work looks to address this question by studying three systems of varying complexity. First, the adsorption and adhesion of a native protein is studied at various pH values with a model metal hydroxide surface. Next, simplified polymeric analogues are used to test the hypothesis that protein adsorption and adhesion is modulating by the local chemical environment within the macromolecule. Finally, short peptide sequences are employed to test the whether these concepts are generalizible.

1. Binding chemistry of catechols and TiO_2

The modified amino acid 3,4-dihydroxyphenylalanine (Dopa) has been shown to be an essential component of the proteins in the adhesive plaques of mussels (*Mytilus edilus, M. californianus)* and the mortar of the sandcastle worm (*Phragmatopoma californica)*. The catecholic moiety of Dopa can participate in a wide variety of interactions including van der Waals forces, hydrogen bonding, and chelation of metal hydr(oxides) or free metal ions.[2] Oxidation of catechol to quinone proceeds rapidly at elevated pH, which can then undergo crosslinking via di-Dopa coupling[3] or Michael addition.[4] Lee *et al* have shown the reduced catechol form of Dopa to be responsible for the adhesive properties of the mussel protein, whereas oxidative crosslinking likely plays a role in cohesion.[5]

Hydrogen bonding and van der Waals interactions lead to physisorption, whereas ligand-exchange processes lead to robust chemisorption. This chemical versatility of catechols allows mussel adhesive proteins to adhere to surfaces ranging from TiO_2 and Fe_3O_4 to polytetrafluoroethylene.[6] The coordination chemistry of Dopa and catecholic compounds has been studied extensively, and the binding interactions of chemisorbed catechols are quite remarkable. Atomic force microscopy (AFM) single molecule adhesion force tests measured a pull-off force between a Dopa residue tethered to a poly(ethylene glycol) linker and a wet titania surface to be $\approx$ 800 pN.[5] In addition, this attachment is completely reversible and, in contrast to electrostatic interactions, has low sensitivity to the dielectric constant of the medium. Strong adhesion forces have also been reported by recent SFA tests of Dopa-grafted peptides and mfp-1 on TiO_2 substrates.[7,8]

Titanium is an important target for the design and optimization of wet adhesives, as it is widely used in medical implant devices. A 2-20nm thick TiO_2 passivation layer is rapidly formed on titanium under physiological conditions, yielding a hydroxyl-terminated surface that is vital in promoting biocompatibility.[9] Robust, permanent attachment to TiO_2 surfaces in physiological conditions is a target for research, as the ability to control the surface functionalization of titania, either with lubricious coatings or biomarkers is desired in biomedical applications. Consequently, the study of the interaction between DOPA-containing proteins and polymers and TiO_2 substrates is of particular interest, both fundamentally as well as for advanced medical applications.

2. Coordinative attachment: controlled by local environment?

Density functional theory studies have shown that the binding of a DOPA group to a TiO_2 surface involves at least three different forms: molecular adsorption (through hydrogen bonding), partially dissociated monodentate adsorption, and fully dissociated bidentate adsorption.[10,11] In aqueous solutions, depending on the pH of the solution, either form of binding can be the dominating binding mechanism. The binding strength of a Dopa–TiO_2 coordination bond (~44 kT) is significantly stronger than the Dopa-Ti hydrogen bond (~4-12 kT).[12] Given the much higher attachment strength of a coordinative bond than a bidentate hydrogen bond, ideal attachment would be one that maximizes coordinative binding.

In the case of chemisorption, the phenolate groups of the catechol act as Lewis bases, capable of coordination with Lewis acidic metal ions. Structural metal ions on the surface of metal oxides can exchange bound hydroxyl groups for the catecholate ligand, as shown in equations 1-3.

$$CatH_2(aq) \leftrightarrow CatH^-(aq) + H^+(aq) \tag{1}$$

$$TiOH(s) + H^+(aq) \leftrightarrow TiOH_2^+(s) \tag{2}$$

$$TiOH_2^+(s) + CatH^-(aq) \leftrightarrow TiCatH\ (s) + H_2O\ (aq) \tag{3}$$

The pK_a of the catecholic ligand, the pH of the solution, and isoelectric point (pI) of the metal oxide surface all influence the degree of chemisorption of the catechol. As summarized by Hidber *et al.*, ideal conditions for maximal surface adsorption between phenolic ligands and metal oxide surfaces are achieved when solution pH ≈ ligand pK_a ≈ substrate pI.[13] When solution pH is much lower than the pK_a of the ligand, the proton affinity of the ligand can outcompete that of the surface and suppress adsorption. When the solution pH is much higher than the pI of the substrate, the concentration of surface hydroxyl species becomes a limiting factor, inhibiting ligand exchange and coordinative binding. Therefore, given the ligand pK_a greater than the isoelectric point of the substrate, maximum adsorption will occur when pH is roughly equivalent to pK_a. The first pK_a of Dopa in aqueous solution has been measured to be 9.8, higher, with few exceptions, than the pIs for various biologically and industrially relevant metal oxides such as vanadium, titanium, aluminum, and iron oxides.[14] Silicates such as mica, with a pI ~ 2, are essentially precluded from coordination binding, with Dopa instead forming bidentate hydrogen bonds.[15,16]

At relatively low pH, pH < 5.5, the Dopa group is well below the pK_a values of the phenolic protons (pK_a ~ 9.8 and 12), and the primary mode of interaction with the surface is expected to be hydrogen bonding with surface-bound oxygen atoms. As the pH increases, the hydroxyl groups are more likely to deprotonate, allowing the catecholate ligands to coordinate in a mono- or bidentate fashion with surface-bound titanium. Therefore the binding of a single Dopa to TiO_2 substrate should be much stronger at pH 7.5 than at pH 3.

Let us investigate the relevant factors in absorption, respectively. As the mussel byssus is completely extracellular, mussels have essentially no control over the pH of the threads after equilibration with seawater (pH ~ 8.2). While incapable of modulating the substrate pI, mussels have been shown to have selection preferences when presented with various surface options.[17] Despite this, the variety of surfaces to which mussels attach suggests an adaptive flexibility to this approach. This leads us to the final factor, the pK_a of the ligand. It is well-established that local microenvironments can widely modulate the pK_as of ionizable amino acids. Mehler et al showed that the pK_a of histidines in hydrophobic pockets could vary by 2 pH units.[18] The pK_a of tyrosine in the active site of ketosteroid isomerase was shown to be shifted down almost 4 pH units.[19] Sun and Toney showed that hydrogen bonding between an arginine and tyrosine in alanine racemase resulted in a pK_a that was effectively 2.5 pH units lower.[20]

While mussel proteins largely lack the secondary structure to hold DOPA in a rigid, defined geometry, it is nonetheless interesting that mfp-3 and mfp-5, the two families of proteins implicated in interfacial adhesion, contain remarkably high levels of lysine and arginine. On this basis, I hypothesized that the primary structure of these proteins may be sufficient to lead to a decreased DOPA pK_a, and the enhancement of coordinative adsorption to metal hydroxide surfaces.

3. Oxidation: A blessing and a curse

Despite having excellent binding ability to mica and TiO_2 surfaces, Dopa has a confounding tendency that presents significant challenges to many potential applications: at alkaline pH and with trace oxidants such as O_2, Dopa can readily undergo a two electron oxidation to Dopaquinone, which greatly diminishes the adhesion of mfp-3 *fast* to mica.[16] Mussels have evolved a strategy to minimize Dopa oxidation by combining an acidic pH, imposed during the formation of the mussel plaque, with the co-secretion of an antioxidant protein, mfp-6. Mussels also use the Dopa-Fe^{3+} coordination complex to temporarily stabilize Dopa in the plaques.[21,22] According to AFM single molecule studies, the pull-off force for the oxidized quinone state, incapable of strong chemisorption, decreased to $\approx$ 150 pN.[5] This 80% decrease is substantial, and suggest that Dopa oxidation can strongly perturb adhesion of mussel foot proteins to TiO_2 or other metal oxide surfaces. Although much attention has been paid to engineering mussel mimetic functional coating materials, few if any studies have systematically examined the effect of Dopa oxidation on the performance of those coating materials on metal oxide surfaces.

4. Resonance Raman spectroscopy: A uniquely capable tool for the study of catecholic coordination binding

Resonance enhanced Raman spectroscopy is a valuable tool to analyze the coordinative binding of Dopa to TiO_2 surfaces. Raman spectroscopy is a vibrational spectroscopic technique, which detects inelastically scattered photons, where the energy of the scattered light quanta differs from that of the primary light quanta. This energy difference can be equated to vibrational or rotational energies of interacting modes in a system. For a molecular vibration to lead to Raman scattering, or be "Raman active", the impinging light must modulate the polarizability of the mode. This is in contrast to infrared spectroscopy, where the frequency of the impinging radiation is in direct resonance with that of the specific vibrational mode. Raman spectra represent intensity changes versus Raman shifts, which are described by Equation 4:

$$\Delta w = \frac{1}{\lambda_o} - \frac{1}{\lambda_1} \tag{4}$$

where Δw is the Raman shift in wavenumber, λ_o is the excitation wavelength, and λ_1 is the wavelength of the Raman scattered light.

When the frequency of the incident radiation falls within the electronic absorption band, the resonance Raman effect may be observed. Rather than exciting a molecule to a virtual energy state, the molecule is excited to an excited electronic state. This can lead to an intensity enhancement of up to 10^6 as compared to the normally weak non-resonance scattering.[23] This allows much increased sensitivity in the detection of chemical species in dilute samples.

Resonance Raman spectroscopy has been proven to be a powerful tool to detect and quantify the binding of catechols to metal ions and metal hydroxide surfaces.[24,8] The binding of catechols from an acidic solution to TiO_2 nanoparticles was investigated extensively by Lana-Villareal *et al.*, who demonstrated that only catechols which bound coordinatively to TiO_2 surfaces formed the charge transfer complex required to observe resonance enhanced Raman signals.[25] Figure 1 shows the shifted absorbance upon complexation, as well as the spectrum obtained for the coordinatively bound catechols. Notable are the modes assigned to catechol-TiO_2 at 396, 516, and 637 cm^{-1}, and those to the catechol ring at 1261, 1329 and 1483 cm^{-1}.

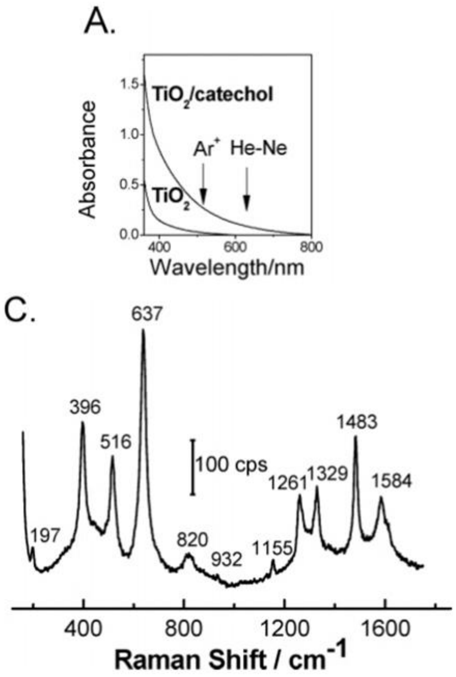

Figure 1: (A) Shift in absorbance upon catechol coordination to anatase titania. (C) Characteristic Raman spectrum for catechol-TiO_2 obtained in 0.1 M $HClO_4$ solution. Adapted from Lana-Villareal *et al*.[25]

Mfp-1 and Dopa grafted synthetic polymers were shown to form stable bis- and tris-catecholate complexes with Fe(III) at pH 7.5 or higher in vitro and in situ (in the mussel plaque).[22,24] Resonance-enhanced signals assigned to mono- and bidentate coordination were seen for a Dopa-containing protein on TiO_2.[8] The fact that only coordinatively bound catechols generate the ligand-to-metal charge transfer complexes that shift the electronic absorption band to the red means that the Raman spectra collected for catechols adsorbed to TiO_2 is dominated by those from coordinatively bound catechols, and not simply by catechols located in the vicinity of the substrate. This distinguishes the mode of binding in a much more direct fashion than could be obtained from other methods such as surface plasmon resonance (SPR) or quartz crystal microbalance (QCM).

II. Adsorption of mfp-3f to TiO_2

1. Background of mfp-3 fast

Mussel foot protein-3 (mfp-3) is a primary adhesive protein of the mussel plaque, located at the plaque/substrate interface. Although more than 35 polymorphs have been identified, these variants are generally of low molecular weight, high Dopa content and basic isoelectric point. For the sake of simplicity in this work, we focus on one variant, mfp-3fast 1α, with a molecular weight of 5200 kDa, a Dopa content of 21 mol-%, and a pI of 10.2. This protein has been shown to exhibit remarkable adhesive properties to mica surfaces. [1] The measured adhesion has been attributed to the propensity of Dopa to form bidentate hydrogen bonds with mica surfaces. Furthermore, the adhesive energy has been found to vary greatly with pH, decreasing sharply as the pH rises from 3 to 7.5, despite this pH range being above the isoelectric point of the mica surface (ca. 2) and below that of the ionizable lysine (pK_a ~ 10.5) and arginine (pK_a ~ 12.5) groups in the protein. The subsequent research looked to investigate whether mfp-3f adhesion to TiO_2 could be directly attributed to the formation of coordination bonds between Dopa and undercoordinated surface Ti sites, and whether protein adsorption varies as a function of pH.

2. The adhesion of mfp-3 fast to TiO_2

The adhesive interactions between mfp-3f and TiO_2 at three pHs have been investigated. The strongest adhesion force, with corresponding adhesion energy of -6.6 mJ/m^2, was measured at pH 3 after a brief compression. Interestingly, the adhesion force measured at pH 3 was not stable, showing strong time dependence. The adhesion force decreased with increasing the approach/separation force run cycles and/or the time of the experiment. In the third force run, the adhesion energy measured dropped to -5 mJ/m^2, about a 25% decrease of the initial adhesion. Unlike on mica surfaces, a longer contact time did not enhance the adhesion force of mfp-3 on TiO_2 surfaces: in the 4th force run, we kept the surfaces in contact for 10 min, and the adhesion force measured during separation decreased to - 4.5 mJ/m^2. DOPA does not undergo oxidation at pH3 in bulk solution.[26,27]

This decrease in adhesion forces is attributed to the photo-oxidation of Dopa by TiO_2 via the strong white light necessitated for interferometric analyses of separation and force in SFA experiments. Although the effect of photo-oxidation was significant in these tests, it is irrelevant to medical coatings applications since exposure to intense light is not typically involved in those processes.

The strong initial adhesion of mfp-3f on TiO_2 surfaces at pH 3 dropped significantly to −0.7 mJ/m^2 when the gap solution pH was increased to pH 5.5 (Figures 2a). Previous SFA studies on mica surfaces have shown similar trends, due to the auto-oxidation of Dopa to Dopaquinone at high pH.

Increasing the pH to 7.5 did not further reduce adhesion, but instead increased it to −1.3 mJ/m^2. Given that Dopa is more susceptible to auto-oxidation at pH 7.5, there should be fewer Dopa groups available for binding, and correspondingly lower adhesion; however, increasing the pH also increases the possibility of monodentate or bidentate binding of Dopa to the TiO_2 surfaces, thereby leading to much stronger binding than the molecular absorption through hydrogen bonds at the single molecular level.[8,10] Ti(IV) complexation by coordination may also significantly improve the stability of Dopa, as shown in mussel plaques. As a result of the two competing effects, the adhesion of mfp-3f on TiO_2 surface is stronger at pH 7.5 than at pH 5.5.

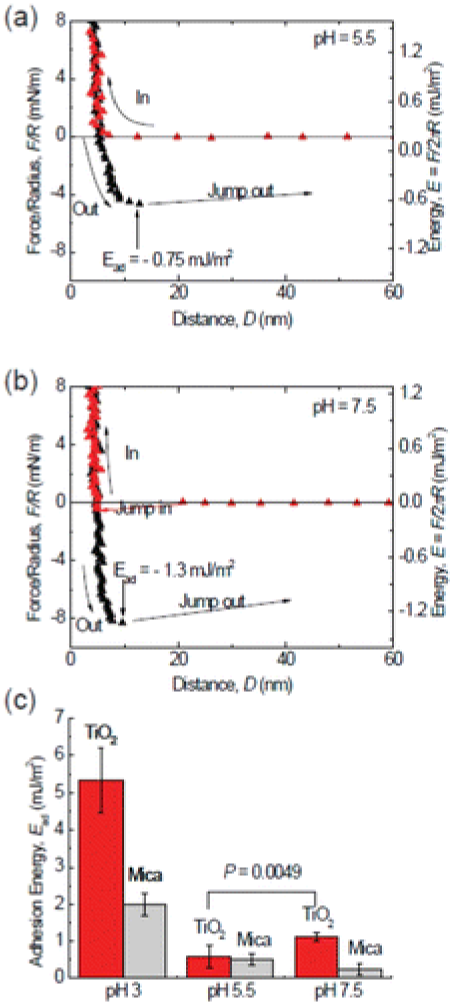

Figure 2: pH dependence of adhesion of mfp-3F to TiO2. Reduced adhesion occurs upon increasing the pH to 5.5 (a). A surprising increase in adhesion by almost 40% occurs upon bringing the pH up to 7.5 (b). Although Dopa loss to oxidation is more severe at high pH, the Dopa–TiO2 coordination bond gives higher adhesion forces. (c) A summary of the adhesion energies of mfp-3 on TiO2 in different pH buffers. The adsorption of Dopa on TiO2 surface is highly pH-dependent. At low pH, the protonated Dopa predominates, whereas at pH 7.5, there exists a mixture of both half- and fully deprotonated catecholates.

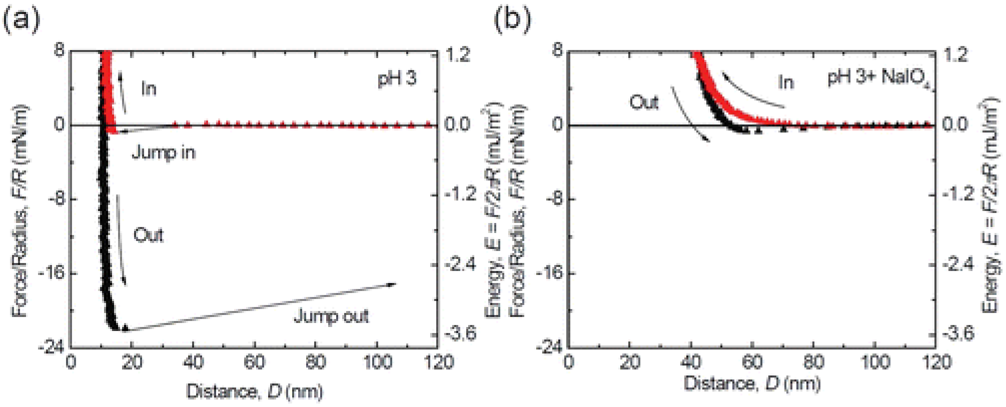

Figure 3: Periodate treatment as an independent measure of the effect of Dopa oxidation on adhesion. At pH 3, before adding periodate, strong adhesion was measured (a). The adhesion is almost completely abolished (96% decrease) by adding periodate at pH 3 (b).

To explore the correlation between the loss of adhesion and DOPA oxidation, we performed a control DOPA oxidation experiment using an oxidant, periodate, at pH 3 where the strongest adhesion was detected. After achieving a final stable adhesion energy of −3.6 mJ/m^2, 20 μL periodate solution (100 μM) was injected into the gap between the surfaces (Figure 3). Only an extremely weak adhesion force, corresponding to an energy of −0.15 mJ/m^2, was detected in the separation after driving two surfaces into contact. The periodate oxidation experiment supports our proposition that oxidation of Dopa to Dopaquinone decreases mfp-3f adhesion to mica at pH 5.5 and 7.5, however, it does not preclude the possibility that electrostatic attraction also contributes to the increased adhesion at pH 7.5. The four-fold increase in the hardwall (from 10 to 40 nm) has been attributed to the effect of dehydroDopa formation on backbone stiffening and is typically reversible with reduction.[15]

3. Resonance Raman spectroscopy of adsorbed mfp-3f on TiO_2

As mentioned previously, resonance Raman spectroscopy is a particularly well-suited method to detect the formation of catechol-Ti coordination bonding. To further investigate the binding mechanism of mfp-3f as a function of global environment, we adsorbed mfp-3f on TiO_2 surfaces at three different pHs (pH 3, 5.5 and 7.5). Figure 4 shows background-subtracted Raman spectra for mfp-3f adsorbed at pH 3 and pH 5.5, normalized to the non-resonant C-H vibrational peak (2800-3000 cm^{-1}) (Appendix A.1). The spectrum for protein adsorption at pH 7.5 is shown in Appendix A.2. Prominent peaks in the spectrum resulting from mfp-3f deposition at pH 5.5 are consistent with those seen for mfp-1-TiO_2 adsorption, and share marked similarity to those originating from the complexation of mfp-1 and Fe^{3+}.[24,21] Low energy resonance peaks (500–700 cm^{-1}) have previously been assigned to vibrations of the oxygen–metal chelation bonds. Specifically, peaks at 585 cm^{-1} and 639 cm^{-1} indicate coordination by the oxygens on C3 and C4 of the catechol ring, respectively, whereas that of 530 cm^{-1} arises upon bidentate coordination and resulting charge transfer. Higher energy resonance peaks (1200–1500 cm^{-1}) have been assigned to catechol ring vibrations.[21] The pronounced spectral features in this region highlight the involvement of the catechol in the interfacial charge transfer upon coordination to TiO_2. Namely, the strong ring stretch at 1488 cm^{-1} is indicative of a catechol-Ti charge transfer and has previously been observed as a charge transfer in the Dopa-Fe^{3+} chelate complex. Similarly, a strong feature at 1331 cm^{-1}, attributed to a C-O stretching mode, indicates the vital role of the catecholate functionality in providing bridging adsorption.[28]

The spectra acquired at pH 3 also show characteristic enhanced signals in both the high and low energy regions shaded in Figure 3. The strength of these signals is notably diminished relative to that of mfp-3f adsorbed at pH 5.5. As anticipated, binding at pH 3

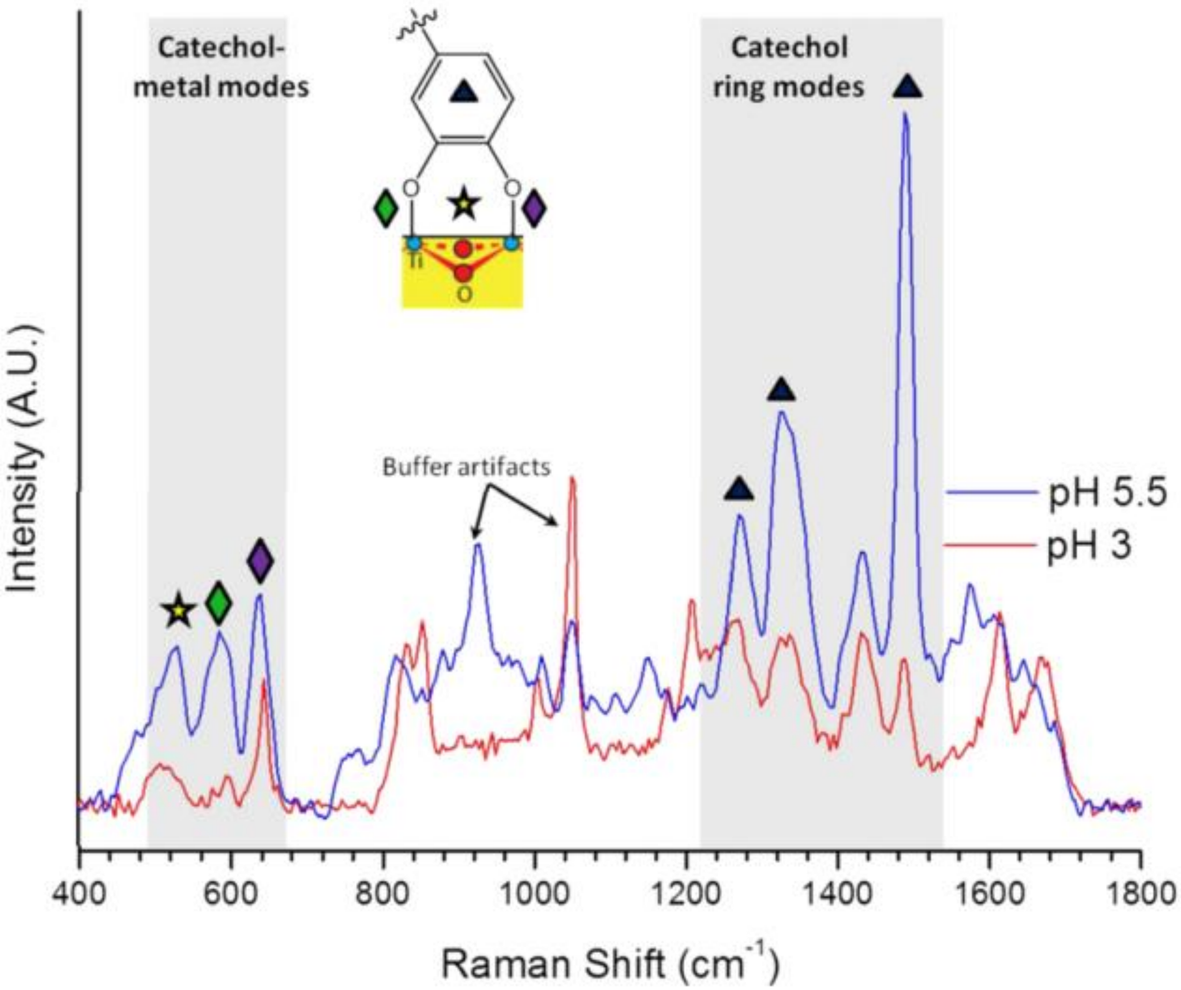

Figure 4: Resonance Raman spectra of Dopa–TiO$_2$ interactions in mfp-3f adsorbed at pH 3 and 5.5. Peaks at 1488 (▲; ν C–Carom + ν C–Harom), 1329, and 1261 cm^{-1} (▲; ν C–O + ν C–Carom) are characteristic catechol peaks which are enhanced upon coordination and charge transfer. Signals at 639 (◆; δ,ν C4–O), 585 (◆; δ,ν C3–O), and 530 cm^{-1} (☆; δ,ν C–O bidentate coordination) are characteristic catechol/metal chelate modes. Resonance enhancement of diagnostic modes for coordination is reduced at lower pH, suggesting predominant Ti-Dopa bridges at pH 5.5 and largely uncomplexed protein at pH 3. Peaks labeled represent artifacts from the buffer solutions (sodium acetate C–C at 930 cm^{-1} and nitrate N–O ν1 at 1050 cm^{-1}).

results in a lower amount of coordination, as protons outcompete surface metal sites for the catecholate anions.

Mfp-3f deposited at pH 7.5 shows a strong fluorescent background (Appendix A.2). A strong fluorescence has previously been observed in resonance Raman investigations of Mefp-1. [29] As described earlier, Dopa is especially prone to auto-oxidation at high pH. This oxidation leads to rapid oligomerization, generating impurities with red-shifted absorption and fluorescence.[30] Under the conditions studied, this shifted absorption leads to a substantial fluorescence background that obscures all other signals; therefore, resonance-enhanced peaks signifying coordination could not be detected. However, it is anticipated that similar coordination peaks would indeed be seen at this pH, explaining the rescue of adhesion measured in the SFA experiments.

Taken together, the Raman spectroscopy measurements support the SFA findings: increased pH favors the possibility of coordination binding of DOPA to the TiO_2 surfaces while also increasing the rate of DOPA oxidation, which decreases the amount of DOPA residues available for binding. These opposing effects strongly alter the adhesive properties of mfp-3f and certainly have a similar effect on other DOPA-containing adhesives. This emphasizes the importance of well-controlled deposition conditions in forming robust interfacial binding. It is known that mussels regulate both the pH in the distal depression during protein secretion and the oxidation by co-secreting a protein, mfp-6, shown to have antioxidant properties.[16]

III. Synthetic catecholic polymers derived from poly(pentafluorophenyl acrylate)s

1. Motivation

As shown in the previous section, the amount of coordinative binding of catecholic proteins to a metal hydroxide surface is dependent on the global pH of the system. While evidence shows that the mussel lowers the local pH during plaque protein secretion, this quickly equilibrates to that of seawater (ca. 8.2). I looked to investigate whether the local chemical environment surrounding catechols can similarly alter the amount of coordinative binding to metal hydroxide surfaces in synthetic polymeric constructs.

To probe this question, I synthesized a library of polyacrylates containing catecholic functionality flanked by positive, negative, and neutral cofunctionality. Similar to the adhesive proteins mfp-3 and mfp-5, these polymers have high catecholic (15 mol-%) and charged residue (20 mol-%) incorporation. Our hypothesis was that, as in the case of the interfacially active mussel foot proteins, polymers with basic flanking units would lead to increased coordinative binding to TiO_2 surfaces.

2. Synthesis of a diverse library of catecholic polyacrylamides

A. Poly(pentafluorophenyl acrylate) (***pPFPA***) *homopolymer and copolymer synthesis and characterization*

Copolymers can be synthesized either by copolymerization of diverse monomers, or by post-functionalization from a reactive polymeric platform. The first requires separate polymerizations, whereas the second can be difficult to functionalize in high yield. In order to minimize the confounding factors of molecular weight, polydispersity, and blocky character, and increase the modularity of the system, I used a post-functionalization strategy. The polymer of the active ester monomer pentafluorophenyl acrylate has been shown to react in nearly quantitative yields with a wide variety of nucleophiles, including catecholamines and amines bearing positive and negative charge.[31–35]

Pentafluorophenyl acrylate was synthesized according to a literature procedure.[32] After purification, the activated ester monomer was polymerized using radical addition-fragmentation chain-transfer (RAFT) polymerization with a trithiocarbonate chain transfer agent. The polymers were purified by precipitation and characterized by nuclear magnetic resonance (NMR) spectroscopy, attenuated total reflectance infrared (ATR-IR) spectroscopy, and gel permeation chromatography (GPC) (Figures 5 and Experimental). In addition to ^{1}H and ^{13}C, the pentafluorophenyl acrylate polymers can also be monitored through ^{19}F NMR. The ^{19}F nucleus has a 100% natural abundance, high sensitivity, and shift parameter range of about 400 ppm, which allows excellent nuclear resolution. Molecular weight and polydispersity index (PDI) were measured by chloroform GPC calibrated with polystyrene molecular weight standards and determined to be M_n =11.0 kDal, with a PDI of 1.31.

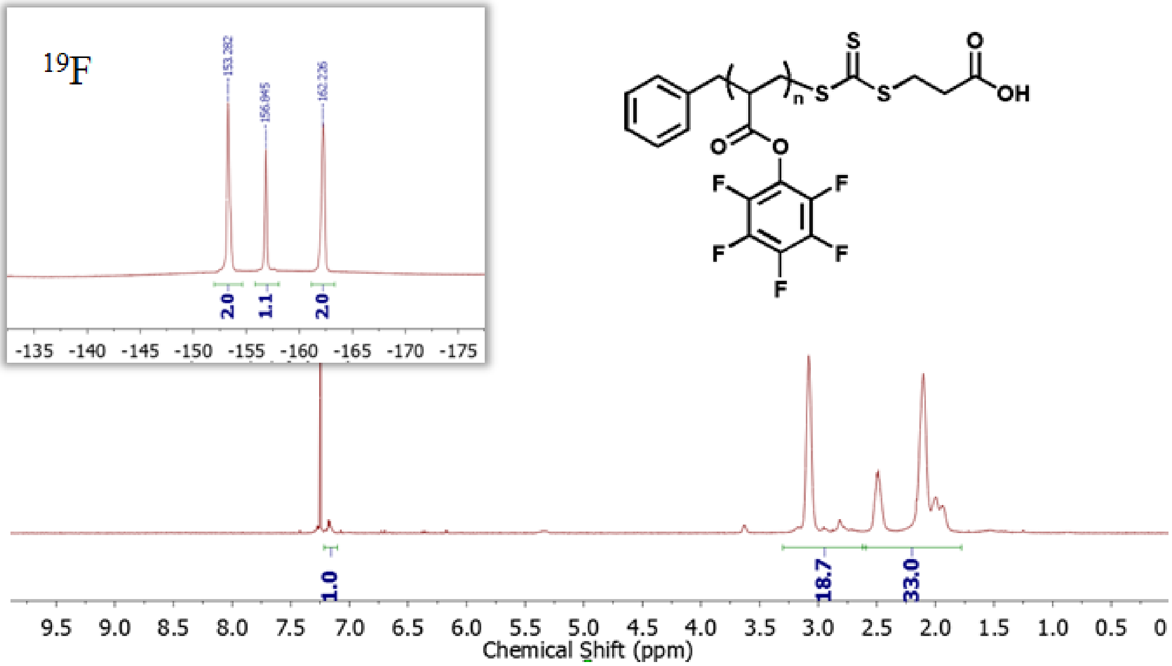

Figure 5. Annotated ^{1}H and ^{19}F nuclear magnetic resonance spectra of poly(pentafluorophenyl acrylate) homopolymer synthesized via RAFT polymerization.

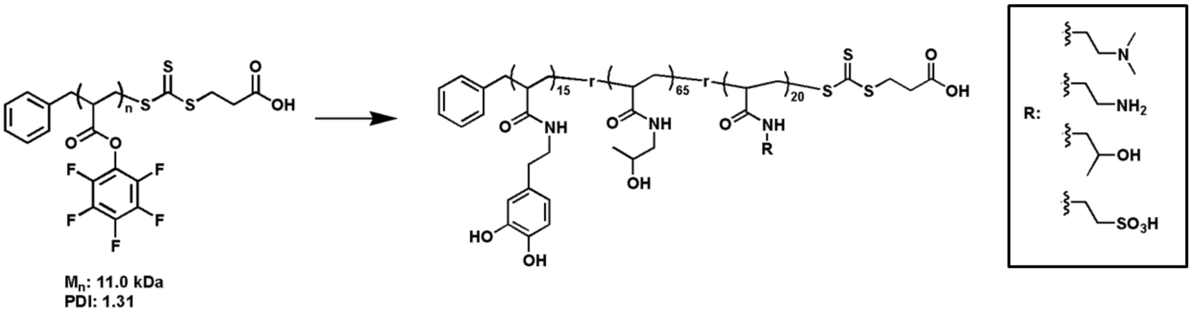

Scheme 1: Stepwise functionalization of PFPA polymer to yield catecholic copolymersbearing charged functionalities.

A library of catecholic polymers with varying cofunctionality was prepared from this starting polymer, as shown in Scheme 1. The procedure of Wang *et al* was be used to sequentially functionalize the active ester polymers with catechol and cofunctionality.[34] First, functionalization with dopamine hydrochloride was monitored by the ratio of free:polymeric pentafluorophenyl signals in via ^{19}F NMR. After 3 hours, dopamine was determined to be completely reacted. To ensure identical catecholic functionality, aliquots of this reaction solution were divided and further functionalized with the desired ionizable amine (hydroxypropylamine, mono-boc ethylenediamine, *N*,*N*-dimethyl ethylenediamine and taurine). Finally, an excess of hydroxypropylamine was added to each vial to react and quench the remaining active ester functionality.

An annotated NMR spectrum of one representative functionalized copolymer is shown in Figure 6. Of note is the complete disappearance of pentafluorophenyl peaks in the ^{19}F spectrum. Detailed characterization information of the remaining copolymers is included in the experimental section at the end of this chapter.

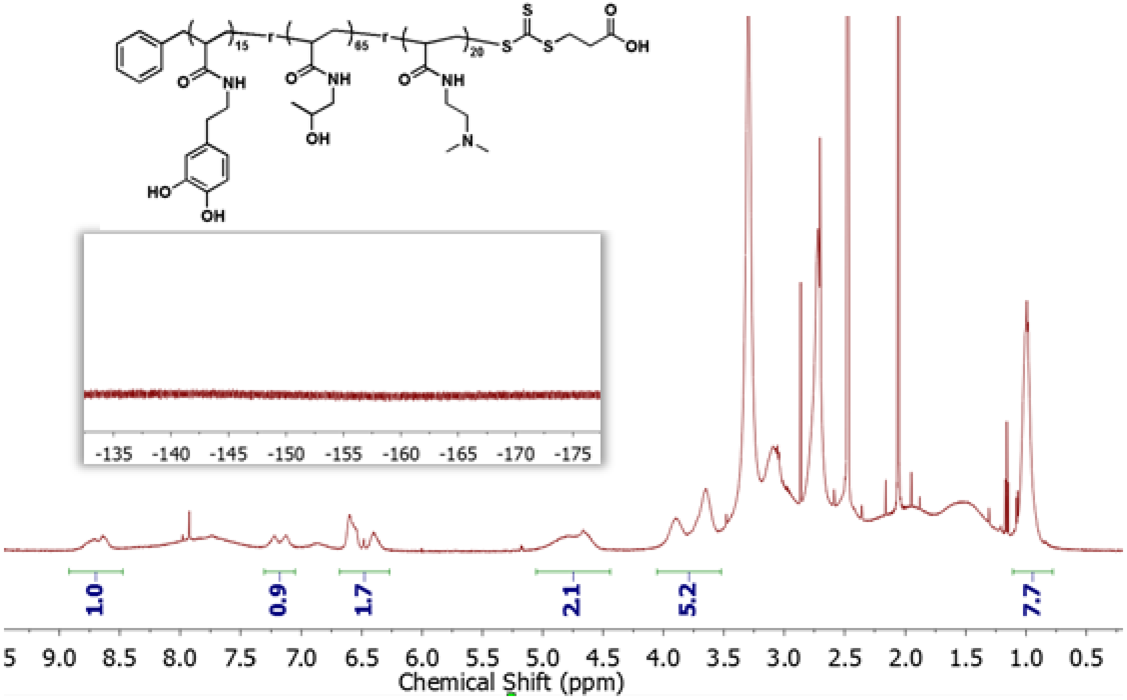

Figure 6. ^{1}H **and** ^{19}F **nuclear magnetic resonance spectra of poly(dopamine acrylamide-co- [2-(Dimethylamino)propyl]acrylamide-co-(2-Hydroxypropyl) acrylamide) P(DA-DPA-HPA) synthesized via sequential functionalization from the starting PFPA.**

3. Interrogating binding via resonance Raman spectroscopy

Next, I looked to investigate the effect of cofunctionality on the coordinative binding of the synthesized acrylic copolymers via resonance Raman spectroscopy. Again, this technique possesses the advantage of selectively enhancing the signal from those catechol moieties bound coordinatively to TiO_2 surfaces. Initially, attempts were carried out under identical conditions to those used for protein adsorption and described above. However, after deposition and rinsing, no resonance signal indicative of coordination binding could be detected for any formulation under any condition. This suggests that the catecholic residues in the acrylic copolymers are notably less surface-active than those in mfp-3*f*, an intriguing finding that speaks to the efficacy of the adhesive proteins and warrants study in further detail.

The adsorption procedure was optimized to allow comparable detection of catechol-Ti coordination binding. To increase the number of surface sites available for binding, I switched from smooth, amorphous TiO_2 surfaces used for protein binding to commercially available TiO_2 nanopowder (Degussa P25). This powder has an average particle size of 27 nm, and is 80% anatase and 20% rutile, with an isoelectric point of 6.2. As a result of the anatase crystallinity, sharp peaks are observed in the spectrum at 409 cm^{-1}, 515 cm^{-1}, and 609 cm^{-1}. This is in agreement with previously assignments for anatase nanoparticles, and notably distinct from those peaks at 530, 585, and 639 cm^{-1} observed as a result of catecholate-TiO_2 resonance-enhanced bands.[36]

A TiO_2 nanoparticle slurry was dropcast and dried onto a mica slide to form a thick nanoparticle film. Copolymers were deposited from a buffered solution of the desired pH at [catechol] = 5 mM. Figure 7 shows the Raman spectrum taken from several deposition conditions for the best-adsorbing copolymer. The resulting spectra represent an average of 300 individual measurements taken over an area of 150 μm x 150 μm. A short integration time of 0.3 seconds and a low laser power of 10-20 mW were necessitated to avoid sample burning and carbonization. As for the proteins, high energy resonance peaks which correspond to catechol ring vibrations are observed at 1488, 1331, and 1285 cm^{-1}, which can be assigned to catechol ring vibrations.[8] The remaining spectral series can be found in Appendix A.3-5.

In order to assess the degree of coordinative binding, the peaks from the anatase titania surface were used as an internal standard. Figure 8 shows the ratio of the intensity of the resonance peak from adsorbed catechol at 1489 cm^{-1} to the anatase peak at 609 cm^{-1} for the 4 selected copolymers adsorbed at pH 3, 5.5, 7.5 and from unbuffered DI water (measured pH 5.3).

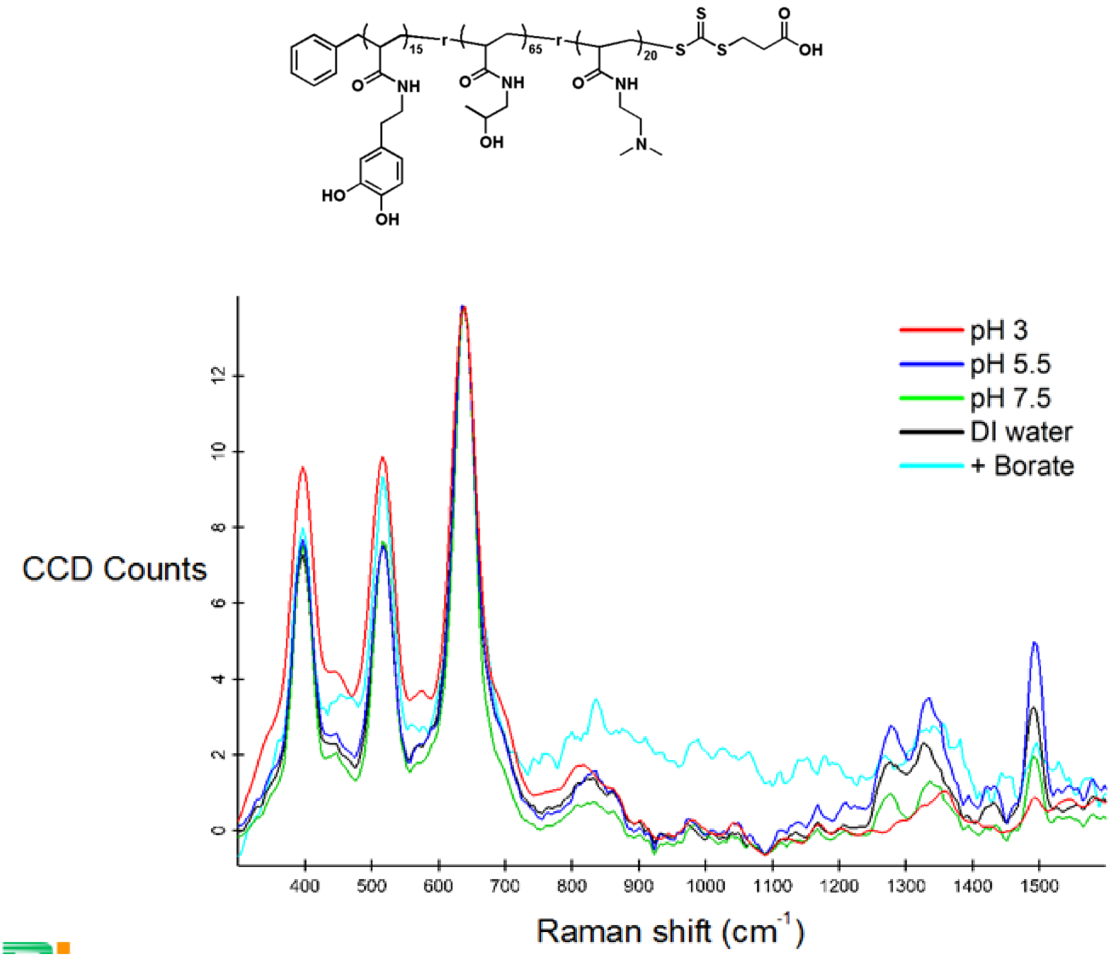

Figure 7. Resonance Raman spectra of P(DA-DPA-HPA) copolymer adsorbed to TiO_2 nanoparticle film. Peaks at 1488 (▲; ν C–C$_{arom}$ + ν C–H$_{arom}$), 1329, and 1261 cm–1 (▲; ν C–O + ν C–C$_{arom}$) are again seen as characteristic catechol peaks which are enhanced upon coordination and charge transfer. Acetate buffers were used for pH 3 and 5.5, phosphate for 7.5, and borate at pH 9.

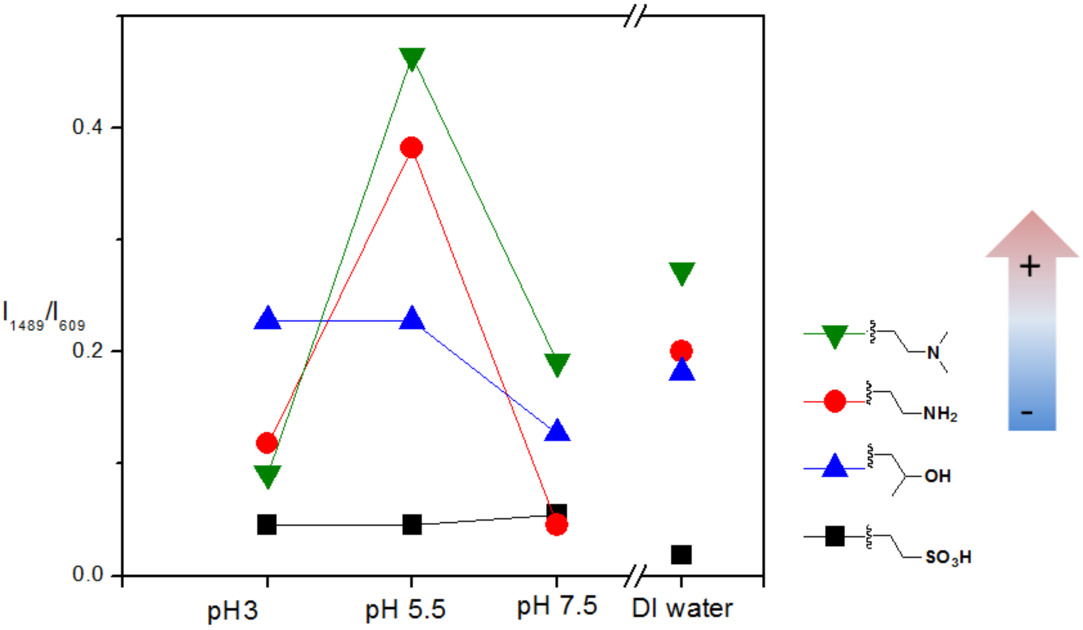

Figure 8: Plot of the relative Raman peak from at 1488 cm^{-1}(ν C–C$_{arom}$ + ν C–H$_{arom}$) for coordinative binding, standardized to that of the non-resonant anatase TiO$_2$ peak at 609 cm^{-1}.

Many interesting features can be gleaned from these data, which follows the general absorption trends established in mfp-3*f*. Most evident is the minimal absorption by the sulfonic acid-functional taurine copolymer under all conditions. The neutral amino-2-propanol functional copolymer shows moderate coordinative adsorption at low pH, and decreased coordination at pH 7.5, which also correlates to higher background fluorescence. We attribute this to the competing effects of adsorption as well as increased rate of auto-oxidation as pH increases, knocking out potential binding functionality. Finally, the cationic copolymers show a similar trend in coordinative binding, with minimal adsorption at low pH, a peak around the pI of the TiO_2 surface, and a decline afterwards. This behavior has been interpreted as such: at low pH, the TiO_2 and the copolymer are both highly positively charged, leading to an electrostatic repulsion which minimizes adsorption as compared to the neutral copolymer. Upon an increase to pH 5.5, the TiO_2 surface is essentially neutral. The increased amount of coordination for both cationic copolymers as compared to the neutral copolymer would match the effect predicted by the fact that a locally basic microenvironment can lead to a shift in the pK_a of the adsorbing catechol species. Finally, there is a decrease in binding at high pH, as the amount of TiO_2 surface hydroxyl sites becomes sparse. Worth noting is the divergence in adsorption between the dimethylamine-functional copolymer and the primary amine functional copolymer at high pH. On the basis of the increased fluorescent background, we attribute this difference to the propensity of the primary amine to undergo a nucleophilic Michael addition or Schiff base reaction to knock out adsorbing catechol species, a characteristic, which is not possible with the tertiary amine. Amine reactivity in the context of catechols was previously noted in the literature as Chawla *et al* utilized a DOPA-lysine motif as the anchoring functionality for PEG brushes on PDMS surfaces.[37] In this study, the presence of the amino-functionality led to dramatically higher oligomerization in solution as compared with the non-lysine-containing derivative.

4. The effect of local environment on metal-binding speciation

The resonance Raman measurements detailed in the preceding section show that the cofunctionality plays a role in the coordinative adsorption of catecholic polymers to inorganic substrates. To demonstrate this further, I investigated the binding stoichiometry of catecholic polymers with Fe^{3+}. For simplicity, a comparison was made between the binding of the neutral poly(dopamine acrylamide-co-(2-hydroxyethyl) acrylamide) (p(DA-HEA)) and the cationic poly(dopamine acrylamide-co-[2-(Dimethylamino)propyl] acrylamide-co-(2-hydroxyethyl) acrylamide (p(DA-DMA-HEA)). Figure 9 shows the absorption spectra for these polymers with 3:1 catechol:Fe^{3+} at pH 8.2. The peak region from 400-750 nm is diagnostic of the ligand-to-metal charge transfer ($d\pi^*$) absorption formed upon coordination, where each stoichiometry has a distinct λ_{max} and known molar absorptivity (*mono* 714 nm ($\epsilon = 1000\ M^{-1}cm^{-1}$), *bis* 570 nm ($\epsilon = 3330\ M^{-1}cm^{-1}$), *tris* 490 nm ($\epsilon = 4190\ M^{-1}cm^{-1}$)).[38] Peaks were fit in order to determine the ratios of *bis* and *tris* coordination in the solution. Figure 10 shows that at pH 8.2, both polymers bind Fe^{3+}in a mix of *bis* and *tris* coordination stoichiometry. Clearly, however, the proportion of binding is different between the neutral and cationic species, providing further evidence that the presence of local positive charges can alter the behavior of neighboring catechols.

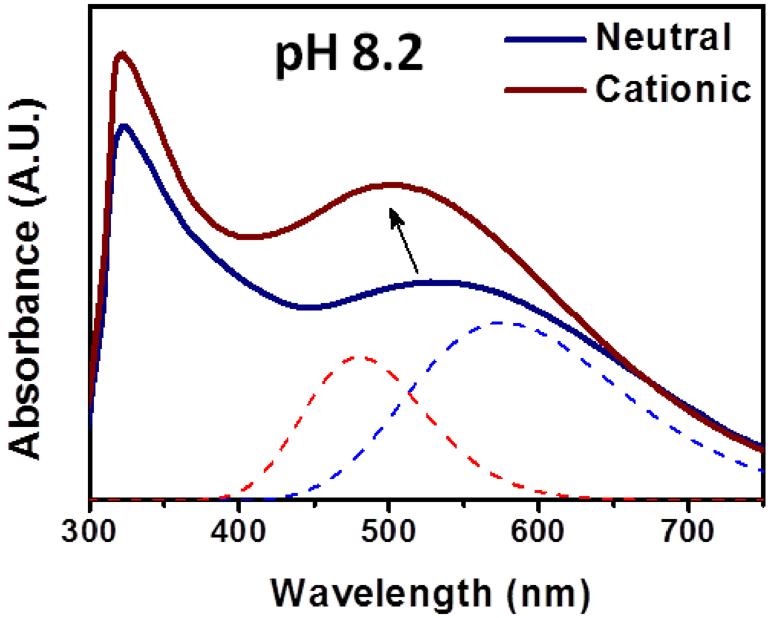

Figure 9. UV-visible absorption spectra of neutral p(DA-HEA) and cationic p(DA-DMA-HEA)-Fe^{3+} solutions.

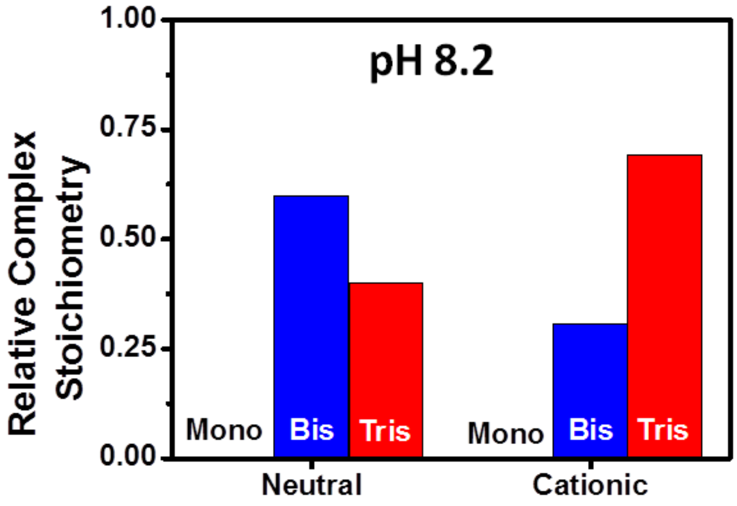

Figure 10. Relative speciation of Fe^{3+}-catechol complexes formed with catecholic acrylamides in solution.

IV. Using Dopa-containing peptides to probe the effect of neighboring lysine residues

1. Motivation

The previous adsorption and metal binding studies highlight the substantially higher amount of coordinative binding and shifted speciation due to the presence of cationic cofunctionality. I next looked to investigate whether this enhanced performance could be duplicated in a simple peptide model system. Wei *et al.*, in a gentler approach to reductionism, derived 3 15-peptide sequences of dramatically different charge states from the interfacial adhesive protein mfp-5.[39] All sequences had similar Dopa content, but the peptide with the most basic isoelectric point was seen to be the most adhesive to mica substrates, hinting again at the importance of co-localization of positive charges and Dopa. A glance at the sequence of mfp-5 shows a remarkable level of tandem cationic-Dopa residues (~70% of Dopa are flanked by lysine or histidine). We looked to scale this finding down another level, using an even simpler peptide series to determine whether the primary structure of Dopa and lysine could be demonstrated to affect the chemical properties of Dopa. To probe this, a series of peptides with Dopa (Y*) and lysine (K) were synthesized with varying lengths of glycine (G) spacer residues (KY*K, KY*, KGY*, KGGY*, KGGGY* and GY*G). I analyzed the chemical environment of these Dopa peptides in dilute solutions by nuclear magnetic resonance and electrochemistry to determine whether the direct primary sequence could be shown to influence the reactivity of Dopa.

2. Electrochemical characterization of KGY* peptides

As the oxidation of Dopa to quinone is a proton-dependent process, the measured reduction potential changes as a result of solution pH as well as the pK_a of substituted catechols. For example, the reduction potential of 4-*tert*-butyl catechol ($pK_{a1} = 9.8$) at pH 3 is 310 mV, while that of 4-nitrocatechol($pK_{a1} = 6.7$) is 570.[40,41] We prepared dilute solutions of the Dopa and lysine-functional peptides, and determined their reduction potentials via cyclic voltammetry. Figure 11 shows the voltammagrams for the KY*, KGY*, KGGY*, and GY*G peptides.

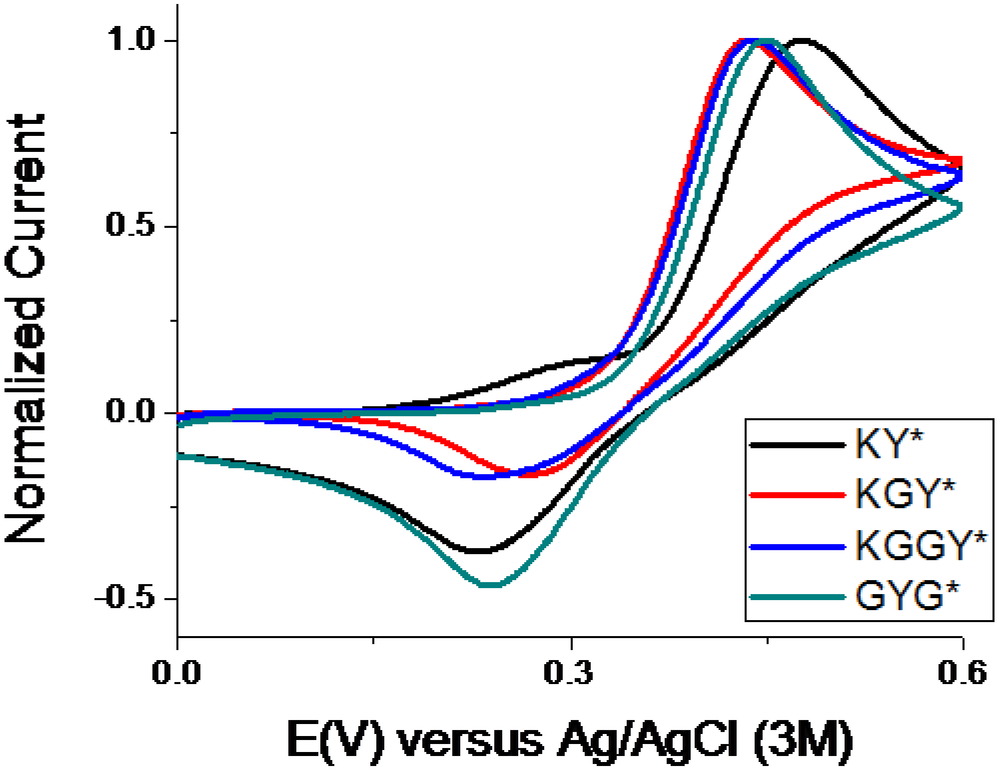

Figure 11: Cyclic voltammetry of a series of lysine and DOPA containing peptides. Spectra were measured at a scan rate of 100 mV/s in 100 mM pH 5.5 acetate buffer.

As shown above, the anodic current peak is virtually identical for the control GY*G peptide and the KGY* and KGGY* peptides ($E_{\text{peak, anodic}}$ = 450, 444, and 441 mV respectively), though it is shifted to slightly higher potentials ($E_{\text{p,anodic}}$ = 477 mV) for KY*. This 30 mV shift in the reduction potential corresponds to a change in free energy equivalent to that of a change in pK_a of approximately 1 unit, suggesting that, indeed, the presence of a directly proximal lysine can measurably alter the adsorptive properties of catechols (Equations 5 and 6).

$$\Delta G_e = -nF(E_1 - E_2) \tag{5}$$

$$\Delta G_e = 2.303RT(pK_{a1} - pK_{a2}) \tag{6}$$

3. NMR spectroscopic characterization of KGY* peptides

A comparison of the NMR spectra for three Dopa-containing peptides, KGY*, KY*K, and KGGGY*, is shown in Figure 12. The chemical shift of protons is dependent upon the electronic environment around the protons. Relatively electron-rich protons are shifted upfield, to higher ppm, while electron-poor protons are shifted downfield. Unfortunately, compared to the results from cyclic voltammetry, the NMR results lack a clear trend in chemical shift. An effect of lysine/Dopa spacer length cannot be detected by this method.

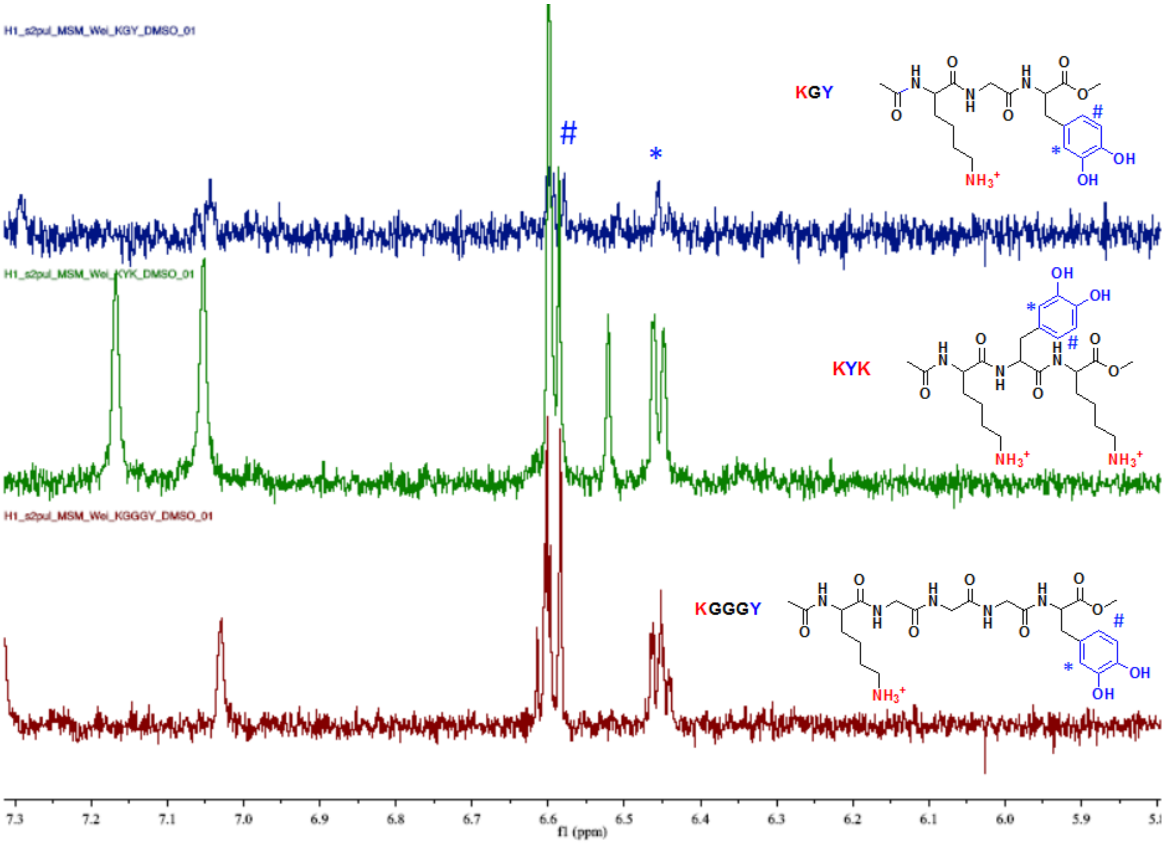

Figure 12: shows a comparison of the aromatic regions for KGY*, KY*K, and KGGGY*. The aromatic proton at postion C_2 shows a chemical shift of approximately 6.45 ppm for all cases (marked with an asterisk), while the C_5 and C_6 aromatic protons give a peak at 6.55 to 6.63 ppm in all cases (marked with a pound sign).

V. Conclusions

Understanding the binding mechanism of Dopa to TiO_2 surfaces is crucial for the development of mussel-inspired polymers as coating materials. The work described in this chapter provides a foundation for the design principles required to optimize the binding of catecholic macromolecules to the model metal hydroxide surface TiO_2. Three systems are utilized to investigate this binding.

The results from Section II demonstrate that mfp-3f binds strongly to TiO_2 surfaces at low pH. Raising the pH gives rise to opposing effects: (1) oxidation, which decreases the amount of Dopa residues available to bind to the TiO_2 surfaces; (2) changing the binding nature of a single Dopa to the TiO_2 from H-bonding to coordination bonding and, therefore, increasing the binding strength of a single Dopa group to the TiO_2 surface.

Section III describes the binding of a series of charged catecholic polyacrylates to TiO_2 surfaces. As with the proteins, coordinative binding was found to be a function of pH. Furthermore, the amount of binding varies with different copolymer compositions. Polymers with positively charged moieties were shown to promote a higher degree of coordinative binding. This effect aligns with the high proportion of positive charges in the interfacial mussel foot proteins, and is believed to modulate the local environment of the catechol to increase the amount of binding.

Having shown that the binding properties of catecholic macromolecules can be optimized by the addition of cationic cofunctionality, Section IV seeks to determine whether the proximity of this cationic charge has a measurable effect on the electrochemical and spectroscopic properties of short peptides. The reduction potential of peptides with directly neighboring lysine functionality was found to be shifted to higher potential, whereas those residues spaced by at least one glycine were identical to the control peptide.

Collectively, the results of this chapter support the initial hypothesis that cationic cofunctionality can increase the amount of coordinative binding of catecholic polymers to TiO_2 surface. The proposed mechanism for this enhanced binding is that this highly basic environment favors catecholic deprotonation, resulting in more highly adsorbing species.

VI. Experimental

Materials and Methods

All reagents were purchased from commercial sources and used without further purification unless otherwise stated. Triethylamine was dried by distillation and stored over molecular sieves.

Instrumentation

^{1}H and ^{13}C NMR spectra were recorded using a Varian 600 MHz spectrometer with the solvent signal as internal reference. Gel permeation chromatography (GPC) was performed on a Waters 2690 separation module equipped with Waters 2414 refractive index and 2996 photodiode array detectors using $CHCl_3$ containing 0.25% triethylamine as eluent at a flow rate of 1 mL/min. Molecular weight distributions (PDIs) were calculated relative to linear poly(ethylene oxide) standards. ESI mass spectrometry was performed on a Micromass QTOF2 quadrupole/time-of-flight tandem mass spectrometer. UV-Vis spectra were recorded on an Agilent 8453 spectrophotometer using quartz cuvettes with 1cm path length and blanked against the relevant buffer solution.

Protein Purification

Purification of mfp-3f was achieved as previously described.(14) The purified proteins were suspended in buffer consisting of 0.1 M acetic acid (EMD Chemicals, Gibbstown, NJ), and 0.25 M potassium nitrate (Aldrich, St. Louis, MO) and with a pH of 3. The protein solutions were divided into small aliquots and stored at −50 °C before experiments.

Surface Forces Apparatus

The adhesion of mfp-3f on TiO2 surfaces was studied using a surface forces apparatus 2000 (SFA 2000) with a reported geometry.(15) A 10 nm thick TiO2 layer was deposited on the mica surfaces glued on the SFA disks using an E-Beam deposition method (Temescal system) at a constant rate of 0.1 nm/s and a pressure <4 × 10–5 Torr and was shown to be free of impurities by XPS (Kratos Ultra, Kratos Analytical Limited, S Figure 1). The surface roughness of the TiO2 substrate was 1 nm measured by AFM (Asylum MFP-3D-SA, S Figure 2). Prior to experiments, a droplet of mfp-3f solution with a mfp-3 concentration of 5 μg/mL (pH = 3) was pipetted on top of one TiO2 surface, letting the protein adsorb for 20 min and ideally forming a monolayer of mfp-3 molecules on the surface. The TiO2 surfaces were then rinsed thoroughly with pH 3 buffer (0.1 M acetic acid, 0.25 M potassium nitrate, Sigma Aldrich) to remove the unabsorbed protein and then mounted into a SFA box. Buffer change was achieved by repeated injection and removal of buffer between the two surfaces. The distance D between two surfaces is measured with an optical interferometry technique (fringes of equal chromatic order, FECO). By applying the Derjaguin approximation, the normalized force F/R between the two cylindrical SFA surfaces is directly proportional to the energy between two flat surfaces with a simple relation of $E(D) = F(D)/2\pi R$. Buffer preparation: 0.1 M sodium acetate (EM Science, Gibbstown, NJ) and 0.25 M potassium nitrate titrated by acetic acid (pH 5.5); 0.016 M potassium phosphate monobasic (Mallinckrodt, Hazelwood, MO) and 0.084 M potassium phosphate dibasic (EMD Chemicals, Gibbstown, NJ; pH 7.5). Milli-Q water (Millipore, Bedford, MA) was used for all the glassware cleaning and solution preparation.

Raman Spectroscopy

For the protein experiments, samples were prepared by drop-casting 20 μL of mfp-3f solution (10 μg/mL) in the appropriate buffer solution onto the TiO2-coated mica surfaces described for the SFA experiments, followed by incubation under ambient conditions for 20 min. After adsorption, surfaces were rinsed with the respective buffer solution and dried with a stream of N_2.

For the synthetic polyacrylates, copolymers were deposited from a 100 mM buffered solution of the desired pH at 5 mM [catechol]. A 25 μL aliquot of the copolymer solution was dropcast onto the TiO_2 surface and incubated for 20 minutes. To remove excess polymer, the wafer was gently dipped into the respective buffer solution.

Raman spectra were collected with a confocal Raman microscope (α300; WITec) equipped with a Nikon objective (100×) and a laser excitation wavelength of 532 nm. Spectra were acquired with a CCD camera (DV401-BV; Andor) behind a spectrometer (UHTS 300; WITec) with a spectral resolution of 3 cm–1. Samples were sensitive to burning by the laser beam; therefore, laser power was restricted to 10–20 mW. Each collected spectrum consisted of 120 accumulations; with an integration time of 1 s. ScanCtrlSpectroscopyPlus software (version 1.38, Witec) was used for measurement setup. The acquired spectra were analyzed and processed with Witec Project software (version 2.08). Spectra were background subtracted (average background subtract function) and smoothed with a 9-point Savitzky-Golay filter (fourth order polynomial). Background spectra of TiO2-coated mica substrate with and without drop-cast buffer solution were also collected.

Polymer synthesis

Poly(pentafluorophenyl acrylate) (1.3 grams, 5.46 mmol repeats, 1 EQ) was dissolved in 15 mL dry DMF in a Schlenk flask. Solution was sparged with argon for 15 minutes. Dopamine HCl (155 mg, 0.819 mmol, 0.15 EQ) was added, followed by dry triethylamine (266 uL, 1.91 mmol, 0.35 EQ, freshly distilled over CaSO4). Solution turned medium yellow upon addition. Solution was stirred under argon at 50°C for 3 hours. Functionalization was monitored by the ratio of free:polymeric pentafluorophenyl signals via ^{19}F NMR. After 3 hours, dopamine was determined to be completely reacted. the reaction mixture was divided into 4 vials. This insured that all subsequent polymers contained the same amount of catecholic functionality (15 mol-%). To each vial was added 0.2 equivalents of the desired amine to impart cofunctionality (hydroxypropylamine, mono-boc ethylenediamine, N,N-dimethyl ethylenediamine and taurine). Again, these reactions were stirred at 50°C under nitrogen and monitored by ^{19}F NMR. After 5 hours, an excess of amino-2-propanol (640 uL, 8.19 mmol, 1.5 EQ) was added with dry triethylamine (1.14 mL, 8.19 mmol, 1.5 EQ) and stirred overnight under argon at 50°C. Solution was concentrated under hi-vacuum to ~1/2 volume and diluted with DI water (~ 10 mL). Solution was dialyzed (MWCO: 3500) against argon-sparged water (first pH3 adjusted with 1M HCl, then DI) w/ positive argon pressure in sealed dialysis vessel for ~ 2 days with frequent reservoir changes. Remaining solution was lyophilized to yield white, fluffy powder. Isolated yield: ~ 200 mg for each copolymer.

Polymer characterization

Poly(pentafluorophenyl acrylate)

^{1}H NMR (600 MHz, $CDCl_3$): δ 1.8-2.6 (br, 2H), 3.2 (br, 1H). ^{19}F (125 MHz, $CDCl_3$): δ -162.2 (2F), -156.9 (1F), -153.3 (2F). ATR-IR (cm^{-1}): 1782, 1519, 1081.

Poly(dopamine acrylamide-co-[3-(Dimethylamino)propyl]acrylamide-co (2-Hydroxypropyl) acrylamide) P(DA-DPA-HPA):

^{1}H NMR (600 MHz, d6-DMSO): δ 1.00 (br, $C\mathbf{H_3}CH(OH)$), 2.2 (br, $N(C\mathbf{H_3})_2$), 2.72 (br, backbone-$C\mathbf{H_2}$), 3.89 (br, $C\mathbf{H}OH$), 6.38-6.60 (br, C**H-**arom.). ATR-IR (cm^{-1}): 3290 (br), 2950, 1651, 1518, **1420,** 1281, 1114.

Poly(dopamine acrylamide-co-(2-Hydroxypropyl) acrylamide) P(DA-HPA):

^{1}H NMR (600 MHz, d6-DMSO): δ 1.00 (br, $C\mathbf{H_3}CH(OH)$), 2.72 (br, backbone-$C\mathbf{H_2}$), 3.89 (br, $C\mathbf{H}OH$), 6.38-6.60 (br, C**H-**arom.). ATR-IR (cm^{-1}): 3250 broad, 2950, 1649, 1517, 1281, 1250.

Poly(dopamine acrylamide-co-(2-sodium sulfate) ethylacrylamide-co-(2-Hydroxypropyl) acrylamide) P(DA-SEA-HPA):

^{1}H NMR (600 MHz, d6-DMSO): δ 1.00 (br, $C\mathbf{H_3}CH(OH)$), 2.72 (br, backbone-$C\mathbf{H_2}$), 3.00 (br, $C\mathbf{H_2}SO_3^-Na^+$), 3.89 (br, $C\mathbf{H}OH$), 6.38-6.60 (br, C**H-**arom.). ATR-IR (cm^{-1}): 3250 broad, 2950, 1649, 1517, **1360**, 1281, **1197**.

Poly(dopamine acrylamide-co-(2-amino)ethylacrylamide-co-(2-Hydroxypropyl) acrylamide) P(DA-AEA-HPA):

^{1}H NMR (600 MHz, d6-DMSO): δ 1.00 (br, $C\mathbf{H_3}CH(OH)$), 2.72 (br, backbone-$C\mathbf{H_2}$), 3.89 (br, $C\mathbf{H}OH$), 6.38-6.60 (br, C**H-**arom.). ATR-IR (cm^{-1}): 3290 (br), 2950, 1651, 1518, 1281, 1114.

UV-Visible Spectroscopy

Polymers were dissolved in deionized water at a concentration of 0.1 mM [catechol]. A small amount of $FeCl_3 \cdot 6H_2O$ was added to reach a 3:1 catechol:Fe^{3+} ratio. The solution was diluted with a 200 mM tris buffer solution to reach pH 8.2. The absorption of the ligand-to-metal charge transfer absorption (dπ^*) was measured in the range of 400-750 nm. The peaks were fit using the Peak Analyzer function in OriginPro2015 with Gaussian peak shapes. Peak constraints implied corresponded to known λ_{max} values for catechol-Fe^{3+} complexes (*mono* 714 nm, *bis* 570 nm, *tris* 490 nm). Peaks were normalized to reported molar absorptivities to calculate the amounts of each stoichiometry.[38]

Peptide synthesis

Peptides were ordered from Genscript in desalt purity, with the N-acetylation and C-amidation. Mushroom tyrosinase was used to catalyze the ortho-hydroxylization of peptidyl Tyr to DOPA.[42,43] as described in earlier work.[39]

Cyclic voltammetry of peptides

Cyclic voltammetry (CV) was performed using a CHI 500/A electrochemical workstation from CH Instruments Inc, with a bare glassy carbon working electrode, a Pt counter electrode and a saturated Ag/AgCl reference electrode. Peptides were dissolved at a concentration of 0.1mg/ml in 100 mM pH 5 acetate buffer and scanned over a range from 0-600 mV at a scan speed of 20 mV/s.

VII. References

(1) Sedó, J.; Saiz-Poseu, J.; Busqué, F.; Ruiz-Molina, D. *Adv. Mater.* **2013**, *25*, 653–701.

(2) Yu, M.; Hwang, J.; Deming, T. J. *J. Am. Chem. Soc.* **1999**, *121*, 5825–5826.

(3) Taylor, S. W.; Luther, G. W.; Waite, J. H. *Inorg. Chem.* **1994**, *33*, 5819–5824.

(4) Sagert, J.; Sun, C.; Waite, J. In *Biological Adhesives*; Springer, 2006; pp. 125–143.

(5) Lee, H.; Scherer, N. F.; Messersmith, P. B. *Proc. Natl. Acad. Sci.* **2006**, *103*, 12999.

(6) Ye, Q.; Zhou, F.; Liu, W. *Chem. Soc. Rev.* **2011**, *40*, 4244–4258.

(7) Anderson, T. H.; Yu, J.; Estrada, A.; Hammer, M. U.; Waite, J. H.; Israelachvili, J. N. *Adv. Funct. Mater.* **2010**, *20*, 4196–4205.

(8) Hwang, D.; Harrington, M.; Lu, Q.; Masic, A.; Zeng, H.; Waite, J. *J. Mater. Chem.* **2012**, *22*, 15530–15533.

(9) Larsson, C.; Thomsen, P.; Lausmaa, J.; Rodahl, M.; Kasemo, B.; Ericson, L. E. **1994**.

(10) Terranova, U.; Bowler, D. *J. Phys. Chem. C* **2010**, 6491–6495.

(11) Liu, Y.; Dadap, J. *J. Phys. …* **1999**, 2480–2486.

(12) Li, S.-C.; Chu, L.-N.; Gong, X.-Q.; Diebold, U. *Science* **2010**, *328*, 882–884.

(13) Hidber, P.; Graule, T.; Gauckler, L. *J. Eur. Ceram. Soc.* **1997**, *17*, 239–249.

(14) Martin, R. *J. Phys. Chem.* **1971**, *75*, 2657–2661.

(15) Yu, J.; Wei, W.; Danner, E.; Israelachvili, J. N.; Waite, J. H. *Adv. Mater.* **2011**, *23*, 2362–2366.

(16) Yu, J.; Wei, W.; Danner, E.; Ashley, R. K.; Israelachvili, J. N.; Waite, J. H. *Nat. Chem. Biol.* **2011**, *7*, 586–588.

(17) GA, Y.; DJ, C. *Marine animals and adhesion*; 1982; pp. 19–39.

(18) Mehler, E. L.; Fuxreiter, M.; Simon, I.; Garcia-Moreno, E. B. *Proteins* **2002**, *48*, 283–292.

(19) Schwans, J. P.; Sunden, F.; Gonzalez, A.; Tsai, Y.; Herschlag, D. **2013**.

(20) Sun, S.; Toney, M. D. **1999**, 4058–4065.

(21) Harrington, M. J.; Masic, A.; Holten-Andersen, N.; Waite, J. H.; Fratzl, P. *Science* **2010**, *328*, 216–220.

(22) Zeng, H.; Hwang, D. S.; Israelachvili, J. N.; Waite, J. H. *Proc. Natl. Acad. Sci.* **2010**, *107*, 12850.

(23) McHale, J. In *Handbook of Vibrational Spectroscopy*; 2006.

(24) Holten-Andersen, N.; Harrington, M. J.; Birkedal, H.; Lee, B. P.; Messersmith, P. B.; Lee, K. Y. C.; Waite, J. H. *Proc. Natl. Acad. Sci. U. S. A.* **2011**, *108*, 2651–2655.

(25) Lana-Villarreal, T.; Rodes, A.; Pérez, J. M.; Gómez, R. *J. Am. Chem. Soc.* **2005**, *127*, 12601–12611.

(26) Nakata, K.; Fujishima, A. *J. Photochem. Photobiol. C Photochem. Rev.* **2012**, *13*, 169–189.

(27) Jribi, R.; Barthel, E.; Bluhm, H. *J. …* **2009**, 8273–8277.

(28) Shoute, L. C. T.; Loppnow, G. R. *J. Chem. Phys.* **2002**, *117*, 842.

(29) Ooka, A. A.; Garrell, R. *Biopolymers* **2000**, 92–102.

(30) Gallas, J.; Eisner, M. *Photochem. Photobiol.* **1987**, *45*, 595–600.

(31) Gibson, M. I.; Fröhlich, E.; Klok, H. *J. Polym. Sci. Part A Polym. Chem.* **2009**, *47*, 4332–4345.

(32) Eberhardt, M.; Mruk, R.; Zentel, R.; Theato, P. *Eur. Polym. J.* **2005**, *41*, 1569–1575.

(33) Eberhardt, M.; Théato, P. *Macromol. Rapid Commun.* **2005**, *26*, 1488–1493.

(34) Wang, J.; Tahir, M. N.; Kappl, M.; Tremel, W.; Metz, N.; Barz, M.; Theato, P.; Butt, H.-J. *Adv. Mater.* **2008**, *20*, 3872–3876.

(35) Tahir, M. N.; Eberhardt, M.; Theato, P.; Faiss, S.; Janshoff, A.; Gorelik, T.; Kolb, U.; Tremel, W. *Angew. Chem. Int. Ed. Engl.* **2006**, *45*, 908–912.

(36) Zhang, W. F.; He, Y. L.; Zhang, M. S.; Yin, Z.; Chen, Q. *912*.

(37) Chawla, K.; Lee, S.; Lee, B. P.; Dalsin, J. L.; Messersmith, P. B.; Spencer, N. D. *J. Biomed. Mater. Res. A* **2009**, *90*, 742–749.

(38) Sever, M. J.; Wilker, J. J. *Dalton Trans.* **2004**, 1061–1072.

(39) Wei, W.; Yu, J.; Gebbie, M. a; Tan, Y.; Martinez Rodriguez, N. R.; Israelachvili, J. N.; Waite, J. H. *Langmuir* **2015**.

(40) Nematollahia, D.; Varmaghania, F. *J. Iran. Chem. Soc.* **2011**, *8*, 803–810.

(41) Nematollahi, D.; Rafiee, M.; Samadi-Maybodi, A. *Electrochim. Acta* **2004**, *49*, 2495–2502.

(42) Taylor, S. W. *Anal. Biochem.* **2002**, *302*, 70–74.

(43) Wilke, P.; Börner, H. *ACS Macro Lett.* **2012**, *1*, 871–875.

3 Catecholic analogues as metal chelation building blocks and their application in supramolecular hydrogels

Reproduced in part with permission from: Menyo, M.S., Hawker, C.J. and Waite, J.H. (2013). Versatile tuning of supramolecular hydrogels through metal complexation of oxidation-resistant catechol-inspired ligands. Soft Matter. 9, 10314-10323. Copyright (2013) Royal Society of Chemistry.

I Introduction

The remarkable functional behavior of biological materials is enabled by, and intimately coupled to, dynamic structural interactions that occur at multiple length and time scales. As demonstrated by the mechanochemical analysis of titin[1] and spider silk,[2] profoundly useful insights can be distilled from a fundamental understanding of these interactions. In synthetic polymeric systems, dynamic bonding has the ability to expand the range of properties due to the inherent responsiveness to local stimuli and healable nature of these bonds.[3] This dynamic nature is dramatically apparent in polymer hydrogels, where factors such as pH[4,5], temperature[5], salt concentration[6], and light[8-12] can trigger reversible gel formation, dissolution, reshaping, and/or internal healing. A variety of supramolecular interactions, including hydrogen bonding[7,8], hydrophobic effects[9], π-π stacking[10], electrostatic attraction[11,12], and metal-ligand coordination[13-14] have been used to drive assembly.

Individual metal/ligand coordination sites can provide stable, yet reversible, crosslinking points between polymers, in contrast to other mechanisms of dynamic crosslinking, where multiple weak interactions must act in concert to achieve self-supporting gels.[15] One particular metal-ligand interaction observed widely in nature is that of catecholic ligands with Fe(III). The coordination of ferric iron with enterobactin (tripodal *tris*-catecholate siderophore from *E. coli*) has a measured stability constant of 10^{52}, equating to a free energy for the complex 2 orders of magnitude higher than a single hydrogen bond, 3 times as high as the “gold standard” noncovalent interaction of biotin and avidin, and comparable to a covalent bond.[16] Similarly, the cuticle of the mussel byssal thread employs DOPA residues to establish catechol-based, Fe(III) crosslinks in composite systems that arrest crack formation and drive recoverability under the repetitive high strain of waves and tides.[17] In addition to its strength and dynamic nature, catechol/Fe(III) complexation is highly pH-dependent. Binding stoichiometry changes from a 1:1 *mono* complex at low pH to a highly stable 3:1 catechol:Fe(III) *tris* state at increased pH.

While biological systems have evolved to take advantage of the uniquely high affinity of catecholic moieties for Fe(III), the task of implementing catechol-Fe(III) coordination in materials systems is fraught with peril. Catechols are prone to rapid auto-oxidation at neutral to alkaline pH,[18] forming a quinone species which shows significantly reduced affinity for Fe(III) and is susceptible to covalent crosslinking through reaction with a variety of nucleophiles, including catechol itself.[19] Furthermore, complexed Fe(III) can catalyze a one-electron ligand-to-metal charge transfer to generate semiquinone and Fe(II), a process which is greatly accelerated at low pH.[20] This complex can quickly dissociate, in which case Fe(II) typically generates free radicals via a Fenton pathway,[21] while the semiquinone is susceptible to further oxidation resulting in quinone and covalent crosslinking.[22] As a result, the dynamic nature of the catechol:Fe(III) bond is undermined by the very conditions which prompt its utility. Furthermore, achieving *tris* complexes, responsible for the strongest metal binding, requires highly alkaline conditions, due to strong proton competition for the catecholate ligand. In a simple hydrogel system formed from DOPA-functionalized poly(ethylene) glycol (PEG), Holten-Andersen et al. found that substantial *tris*-catecholate-iron complexation did not occur until pH 8, with complete complex formation requiring ~ pH 12.[13]

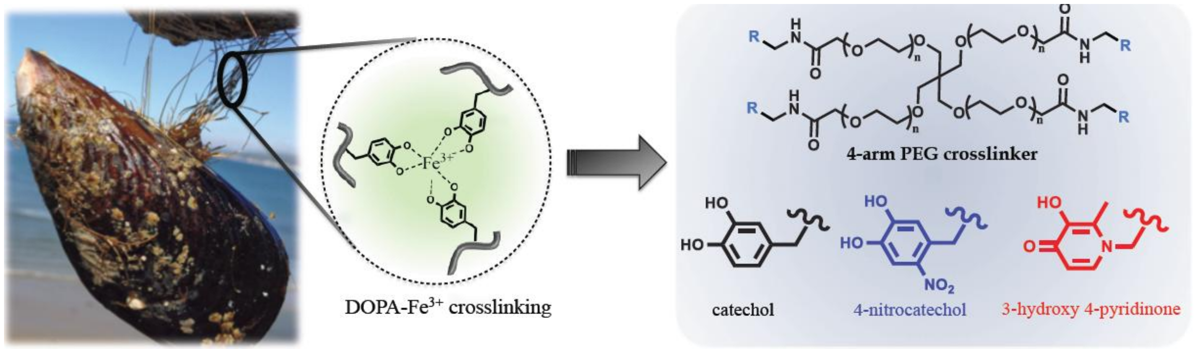

Figure 1. Cartoon highlighting translation of the strong, healable DOPA-Fe^{3+} crosslinks of the cuticle of *Mytilus californianus*, and the structure of the 4-arm poly(ethylene glycol) (PEG) backbone with pendant catechol (Cat), nitrocatechol (nCat) and 3-hydroxy-4-pyridinone (HOPO) chelating moieties.

Given these limitations and to address the above challenges, alternative chelating functionalities with high coordination affinity, pH-dependent speciation and lower susceptibility to oxidation were examined. Focus was directed to two analogues based on the parent catechol derivative: 4-nitrocatechol (nCat) and 3-hydroxy-4-pyridinone (HOPO), as shown in Figure 1. These analogues withdraw electron density from the phenolate moieties both inductively and through resonance effects, while maintaining the desired bidentate phenolate nature of the catechol. The net effect manifests in reduced phenolic pK_a values (pK_{a1} HOPO = 3.6, pK_{a1} nCat = 6.6, pK_{a1} catechol = 9.2)[23], increased oxidation potentials, and shifted metal/ligand stoichiometry. Measured stability constants for tris-Fe(III) complexed nCat ($\log\beta_3 = 39.2$)[23] and HOPO ($\log\beta_3 = 37.6$)[24] are remarkably high, though slightly lower than catechol ($\log\beta_3 = 43$) due to the "softer" nature of the phenolate ligands.

In this chapter, I will show that these electron-deficient catechol analogues demonstrate metal binding stoichiometry which is shifted to lower pH values, as well as enhanced oxidative stability. I will then discuss how incorporation into simple hydrogel constructs allows coordination chemistry to be definitively related to mechanical properties. A 4-arm PEG backbone, where each chain end is functionalized with a chelating group, was chosen as the scaffold for hydrogel formation. This simple construct allows clear determination of the relationship between metal/ligand coordination and bulk hydrogel properties. The presence of a single chelating functional group at each chain end, rather than multiple moieties interspersed within a domain, is expected to drive "crosslinking" intermolecular coordination rather than "looping" intramolecular complexes, and allow for rapid gel equilibration. This architecture is also advantageous for potential biological application, as the high water content and biocompatibility of PEG-based hydrogels are well established.[25]

II Supramolecular coordination hydrogels

1. Chelator synthesis and characterization

Initial studies focused on the synthesis and characterization of amino-functional nitrocatechol and HOPO molecules. The hemisulfate salt of 6-nitrodopamine was synthesized by reaction of dopamine with sodium nitrite in the presence of sulfuric acid following a literature procedure.[26] The dihydrochoride salt of 1-(2’-aminoethyl)-2-methyl-3-hydroxy-4-pyridinone HOP O was synthesized starting from maltol following a literature procedure.[24] Literature values for pK_a values and stability constants with Fe^{3+} were used to construct the speciation plots shown in Figure 2.[23,24] These results are in agreement with previous speciation shown in catechol-Fe^{3+} hydrogels, where pH > 10 is necessary to achieve complete *tris* crosslinking. Conversely, the addition of electron-withdrawing substituents shifts the speciation to lower pH values, to the point where near-complete *tris* complexation is predicted at physiological pH 7.4 for HOPO-Fe^{3+} complexes.

Oxidation kinetics were investigated via NMR time studies. Amino-functional small molecule chelators were dissolved in deuterium oxide at a concentration of 25 mM and the pD was adjusted to 9 with NaOD. Spectra were collected periodically, and the integration of the aromatic region was monitored as a function of time. Figure 3 (top) shows stacked spectra for dopamine isobutyrlamide at t=5, 20 and 120 minutes on top, where substantial changes in the chemical shifts are complete disappearance of the initial aromatic protons is accompanied by a browning of the solution. Figure 3 (bottom) shows the spectra for nitrodopamine isobutyrlamide at 5 mins, 24 hours and 1 week, slowing much slower oxidation kinetics..

These initial findings were encouraging, and motivated the synthesis of hydrogels to test whether the shifted binding stoichiometry and decreased susceptibility to oxidation carried over into a functional materials construct.

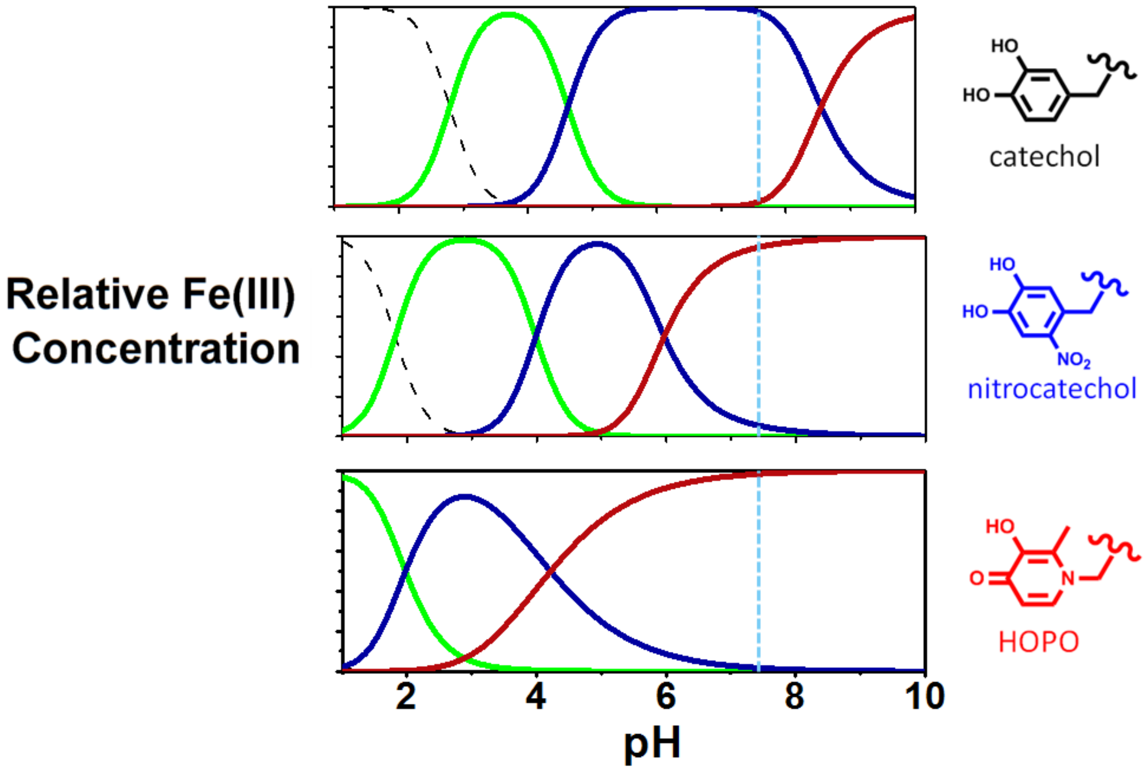

Figure 2: Speciation plots for catechol, nitrocatechol and HOPO. Lines show free Fe^{3+} (black dotted), *mono* (green), *bis* (blue), and *tris* (red) at 25°C, μ = 0.1 M, 1 mM chelator, 0.33 mM Fe^{3+}.

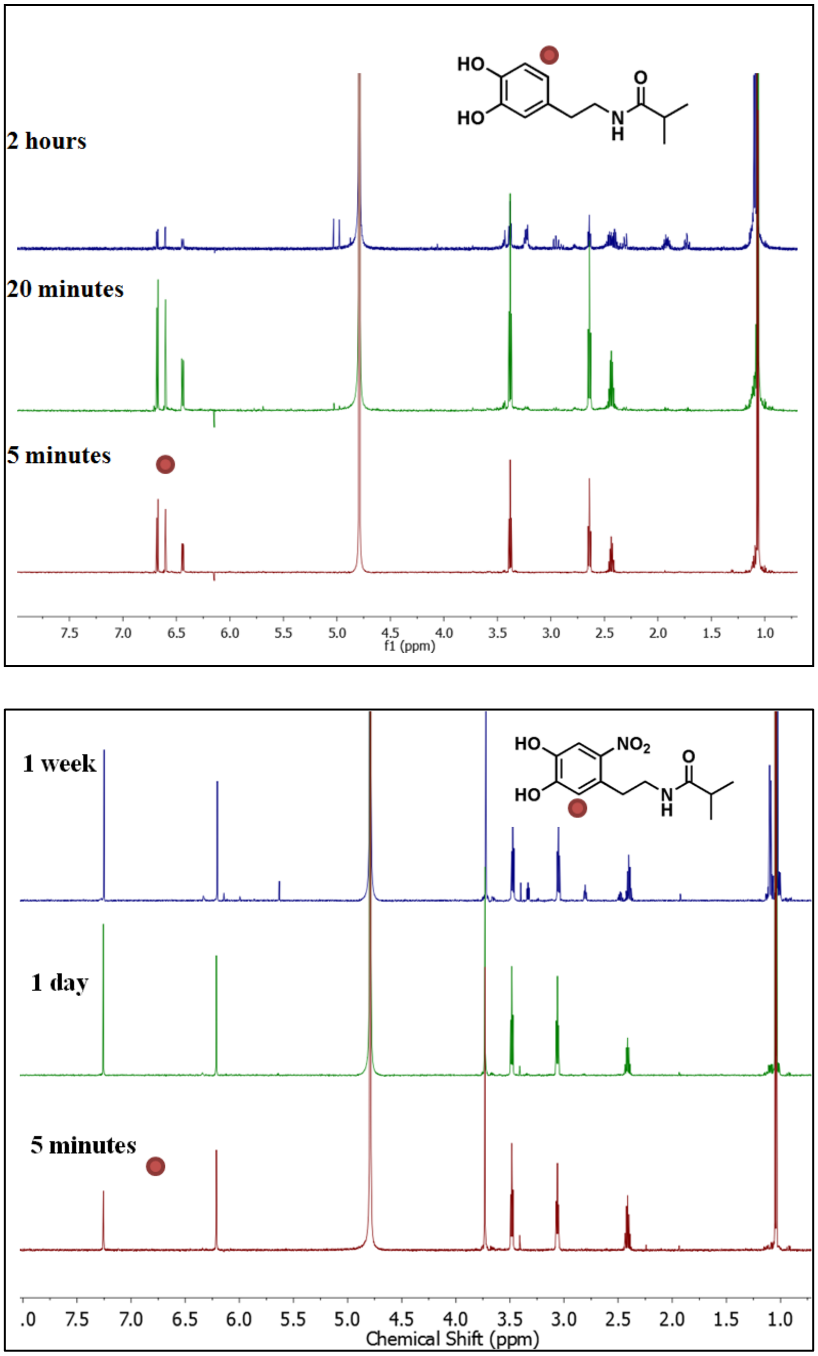

Figure 3: NMR time studies of 25 mM dopamine isobutyramide (DIB) (top) and nitrodopamine isobutyramide (NIB) (bottom) in D_2O at pD 9.

2. Hydrogel Synthesis and Gelation

A commercial 4-arm PEG-OH derivative (MW: 10,000 Da) was selected as a common platform for chain end functionalization and subsequent hydrogel formation studies. Chain end functionalization was accomplished by initial reaction of the terminal hydroxyl groups with ethyl bromoacetate followed by hydrolysis of the ester groups to yield the desired 4-arm PEG-COOH system with almost quantitative conversion of chain end groups. From this common functional PEG derivative, the different chelating units (dopamine, 6-nitrodopamine, 2-methyl-3-hydroxy-4-pyridinone ethylamine) were attached through an amide coupling reaction with HBTU. Chain end functionalization efficiencies were again shown to be high with 90%, 95%, and 96% conversion being observed respectively which is in agreement with literature results.[27] Hydrogels were then formed through crosslinking metal/ligand coordination between the 3 chelators investigated and metal ions known to exhibit high binding affinities for bidentate catechol ligands. Initial hydrogel formation followed the procedure of Holten-Anderson et al.[13] Briefly, the 4-arm chelator was dissolved in deionized water, and a solution of the metal chloride was added to achieve a 3:1 chelator:metal ion ratio. The acidity of the metal salt solution and protons released during chelation ensured predominantly *mono*- coordination and, as expected, no gelation was observed in these cases. Final gel concentration and pH values was achieved by addition of an appropriate buffer solution, and verified with a pH probe electrode. Gelation is attributed to the pH-driven increase in binding stoichiometry leading to crosslinking *bis* and *tris* complexes. For Fe(III)-bound gels, this speciation could conveniently be tracked through distinct spectrophotometric signatures for each stoichiometry. For gels with more labile crosslinks, rigorous mixing led to uniform gels in short order, however for hydroxypyridinone-based gels, which exhibited notably longer effective bond lifetimes, equilibration required long times (~2 hours).

3. Effect of pH and chelating group

The dynamic mechanical properties of metal-ligand crosslinked hydrogels are determined primarily by the dissociation and reformation of the coordination bonds, though these are difficult to measure quantitatively for high affinity complexes. According to Bell Theory,[28] bond lifetime scales with the exponential of bond energy, however, metal/ligand dissociation dynamics have been shown to dominate the dynamic mechanical properties of lower affinity pincer-Pt/pyridine organogels.[15] Studies of iron dissociation from natural and synthetic siderophores have established that chelator protonation is often the rate-limiting step in the dissociation process of a high affinity Fe(III) complex.[29] While catechol-based derivatives have the highest stability constants with Fe(III), they also have the highest proton affinity, as reflected by pK_a values (9.1 and 14 for catechol, 6.7 and 10.3 for nitrocatechol, 3.6 and 9.9 for HOPO) and pH-dependent coordination stoichiometry.[23,30,31]

Based on these predictive small molecule data, we hypothesized that hydrogels with nitrocatechol and HOPO-based crosslinks would form robust hydrogels at pH values lower and more feasible for biological application than catechol-based gels. To test this hypothesis, 10% w/v hydrogels were prepared from the same 4-arm PEG backbone with catechol, nitrocatechol and 3-hydroxy-4-pyridinone (HOPO) chain ends and Fe(III) at pH 9. This pH was necessary to yield gelation in the case of catechol-based crosslinkers.

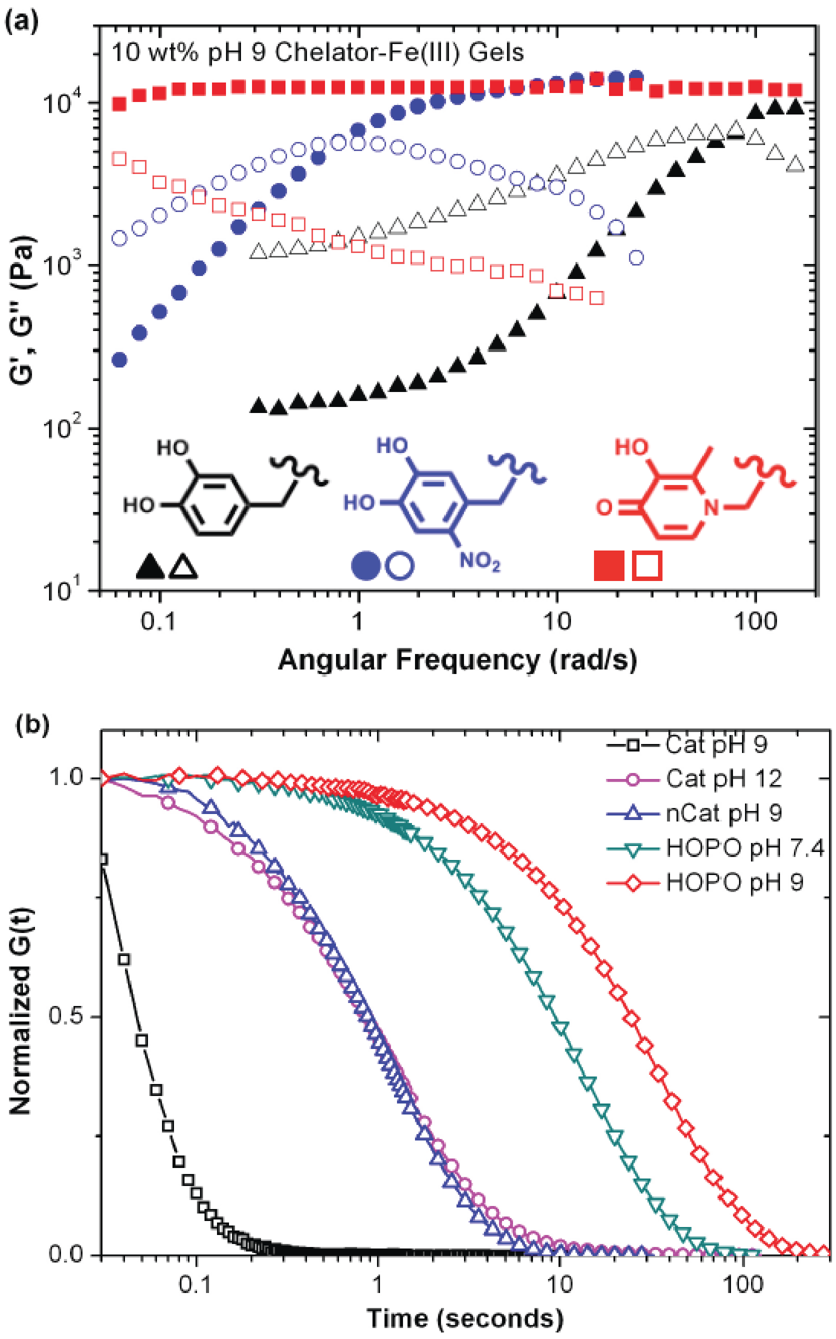

Figure 4 (a) Frequency sweep of hydrogels at pH 9 with storage (G') and loss (G") moduli reported as closed and open symbols, respectively. (b) Relaxation of hydrogels after subjection to a 20% shear step strain

Oscillatory rheology (Figure 4a) was used to probe the dynamic mechanical properties of the hydrogels, and by extension, the nature of the metal/ligand crosslinks. The hydrogels tested show similar plateau moduli around 12 kPa, but characteristic relaxation time τ varied greatly: $\approx$ 0.09 seconds for catechol-, $\approx$ 8 seconds for nitrocatechol- and >125 seconds for HOPO-based gels. Step-strain experiments (Figure 4b) show that all freshly synthesized gels exhibit relaxation to a zero stress state after 20% shear strain, indicative of gel networks crosslinked through dynamic and not covalent bonding.

Both nitrocatechol and HOPO-based gels are predominantly *tris*-coordinate at pH 9, whereas catechol-based gels have a large amount of *bis* coordination, a supposition supported by spectrophotometric evaluation of the gels in comparison to solutions and published data. *Tris* complexes are much more stable than complexes of lower stoichiometry; a *bis* catechol-Fe(III) complex ($\log\beta = 33$) has an associated free energy of complexation almost an order of magnitude lower than that of the *tris* complex ($\log\beta = 43$), and lower than the stability constants of both nitrocatechol and HOPO *tris* chelates. Interestingly, catechol-based gels at pH 12 and nitrocatechol-based gels at pH 9, where small molecule speciation plots predict essentially complete *tris* crosslinking, exhibit notably shorter characteristic relaxation than HOPO-based gels at either pH 7.4 or pH 9. One proposed explanation is that the kinetics of ligand exchange between HOPO-Fe(III) complexes are slower than that of catechol-Fe(III). Additionally, the higher concentration of hydroxide ions at pH 12 results in increased competition for catechol complexation with Fe(III).

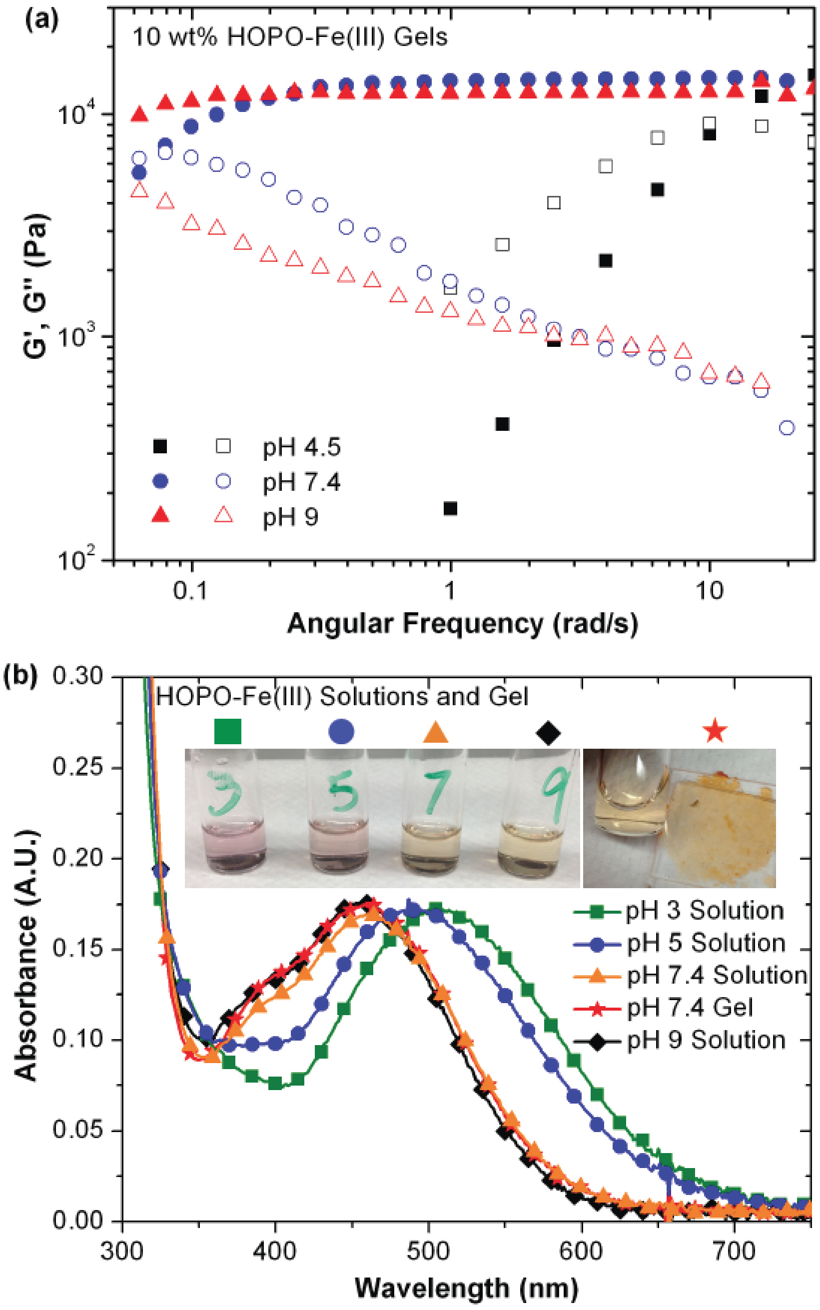

Figure 5 (a) Effect of pH on rheological behavior of HOPO hydrogels at pH 4.5 (black), 7.4 (blue) and 9 (red) and (b) the absorbance of 1% w/v HOPO crosslinker/Fe^{3+} solutions and 10% w/v hydrogel with annotated photographs.

With HOPO identified as a promising crosslinking functionality, the effect of pH on the viscoelastic properties was further investigated. Figure 5a shows dynamic oscillatory rheology on HOPO-Fe(III) gels synthesized at pH 4.5, 7.4 and 9. As gel pH is raised from 4.5 (a mixture of *bis* and *tris* stoichiometry) to 7.4 (predominantly *tris*-crosslinked), increased elastic character in the gels is readily apparent, though all gels exhibit the same plateau modulus. Figure 5b highlights the changing absorbance as pH increases from pH 3 to pH 9 in solutions of diluted 4-arm HOPO and that of the gel formed at pH 7.4. Notable are the virtually identical spectra for HOPO solution and gel at 7.4 and 9, confirming unchanged chelation stoichiometry above pH 7.4 in either gel or solution. Absorptions match previously assigned spectrophotometric signatures for HOPO-Fe(III) binding stoichiometries determined for the small molecule deferiprone[32] Therefore, the increased bond lifetime of hydrogels at pH 9 compared to pH 7.4 is attributed to slower ligand dissociation kinetics due to decreased proton concentration at higher pH values, and not to a change in the degree of coordination.

4. Supramolecular assembly

The rapid and stable gelation seen for HOPO-based hydrogels at physiological pH strongly suggests that gels could be formed upon injection into a bulk buffer solution. To test this hypothesis, unbuffered polymer solutions with a 3:1 chelator:Fe(III) ratio were prepared to the desired final gel concentration and either dropped or injected into a buffer solution at the desired gel pH (7.4 or 9). Indeed, this rapid change in pH led to immediate formation of a distinct hydrogel. Injected gels were equilibrated for 30 seconds, removed from the buffer, briefly blotted dry, and weighed. UV-vis spectroscopy detected no

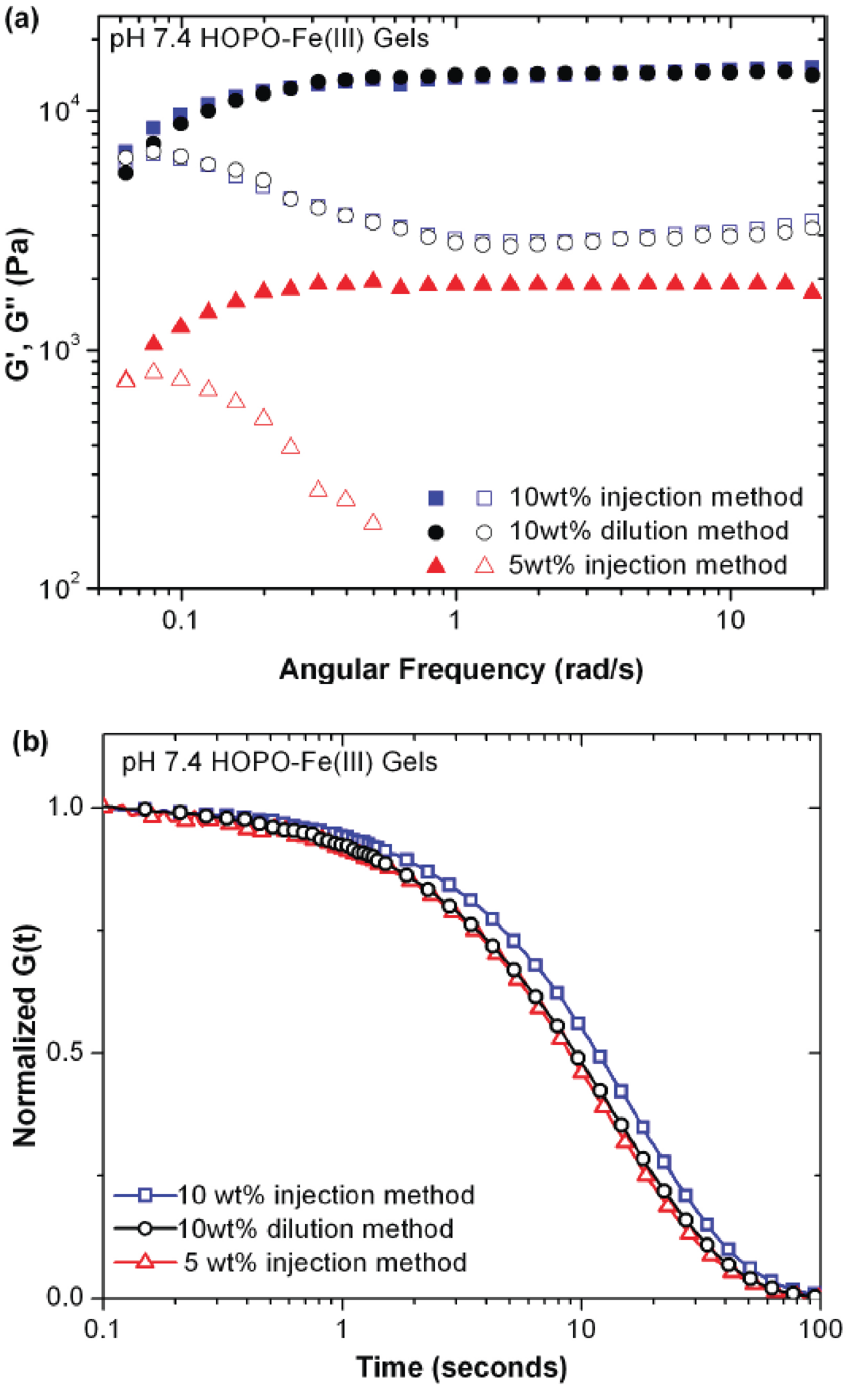

Figure 6 Effect of hydrogel preparation method and conditions on rheological behavior evaluated by (a) frequency sweep and (b) step strain experiments.

measureable absorption from the high extinction coefficient chelator/metal complex in the buffer solution.

Hydrogels prepared by injection from a 10% w/v polymer solution show virtually identical rheological behavior to those synthesized through the conventional “dilution” approach, as shown in Figure 6. Furthermore, gels synthesized by injection of a 5% w/v solution had a plateau modulus an order of magnitude lower than those from a 10% w/v solution, though exhibiting similar characteristic bond lifetimes. This suggests that, while the nature of the crosslinks is similar, the initial stiffness and water incorporation of the gels is determined by the injection solution, and hydrogels are not prone to equilibration with the bulk solution over the time frame required for robust gelation. In contrast, catechol and nitrocatechol-based gels showed no gelation upon injection into pH 7.4 buffer solutions, and significant dissolution even into higher pH solutions (12 for catechol and 9 for nitrocatechol). (Appendix B.1)

5. Gel stability

In all prior work on catechol-based, supramolecular hydrogels, long-term stability is a major issue. This is due to the relative ease with which catechol groups can be oxidized to quinone, a reactive functionality prone to nucleophilic attack and phenolic coupling reactions to yield covalent crosslinks and loss of supramolecular characteristics.[33] This oxidation can proceed rapidly at neutral to alkaline pH in the absence of oxidizing agents, with only trace amounts of oxygen necessary to trigger this cascade. It is also well described in literature that catechol-Fe(III) complexes are susceptible to a one-electron intracomplex redox process, generating Fe(II) and a semiquinone, which again is susceptible to further oxidation and crosslinking. This process has been thoroughly and eloquently characterized for PEG-based gel systems, and it was shown that 1:1 catechol/Fe complexes at low pH values are especially vulnerable.[22]

With this in mind, the long-term stability of the hydrogels synthesized was examined by initially storing a series of catechol-Fe(III) gels, synthesized at pH 9, at room temperature and exposure to light and oxygen for one week. Aging was visually apparent in all samples with the initially wine red gel slowly becoming muddy-brown in color, characteristic of catechol-based oligomerization, with time. UV-visible spectroscopy of the gel and representative solutions initially show a characteristic 3:1 catechol/Fe *tris* complex absorbances of the charge transfer complex (λ_{max} = 480 nm) and the catechol (λ_{max} = 280 nm), shifting to a broad, tailing absorbance with λ_{max} = 267 nm, indicative of covalent coupling of the catechol (Figure 7a and b).[34] Significantly, the aged gels exhibit fundamentally different rheological behavior than the freshly synthesized gels, evident in dynamic oscillatory shear and stress relaxation experiments (Figure 8 and Appendix B.2). Rather than rapid equilibration to a zero stress state, as seen for the freshly synthesized gel, the aged samples show an extended stress decay profile with ~ 40% residual stress. The combined mechanical and spectroscopic evidence support the observation that the parent catechol system is prone to oxidation and covalent crosslinking, leading to a shift in properties towards a mixed mode covalent/dynamic gel. This loss of supramolecular character was further corroborated by dissolution studies which clearly show that newly synthesized catechol-based gels quickly dissolve in pH 3 acetic acid buffer (~15 seconds) while aged gels were not dissolved over the course of 4+ months.

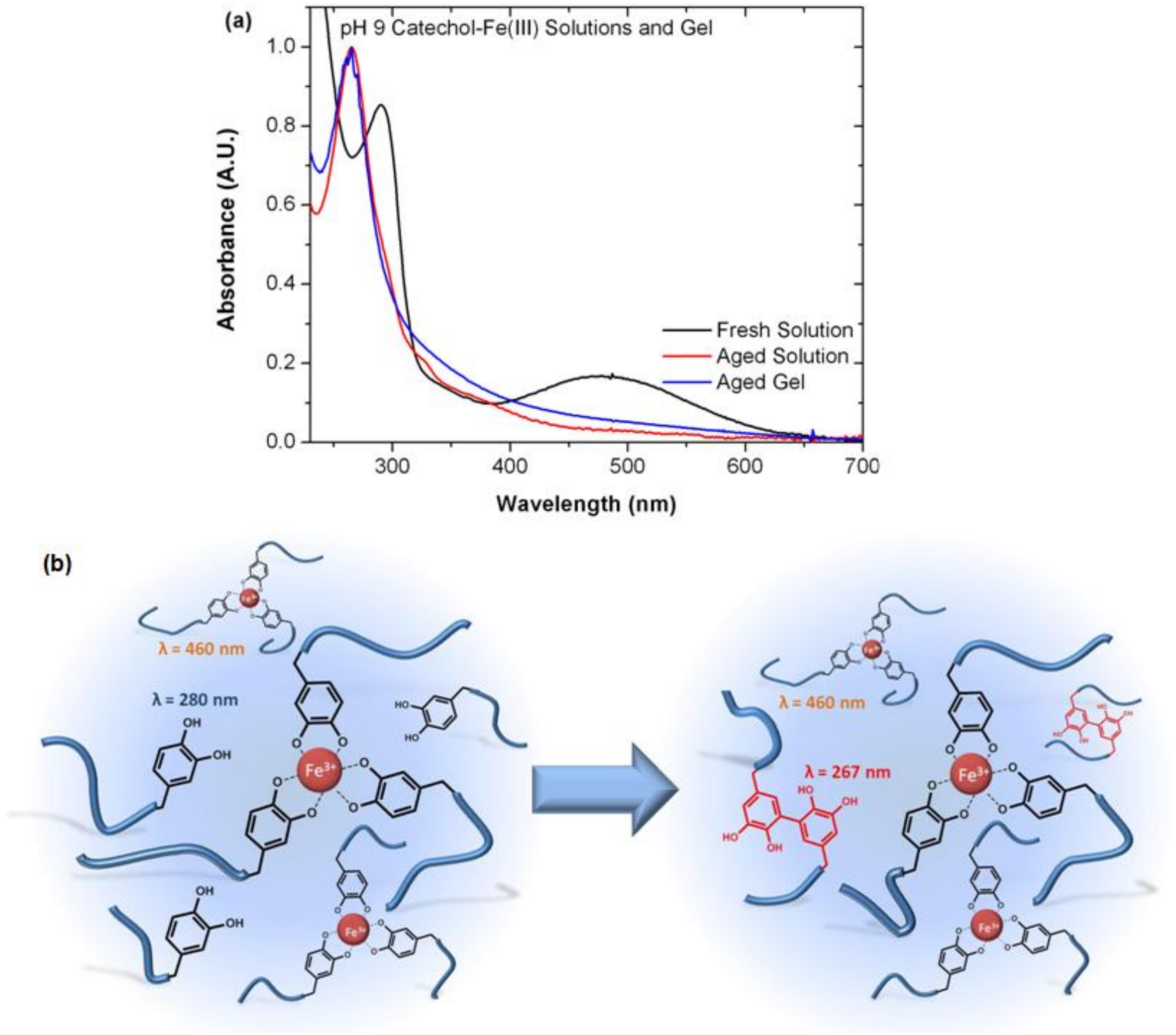

Figure 7 (a) Absorbance of 1 wt% of catechol/Fe^{3+} crosslinker solutions at pH 9 immediately upon mixing (black squares) and after one week incubation at ambient conditions (red circles), and compared to 10wt% hydrogel after one week (blue triangles). (b) Schematic depiction of the oxidative crosslinking.

To further delineate the relative roles of auto-oxidation and iron-catalyzed oxidation, hydrogels were also synthesized from catechol-Al(III) crosslinks. As Al(III) does not have an available Al(II) state, the one-electron metal-triggered oxidation seen for catechol-Fe(III) cannot occur in this system. In analogy with the catechol-Fe(III) system, the rheological behavior of the catechol-Al(III) gels formed at pH 12 switched from purely dynamic to a mixed mode over the course of a week (Supplemental Figure 4). This variation in rheological properties was accompanied by a change in the color of the gel, from colorless to brown, which was similar to that previously observed for catechol gels crosslinked by chemical oxidation in the absence of Fe(III).[13]

From these results it can be concluded that auto-oxidation proceeds even in the presence of strongly *tris*-chelated catechol species under ambient conditions.

The oxidative instability of the parent catechol systems then prompted an examination of HOPO-based hydrogels with a view to retaining the dynamic, supramolecular properties of these materials. It was therefore pleasing to observe that after 1 month of incubation under ambient conditions, HOPO-Fe(III) gels at pH 9 displayed only minimal change in dynamic oscillatory or stress relaxation behavior (Figure 8).[35] Further evidence for the lack of covalent crosslinking could be obtained from dissolution studies. Both as-synthesized and aged HOPO gels dissolve in pH 3 buffer (~30 minutes) and almost instantaneously under more acidic conditions, yielding solutions that are spectrophotometrically identical to freshly synthesized solutions at the corresponding pH. Isolation of the 4-arm PEG precursor by Fe/EDTA chelation and centrifuge filtration followed by size exclusion chromatography analysis showed no change in molecular weight or polydispersity.

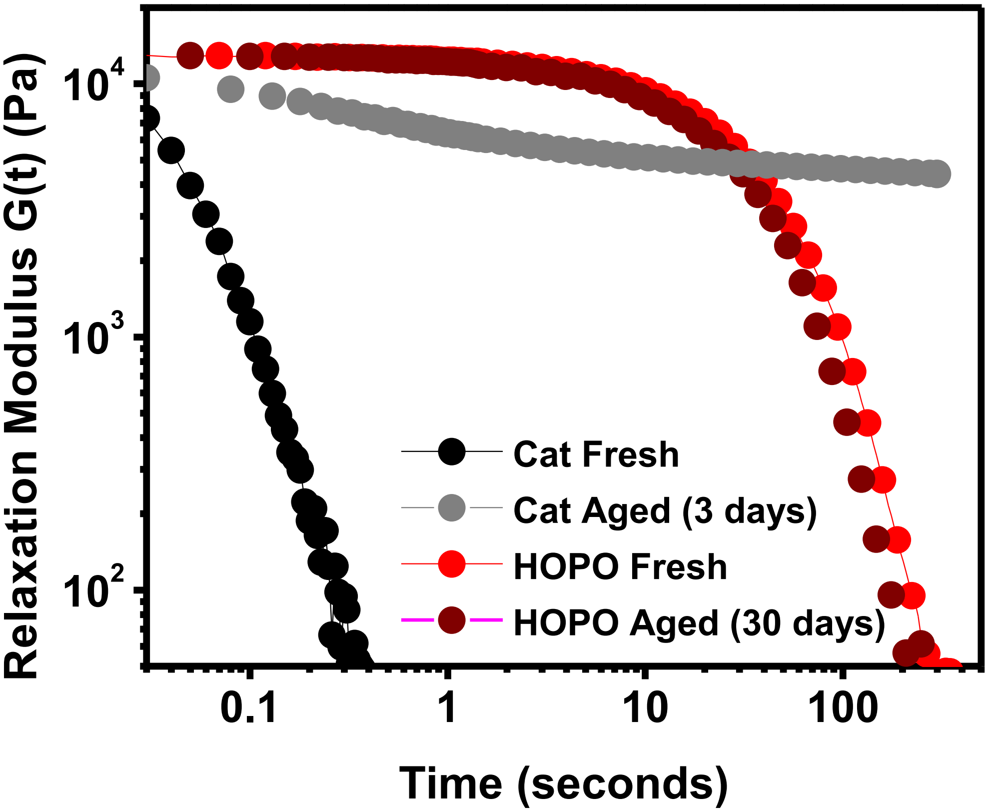

Figure 8 Relaxation of catechol and HOPO hydrogels after aging under ambient conditions.

6. Influence of different metal ions

Based on the advantages of Fe(III)-HOPO gels described above when compared to traditional catechol systems, the versatility of this design was further explored using additional metal ions which have high affinities for hydroxypyridinone-based ligands.

Al(III) and Ga(III) are trivalent ions with similar atomic radii and *tris* binding constants to Fe(III). (Fe(III) = 37.2, Al(III) = 32.3, Ga(III) = 38.4)[30] Furthermore, speciation plots for model 3-hydroxy-4-pyridinones predict a similar coordination stoichiometry profile for Fe(III), Al(III) and Ga(III), with predominantly *tris* complexation at pH 7.4.[36] For comparison, systems based on Cu(II), only capable of *mono* and *bis* coordination modes, though with a high binding constant (β_2 = 21.7)[37] and Gd(III) which has a lower stability constant (β_3 = 17.3), but is capable of tris chelation, were examined.

HOPO-Al(III) gels were found to form strong hydrogels with slightly shorter bond lifetimes than gels formed with Fe(III), as reflected by step strain (Figure 9) and dynamic oscillatory experiments.[38] In contrast, Ga(III)-based gels showed markedly lower values for plateau moduli and characteristic relaxation time. From a thermodynamics standpoint, Ga(III)-based hydrogels would be expected to exhibit similar characteristics to Fe(III)-based crosslinks, while Al(III) would exhibit less elastic behavior, a result that is contrary to the observed rheology, and suggests that ligand exchange kinetics play a role in the observed mechanical properties. Water exchange rates have generally been used as an approximation of ion lability in ligand exchange reactions in aqueous media. Ga(III) is known to be more labile than Fe(III), which in turn is several orders of magnitude more labile than Al(III).[39] As the observed hydrogel elasticity trends do not correspond to predictions based solely on thermodynamic or kinetic considerations, it appears that the

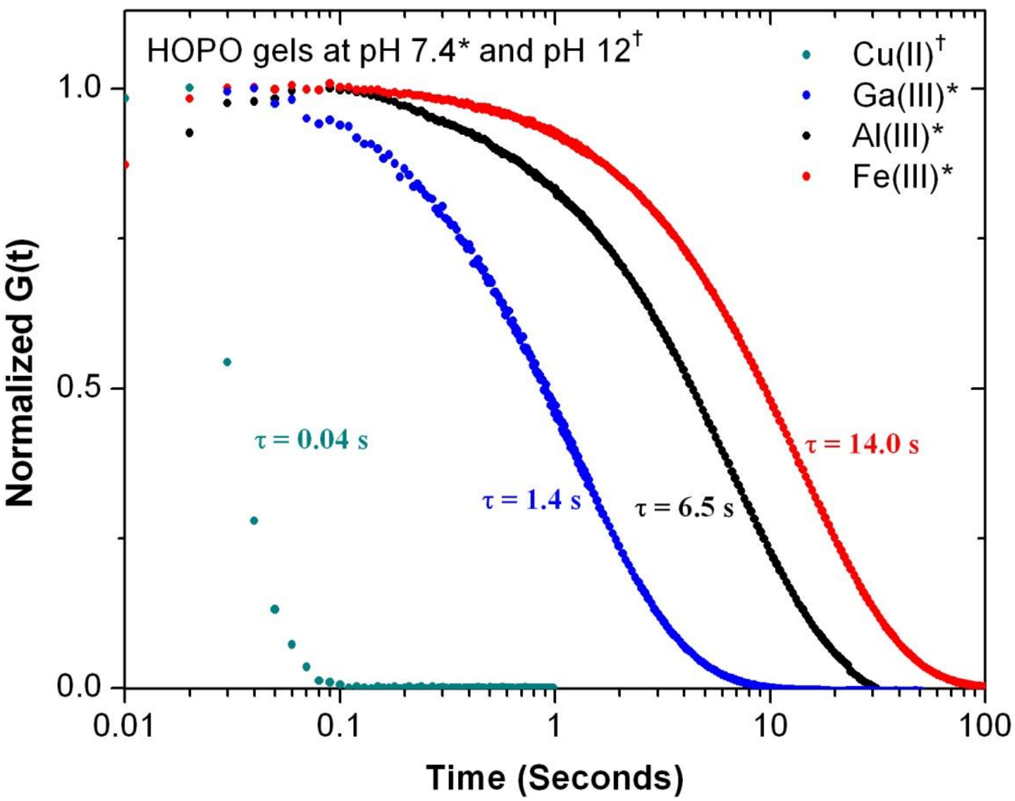

Figure 9 Effect of metal ion identity on relaxation of HOPO hydrogels sheared by a 20% step strain.

mechanical properties of the hydrogel are determined by a combination of these factors that remain to be explored.

No gelation was seen upon raising the pH of a polymer-Gd(III) bound solution to 7.4, whereas increasing pH beyond this point led to cloudiness in the solution, presumably due to hydrolysis and higher order GdO_x complexes. The fact that this is not observed for higher affinity metal ions, especially Fe(III), which have extremely low solubility at higher pH, highlights the ability of the gels to bind and sequester the metal ions from bulk solution. Finally, gelation with Cu(II) was explored. An initially blue solution turned green upon titration to pH 9, forming a very weak green gel upon pH adjustment to 12. In agreement with this observation, dynamic rheological characterization revealed very short characteristic bond lifetimes with a high plateau modulus at high oscillatory shear frequencies.

7. Degradation and release properties

These promising properties for HOPO systems then prompted a basic study of the degradation properties of Fe(III)-HOPO gels formed by injection into physiological buffer solution. In assessing potential stability for *in vitro* application, hydrogel samples (150 μL) were incubated in a sealed vial at 37°C with gentle agitation in the presence of a ten-fold excess of pH 7.4 phosphate buffer solution. The buffer solution was changed regularly, and the characteristic absorbance of the 3:1 HOPO-Fe(III) *tris*-complexes was used to determine polymer concentration in the supernatant. As Figure 10 shows, gradual polymeric mass loss results in complete dissolution after 4 days. The iron chelation efficacy of the clinically prescribed ligand Deferiprone and similar HOPO analogues under biological conditions suggests that the degradation process would not release a substantial amount of Fenton-active Fe(II).[40]

Finally, the small molecule release profiles were examined for the HOPO-based hydrogels. The water soluble dye Amaranth (Acid Red 27) was selected as a model small molecule drug having no specific interactions with the gel being used, as the *tris* HOPO crosslinks with trivalent ions carry no charge. The hydrogel was synthesized through the previously described injection strategy, where a 0.4% w/v loading of dye was incorporated into the pre-gel solution. The solution was dropped into pH 7.4 phosphate buffer solution and incubated in a manner consistent with the mass erosion studies, where the buffer solution was changed at the indicated times. The concentration of released dye was determined by measuring the absorbance of the supernatant at 520 nm, and the normalized results are shown in Figure 11. Hydrogels with HOPO-Al(III) crosslinks were used as these coordination complexes have no absorbance in the analytical range, in comparison to HOPO-Fe(III) complexes, which absorb strongly in this region. Spectroscopic measurements show very high initial incorporation of dye, with just 2.2 +/- 0.5% of the initial dye payload released through the injection and 30 second gelation period. Drug release can be modeled by the Korsmeyer-Peppas equation,

$$\frac{Q_t}{Q} = kt^n \tag{1}$$

where Q_t is the release amount at time t, Q is the total amount released, k is the kinetic constant, and n is the release index. A release index of less than 0.45 indicates a purely Fickian diffusion release mechanism, while a release index between 0.45 and 0.89 indicates a mixed mode release where both diffusion and erosion play a role. A power law fit of the data, shown on Figure 8 (correlation constant, R = 0.99) yields a value for n of 0.49. This

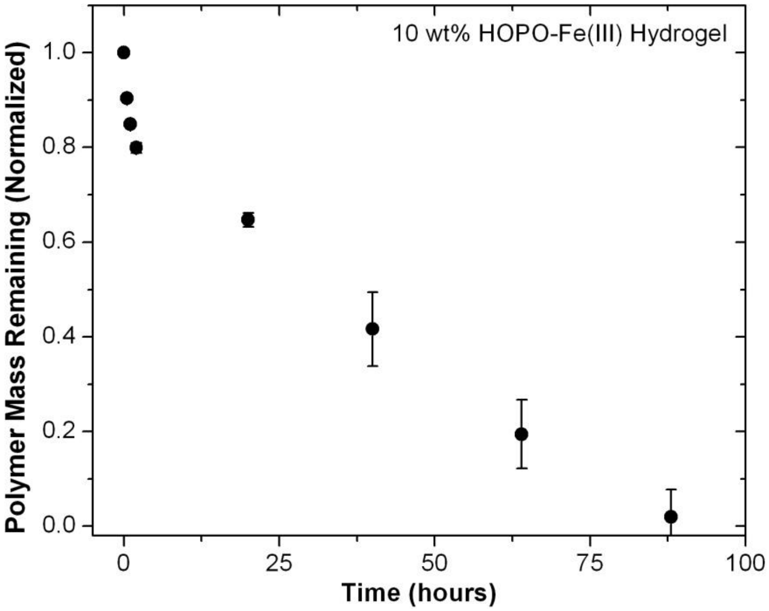

Figure 10 Degradation of HOPO-Fe(III) hydrogel samples in pH 7.4 buffer at 37°C (n=3, error bars represent standard deviation)

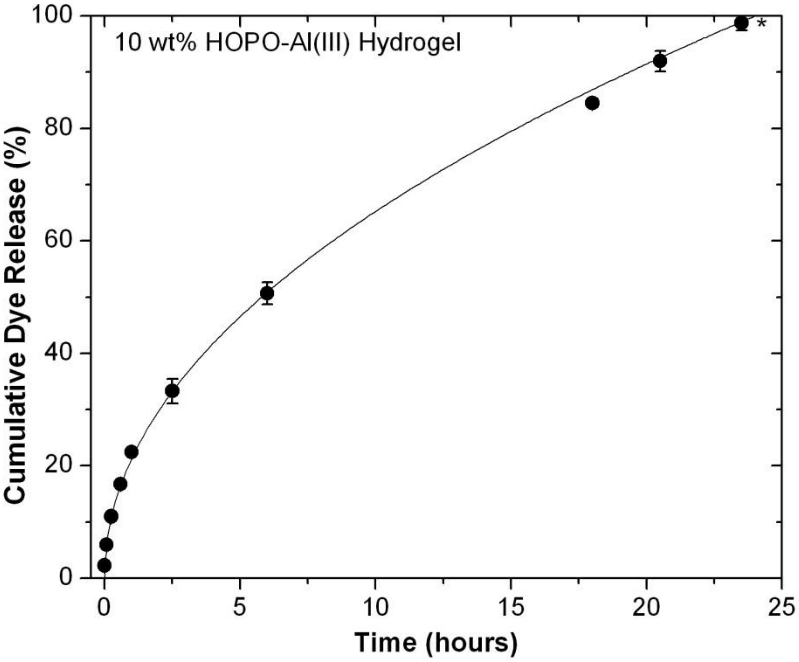

Figure 11 Dye release profile of Acid Red 27 from HOPO-Al(III) hydrogel into pH 7.4 buffer (n=3, error bars represent standard deviation)

implied mixed release mechanism is in agreement with experiment observation, as final dye release occurs concurrently with gel dissolution. As release is controlled in part by hydrogel pore size, release kinetics could conceivably be tuned by changing the distance between crosslinks in gels of this construct.

III. Conclusions

Examination of a number of catechol-based ligands for metal-ion induced hydrogel formation has clearly demonstrated the utility and advantages of HOPO as structural motif and showcases its function in a load-bearing role under biologically mimetic conditions. Hydrogels formed by the chelation of Fe(III) by 4-arm HOPO-terminated polyethylene glycol molecules exhibit several advantages over more traditionally used catechol-Fe(III) chemistry. First, the chelation stoichiometry of HOPO is much better attuned to physiological conditions, allowing almost instantaneous formation of robust gels upon injection into physiological buffer without the need for an external oxidizing agent. Gels encapsulated a model dye compound with high efficiency, and slowly degraded over 4 days in buffer solution, while catechol-based gels could not be formed in this manner. Second, whereas the catechol-Fe(III) complex is shown to be vulnerable to oxidative covalent crosslinking under a wide variety of conditions, HOPO-Fe(III) hydrogels were found to maintain robust, dynamic crosslinking and subsequently stable rheological properties over the course of months. Finally, HOPO is a versatile metal binding species, capable of gelation at physiological pH with Al(III) and Ga(III), and at higher pH with Cu(II) metal ions.

Herein, we describe the synthesis and characterization of hydrogels prepared from catechol-, nitrocatechol-, and 3-hydroxy-4-pyridinone-based 4-arm crosslinkers upon complexation with Fe(III) and other metal ions with high affinity for this class of chelators. The mechanical properties of the hydrogels are found to be strongly dependent on pH, preparation conditions, and metal ion identity. HOPO in particular was shown to be particularly attractive as a chelating functionality in this architecture. It is able to rapidly shift to a *tris* coordinative mode upon exposure to physiological pH buffer, allowing liquid-to-gel transition with limited dissolution of the polymeric crosslinker or leakage of water-soluble cargo, as studied with Acid Red 27 dye. These hydrogels exhibit high stiffness and have long characteristic bond lifetime, leading to gels that behave elastically over a wide range of frequencies. Furthermore, these gels have long-term stability both on the benchtop, where the gels maintain their rheological behavior and dynamic character, and in physiological buffer, where the gels were observed to slowly dissolve over the course of several days. Taken together, these characteristics make HOPO-based hydrogels an appealing target for injectable gelling agents with excellent encapsulation behavior and mechanical properties.

IV. Experimental

Materials

Chemicals were purchased from Sigma Aldrich and used as received. 6-nitrodopamine was synthesized following a previously published method.[26] 1-(2'-aminoethyl)-2-methyl-3-hydroxy-4-pyridinone dihydrochloride (HOPO) was synthesized following the procedure of Dobbin *et al*.[24] 4-arm PEG-OH (Mw: 10,000 Da) was purchased from Nanocs, Inc. N,N-dimethylformamide (DMF) and dichloromethane (DCM) were collected directly from a solvent purification system (PureSolv, Innovative Technology). Deuterated solvents were obtained from Cambridge Isotope Laboratories, Inc.

Instrumentation

^{1}H and ^{13}C NMR spectra were recorded using a Varian 600 MHz spectrometer with the solvent signal as internal reference. Gel permeation chromatography (GPC) was performed on a Waters 2690 separation module equipped with Waters 2414 refractive index and 2996 photodiode array detectors using $CHCl_3$ containing 0.25% triethylamine as eluent at a flow rate of 1 mL/min. Molecular weight distributions (PDIs) were calculated relative to linear poly(ethylene oxide) standards. ESI mass spectrometry was performed on a Micromass QTOF2 quadrupole/time-of-flight tandem mass spectrometer. UV-Vis spectra were recorded on an Agilent 8453 spectrophotometer using quartz cuvettes with 1cm path length and blanked against the relevant buffer solution.

Methods

SYNTHESIS OF 4-ARM PEG-COOH: A solution of 10 kDa 4-arm PEG-OH (2.14 g, 0.856 mmol –OH) in toluene (50 mL) was azeotropically dried by removal of 10 mL of solvent. A mixture of tert-butanol (2 ml) and potassium tert-butoxide (0.192 g, 1.712 mmol, 2 EQ/OH) was added to the solution and stirred for 3 hours at 50℃. Ethyl bromoacetate (380.7 ml, 3.424 mmol, 4 EQ/-OH) was added, and the mixture was stirred overnight at 50℃ under an inert atmosphere. The solvent was removed *in vacuo* and the residue was redissolved in 1 M NaOH (10 mL) and stirred for 4 hours to hydrolyze the ethyl ester. The pH was then adjusted to 1.5 with 1M HCl, and the product extracted with dichloromethane, dried with anhydrous sodium sulfate, concentrated and precipitated in cold ether. The precipitated product was filtered and dried under reduced pressure, to yield 2.01 g of white powder. NMR ($CDCl_3$): 3.41 pρm (s, C-CH_2-O, 8H), 4.16 ppm (s, CH_2-COOH, 8H), 98% functionalization.

SYNTHESIS OF 4-ARM PEG-CHELATORS. PEG-$(COOH)_4$ (500 mg, 0.2 mmol -COOH) was dissolved in 4 mL of a degassed 50/50 mixture of DCM and DMF with the desired chelator amine (0.4 mmol), HOBt (1-Hydroxybenzotriazole) (108 mg, 0.8 mmol), and triethylamine (139.5 µL, 1 mmol) to form a cloudy solution. [2-(1h-benzotriazol-1-yl)-1,1,3,3-tetramethyluronium hexafluorophosphate] (HBTU) (151.8 mg, 0.4 mmol) in 2 mL of dry dichloromethane was added, and the coupling reaction was carried out under argon at room temperature for 1 hour. The solution was concentrated, redissolved in 0.5 M HCl (10 mL), and then purified via centrifuge dialysis (2 x 15 mL pH 3 HCl, 2x 15 mL milliQ water, 5000g, 20 min, MWCO: 3 kDa). Freeze drying gave the desired PEG-$(chelator)_4$ as a fluffy white powder.

PEG-$(catechol)_4$ NMR ($CDCl_3$): 2.70 (t, CH_2-CH_2-NH-C=O, 8H), 3.41 ppm (s, C-CH_2-O, 8H), 3.93 (s, -CH_2-CO-NH-CH_2-, 8H), 6.57-6.82 (m, Ar-H, 12H), 90% functionalization, 90% yield.

PEG-(nitrocatechol)$_4$ NMR ($CDCl_3$): 3.01 (t, CH_2-CH_2-NH-C=O, 8H), 3.41 ppm (s, C-CH_2-O, 8H), 3.95 ppm (s, -CH_2-CO-NH-CH_2-, 8H), 6.96 (s, Ar-H, 4H), 7.88 (s, Ar-H, 4H), 95% functionalization, 87% yield.

PEG-(HOPO)$_4$ NMR ($CDCl_3$): 2.68 (s, CH_3-Ar, 12H), 3.41 ppm (s, C-CH_2-O, 8H), 3.95 ppm (s, -CH_2-CO-NH-CH_2-, 8H), 4.42 (t, CH_2-CH_2-NH-C=O, 8H), 7.07 (s, Ar-*H*, 4H), 7.96 (s, Ar-H, 4H), 96% functionalization, 92% yield.

Formation of Hydrogels

"Dilution" gelation followed a slightly modified version of the procedure established by Holten-Andersen et al.[13] Briefly, a 200 μL 10% w/v hydrogel was made by dissolving 20 mg of the relevant 4-arm crosslinker in a minimum amount (25 μL) of unbuffered Milli-Q water. To this solution was added 10 μL of a 0.19 mM $FeCl_3$ $6H_2O$ solution to achieve a chelator:Fe(III) ratio of 3:1. Finally, the hydrogel was formed by addition of 120 mM buffer solution (165 μL). This buffer addition was verified to yield the desired hydrogel pH by determination with a pH probe electrode.

"Injection" gelation followed the same initial dissolution and $FeCl_3$ binding steps. This iron-bound polymer solution was diluted with unbuffered Milli-Q water to achieve 200 μL of solution which remained below the gel point for all chelators (pH ~ 3). This solution was dropped or injected into a 3 mL reservoir of the desired 120 mM buffer solution. In the case of Fe(III)-HOPO solutions into pH 7.4 phosphate buffer or pH 9 bicarbonate buffer, distinct gelation was immediately apparent.

Dynamic Rheology

Rheological experiments were performed on a Rheometrics Scientific ARES II rheometer with parallel plate geometry (25 mm or 8 mm diameter rotating top plate) at 23°C. Initial time sweeps were carried out (1% strain, 1 Hz) to ensure gel equilibration, and further rheological testing proceeded only after a stable G' value had been achieved (up to 10 minutes for highly elastic hydrogels). Strain sweep experiments (1 Hz) determined the linear viscoelastic region to extend to 30-50% strain for all hydrogels tested. Oscillatory shear testing of gels as a function of frequency was performed using 5% strain. Characteristic relaxation time, τ, was determined as the inverse of the crossover frequency of the storage (G') and loss (G") moduli. Step strain testing was performed by applying a 20% strain and monitoring the relaxation modulus G(t). Initial relaxation modulus values were normalized to allow comparison between hydrogels of different pH, chelator and metal ion identity. Sample dehydration was minimized through the use of an enclosed, humidified chamber during testing. Data points represent the average of testing on two separate gels each measured in duplicate.

Hydrogel dissolution studies

150 μL HOPO-Fe(III) hydrogel samples (n = 2) were placed in a 2 mL vial on a shaker in a 37°C incubator. The gels were covered with 1.5 mL of 0.12 M phosphate buffer solution (pH 7.4) and gently shaken. The supernatant was collected every 30 minutes for the first 2 hours, and once a day thereafter. The gels were patted dry and weighed, and the supernatant was subjected to UV-Vis. Reference 4-arm HOPO-Fe(III) solutions allowed the determination of molar absorptivities for the HOPO ligand (272 nm, $\epsilon = 8010\ M^{-1}\ cm^{-1}$) and

the charge transfer absorbance (460 nm, $\epsilon = 653\ M^{-1}\ cm^{-1}$). The concentration of the 4-arm chelator complex in the supernatant was determined by measurement of these absorbances, and used to calculate the mass of hydrogel remaining.

Small Molecule Release Studies

Samples for small molecule release studies were synthesized in a manner analogous to the “injection” gelation strategy outlined above. 150 µL of a 10% w/v “pre-gel” solution was prepared by dissolving 15 mg of 4-arm PEG-HOPO in 102 µL of Acid Red 27 dye solution (0.66 mg, 0.4 µmoles) in deionized water and 48 µL of $AlCl_3$ solution to achieve a 3:1 chelator:Al^{3+} stoichiometry. This dark red solution was injected in 50 µL aliquots into 1 mL reservoirs of 120 mM PBS buffer (pH 7.4), leading to immediate gelation. The supernatant was removed after 30 seconds of setting and the gels were centrifuged to collect at the bottom of 1.5 mL Eppendorf tubes. The samples were then covered with 0.5 mL of fresh pH 7.4 buffer solution. Samples were incubated with gentle shaking. At the times indicated, the supernatant was removed and replenished. The concentration of eluted dye was determined by measuring the absorbance at 520 nm.

V. References

(1) Li, H.; Linke, W. a; Oberhauser, A. F.; Carrion-Vazquez, M.; Kerkvliet, J. G.; Lu, H.; Marszalek, P. E.; Fernandez, J. M. *Nature* **2002**, *418*, 998–1002.

(2) Becker, N.; Oroudjev, E.; Mutz, S.; Cleveland, J. P.; Hansma, P. K.; Hayashi, C. Y.; Makarov, D. E.; Hansma, H. G. *Nat. Mater.* **2003**, *2*, 278–283.

(3) Appel, E. a; del Barrio, J.; Loh, X. J.; Scherman, O. a. *Chem. Soc. Rev.* **2012**, *41*, 6195–6214.

(4) Lundberg, P.; Lynd, N. a.; Zhang, Y.; Zeng, X.; Krogstad, D. V.; Paffen, T.; Malkoch, M.; Nyström, A. M.; Hawker, C. J. *Soft Matter* **2013**, *9*, 82.

(5) Jeong, B.; Bae, Y. H.; Lee, D. S.; Kim, S. W. *Nature* **1997**, *388*, 860–862.

(6) Zhang, R.; Tang, M.; Bowyer, A.; Eisenthal, R.; Hubble, J. *Biomaterials* **2005**, *26*, 4677–4683.

(7) Cui, J.; del Campo, A. *Chem. Commun. (Camb).* **2012**, *48*, 9302–9304.

(8) Sijbesma, R. P. *Science (80-.).* **1997**, *278*, 1601–1604.

(9) Tuncaboylu, D. C.; Sari, M.; Oppermann, W.; Okay, O. *Macromolecules* **2011**, *44*, 4997–5005.

(10) Burattini, S.; Greenland, B. W.; Merino, D. H.; Weng, W.; Seppala, J.; Colquhoun, H. M.; Hayes, W.; Mackay, M. E.; Hamley, I. W.; Rowan, S. J. *J. Am. Chem. Soc.* **2010**, *132*, 12051–12058.

(11) Wang, Q.; Mynar, J. L.; Yoshida, M.; Lee, E.; Lee, M.; Okuro, K.; Kinbara, K.; Aida, T. *Nature* **2010**, *463*, 339–343.

(12) Hunt, J. N.; Feldman, K. E.; Lynd, N. a; Deek, J.; Campos, L. M.; Spruell, J. M.; Hernandez, B. M.; Kramer, E. J.; Hawker, C. J. *Adv. Mater.* **2011**, *23*, 2327–2331.

(13) Holten-Andersen, N.; Harrington, M. J.; Birkedal, H.; Lee, B. P.; Messersmith, P. B.; Lee, K. Y. C.; Waite, J. H. *Proc. Natl. Acad. Sci. U. S. A.* **2011**, *108*, 2651–2655.

(14) Li, Z.; Buerkle, L. E.; Orseno, M. R.; Streletzky, K. a; Seifert, S.; Jamieson, A. M.; Rowan, S. J. *Langmuir* **2010**, *26*, 10093–10101.

(15) Yount, W. C.; Loveless, D. M.; Craig, S. L. *J. Am. Chem. Soc.* **2005**, *127*, 14488–14496.

(16) Raymond, K. N.; Dertz, E. a; Kim, S. S. *Proc. Natl. Acad. Sci. U. S. A.* **2003**, *100*, 3584–3588.

(17) Harrington, M. J.; Masic, A.; Holten-Andersen, N.; Waite, J. H.; Fratzl, P. *Science* **2010**, *328*, 216–220.

(18) Herlinger, E.; Jamesonb, R. F.; Linerta, W. *J. Chem. Soc., Perkin Trans. 2* **1995**, 259–263.

(19) Lee, B. P.; Dalsin, J. L.; Messersmith, P. B. *Biomacromolecules* **2002**, *3*, 1038–1047.

(20) Jang, H. G.; Cox, D. D.; Que, L. *JACS* **1991**, 9200–9204.

(21) Kawabata, T.; Schepkin, V.; Haramaki, N.; Phadke, R. S.; Packer, L. *Biochem. Pharmacol.* **1996**, *51*, 1569–1577.

(22) Barrett, D. G.; Fullenkamp, D. E.; He, L.; Holten-Andersen, N.; Lee, K. Y. C.; Messersmith, P. B. *Adv. Funct. Mater.* **2012**, 1111–1119.

(23) Nurchi, V. M.; Pivetta, T.; Lachowicz, J. I.; Crisponi, G. *J. Inorg. Biochem.* **2009**, *103*, 227–236.

(24) Dobbin, P. S.; Hider, R. C.; Hall, a D.; Taylor, P. D.; Sarpong, P.; Porter, J. B.; Xiao, G.; van der Helm, D. *J. Med. Chem.* **1993**, *36*, 2448–2458.

(25) Lutolf, M. P.; Lauer-Fields, J. L.; Schmoekel, H. G.; Metters, a T.; Weber, F. E.; Fields, G. B.; Hubbell, J. a. *Proc. Natl. Acad. Sci. U. S. A.* **2003**, *100*, 5413–5418.

(26) Napolitano, a. *Tetrahedron* **2000**, *56*, 5941–5945.

(27) Mizrahi, B.; Shankarappa, S. a.; Hickey, J. M.; Dohlman, J. C.; Timko, B. P.; Whitehead, K. a.; Lee, J.-J.; Langer, R.; Anderson, D. G.; Kohane, D. S. *Adv. Funct. Mater.* **2012**, n/a–n/a.

(28) Israelachvili, J. N. *Intermolecular and Surface Forces Third Edition*; Third.; Elsevier Inc.: Burlington, MA, 2011.

(29) Monzyk, B.; Crumbliss, A. L. *JACS* **1982**, *104*, 4921–4929.

(30) Burgess, J.; Rangel, M. *Advances in Inorganic Chemistry*; Eldik, R. V., Ed.; 2008; pp. 167–243.

(31) Zhou, T.; Ma, Y.; Kong, X.; Hider, R. C. *Dalton Trans.* **2012**, *41*, 6371–6389.

(32) Nurchi, V. M.; Crisponi, G.; Pivetta, T.; Donatoni, M.; Remelli, M. *J. Inorg. Biochem.* **2008**, *102*, 684–692.

(33) Patai, S. *Chemistry of the Quinonoid Compounds: Volume 2*; Patai, S., Ed.; Volume 2.; Wiley, London, 1974.

(34) Olav, S.; Jacobsen, J. P.; Bojesen, G.; Roepstorff, P. *Biochim Biophys Acta* **1992**, *1118*, 134–138.

(35) Yadegari, H.; Jabbari, a; Heli, H.; Moosavimovahedi, a; Karimian, K.; Khodadadi, a. *Electrochim. Acta* **2008**, *53*, 2907–2916.

(36) Santos, M. A.; Gil, M.; Gano, L.; Chaves, S. *J. Biol. Inorg. Chem.* **2005**, *10*, 564–580.

(37) el-Jammal, a; Howell, P. L.; Turner, M. a; Li, N.; Templeton, D. M. *J. Med. Chem.* **1994**, *37*, 461–466.

(38) Menyo, M.; Hawker, C.; Waite, J. *Soft Matter* **2013**, *9*, 10314–10323.

(39) Helm, L.; Merbach, a. E. *Coord. Chem. Rev.* **1999**, *187*, 151–181.

(40) Merkofer, M.; Kissner, R.; Hider, R. C.; Brunk, U. T.; Koppenol, W. H. *Chem. Res. Toxicol.* **2006**, *19*, 1263–1269.

4 Strong, sacrificial metal coordination bonds enhance toughness and recovery in interpenetrating network hydrogels

I Introduction

Living organisms utilize locally available resources to create structural materials that are uniquely tailored to the demands of their local environment. A widely-employed strategy for mechanical reinforcement is the binding of metal ions with chelating amino acid residues in proteins to form metal coordination bonds.[1] *Glycera* and *Nereis*, two polychaetes (phylum Annelida), incorporate Zn- and Cu-histidine crosslinks localized to their jaw tips to invoke a dramatic increase in both hardness and wear-resistance.[2–5] Mussels (genus *Mytilus*) produce attachment threads wrapped in a protective sheath known as a cuticle, which exhibits high stiffness (E = 0.4 GPa) hardness (H = 23 MPa), but can be extended up to 100% strain without complete failure.[6] The cuticle draws toughness from its nanocomposite-like microstructure, consisting of 100-1000nm inclusions enriched in 3, 4-dihydroxyphenylalanine (Dopa)-Fe^{3+} coordination-based crosslinking.[7] Biological filaments in environments susceptible to cyclic strain events show yield and recoverable hysteresis attributed to the sacrificial rupture of metal coordination bonds. The byssal threads in *Mytilus sp.* consist of core collagen domains with flanking His- and Dopa-enriched regions, and are significantly weakened upon treatment with a broad spectrum metal chelator.[8–10] Ashton and Stewart have shown that Ca^{2+}-phosphate and -carboxylate complexes contribute key roles in the yield and recovery in threads from the larval thread of the caddisfly *Hesperophylax occidentalis*.[11]

The chemical properties characteristic of metal coordination bonds can be also be translated to synthetic platforms. Coordination complexes are dynamically exchangeable and thus have an inherent capacity for self-healing and recovery. The timescale of this lability is tied to the dissociation kinetics of the complex, which can be varied by metal ion, ligand, pH, and solvent. [12–16] Craig *et al*. investigated the mechanical properties of 4-vinylpyridine in DMSO, showing that the incorporation of transient Pd(II)- and Pt(II)-pincer crosslinks result in the formation of organogels with viscoelastic properties dependent on ligand dissociation kinetics.[17,18].

The strength of these complexes as determined by $\Delta G_{complex}$ varies widely, from negligible in very weakly chelating systems to >100 kT for strongly chelating metal-ligand pairs like catechol-Fe^{3+}.[19] As with other non-covalent strategies, substantial mechanical reinforcement generally requires the additive or cooperative domain effects from high amounts of lower-affinity complexes such as Fe^{3+}-carboxylate[20], Cu^{2+}-nitrilotriacetic acid[21] or Ca^{2+}-alginate systems.[22] Recently, several studies have shown that robust hydrogels can be formed through small amounts of high-affinity, biologically inspired Dopa-M^{3+} or His-M^{2+}complexes.[14–16]

We have demonstrated previously that 3-hydroxy-4-pyridinones (HOPO) are especially suitable for use as dynamic crosslinkers in hydrogels under physiological conditions.[23] Hydrogels constructed from 4-arm poly(ethylene glycol) (tetraPEG) molecules end-functionalized with HOPO moieties and hard metal ions show efficient crosslinking, pH-responsive viscoelasticity, and stable dynamic behavior. However, the short, extended hydrogel chain architecture and the wholly dynamic nature of this system results in brittle hydrogels with no elastic recovery force.

In this work, we show that the incorporation of this HOPO-tetraPEG coordination network into a loosely crosslinked hydroxyethylacrylamide covalent scaffold allows the formation of an interpenetrating network (IPN) hydrogel in which the coordination network serves as a sacrificial, energy-dispersive component (Figure 1). By employing three different high-affinity metal ions with different dissociation rates, we demonstrate reinforced hydrogels with strain-rate dependent mechanical properties and tunable recovery kinetics.

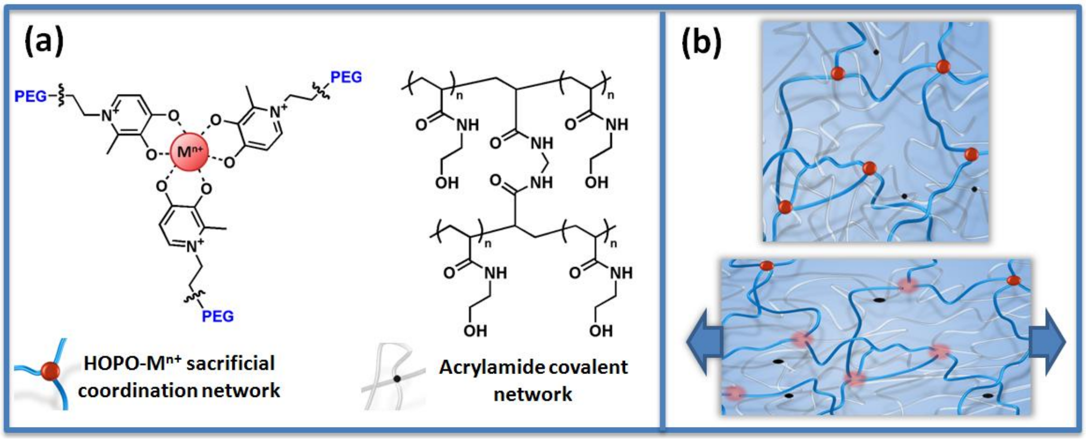

Figure 1: (a) Chemical structures of the crosslinks of the 3-hydroxy-4-pyridinone-M^{n+}-tetraPEG coordination network and the hydroxyethylacrylamide-methylene bisacrylamide covalent networks. (b) Upon loading, the tightly crosslinked coordination network ruptures sacrificially, contributing recoverable toughness in the interpenetrating network.

II. Characterization of coordination network hydrogels

Coordination network crosslinkers were synthesized by reaction of amino-functional 2-methyl 3-hydroxy-4-pyridinone with an NHS-activated tetraPEG starting reagent (M_w: 10,000 g/mol). This reaction led to a high degree of chain-end functionalization (96% by ^{1}H NMR integration, Appendix C.1). Coordination hydrogels (10wt-% polymer) were formed in a three-step process. The tetraPEG crosslinker was dissolved in deionized water, followed by addition of a small volume of trivalent metal chloride stock solution to achieve a 3 HOPO:1 M^{n+} ratio. At $pH < 4$, the metals are bound in low stoichiometry *mono* and *bis* complexes. Gelation was triggered upon addition of 0.1M NaOH to achieve the desired pH.

We first looked to characterize the rheological properties of the coordination networks alone. It has been shown that the dissociation kinetics of the coordination bonds are the principle determinant of the viscoelastic behavior of hydrogels of this nature.[17] We hypothesized that by using three trivalent metal ions with high affinity for HOPO ligands that differed in exchange kinetics, we could control the lifetime over which these bonds are mechanically active, allowing tunable, strain-rate dependent stiffening and recovery. Three metal ions with similarly high affinity for 3,4-HOPO ligands but varying water exchange rates were chosen: Al^{3+} ($\log\beta = 34$, $k_{exchange} = 1\ s^{-1}$), Fe^{3+} ($\beta = 37$, $k_{exchange} = 200\ s^{-1}$) and In^{3+} ($\beta = 33$, $k_{exchange} = 10^6\ s^{-1}$).[24–27]

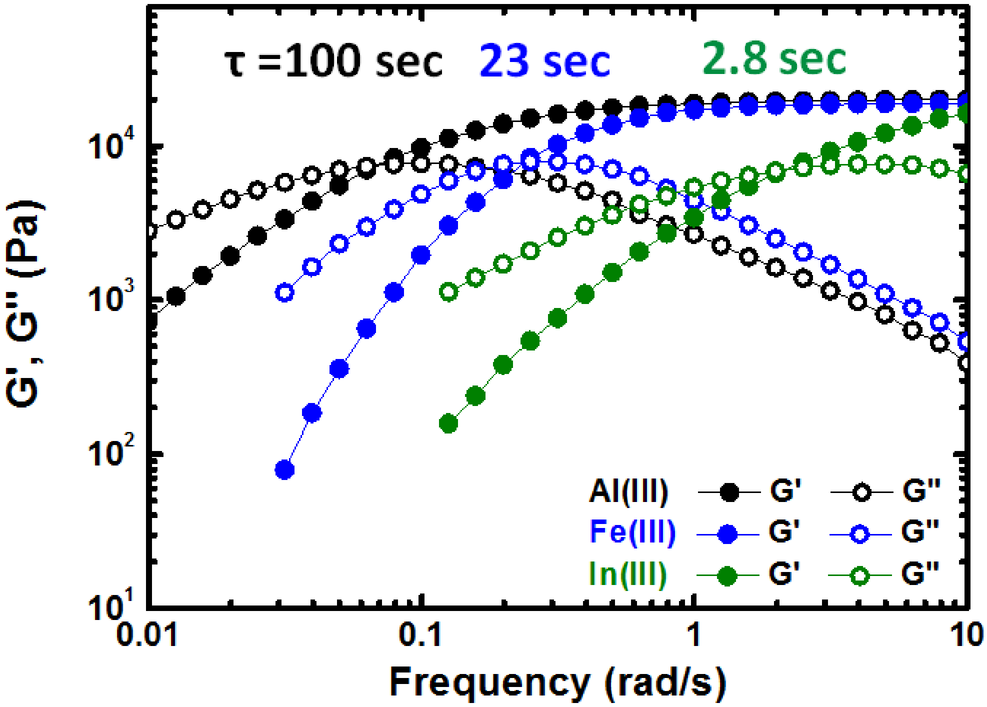

Figure 2: Dynamic shear moduli (G', closed symbols; G", open symbols) as a function of frequency for Al(III), Fe(III) and In(III)-HOPO hydrogels at pH 8.2.

Figure 2 shows linear viscoelastic oscillatory shear measurements of hydrogels formed from Al^{3+}, Fe^{3+} and In^{3+}-HOPO coordination crosslinks at pH 8.2. All gels show predominantly elastic behavior at high ω and similar plateau moduli ($G'_{plateau}$ = 18.9-21.3

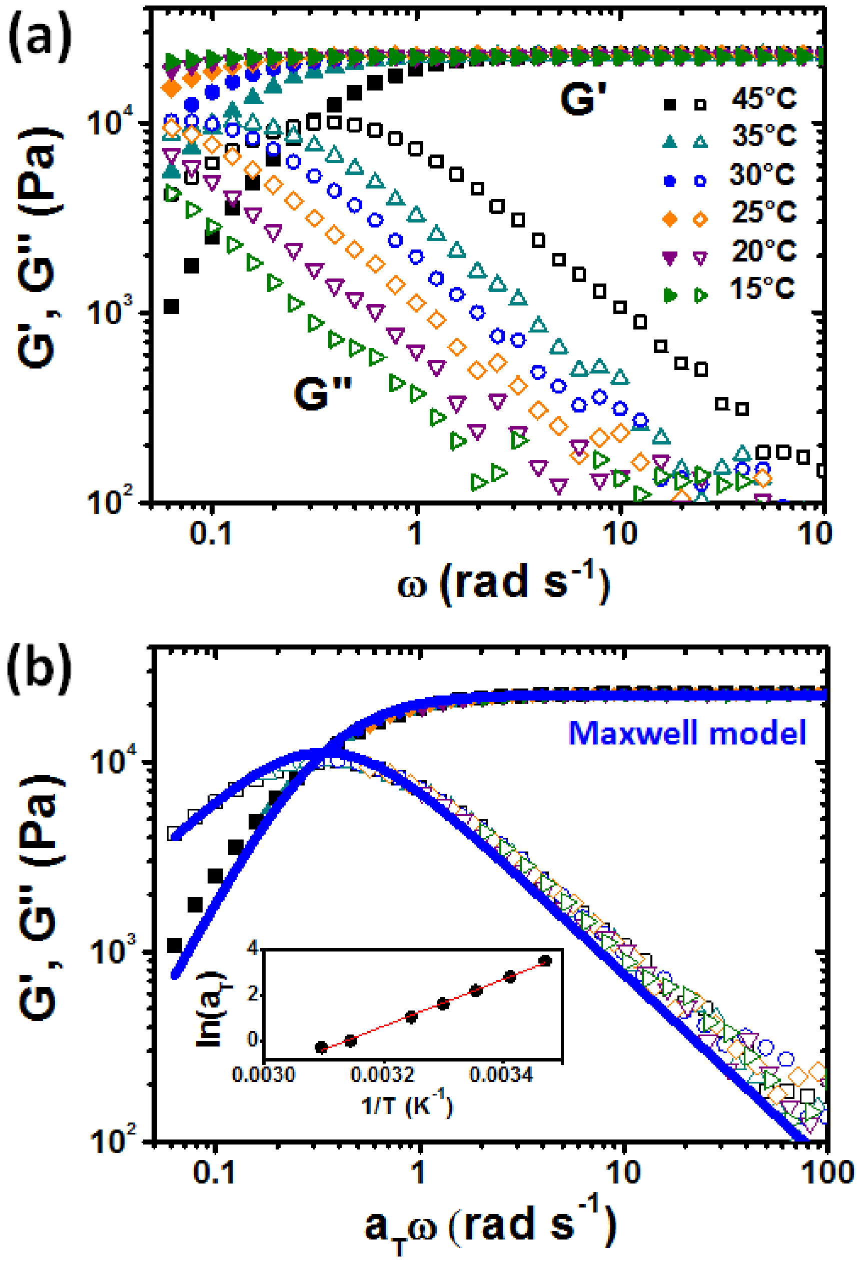

Figure 3: (a) Dynamic shear moduli of Al^{3+}-HOPO coordination hydrogel (pH 8.2) as a function of frequency from 15°C to 45°C. (b) Frequency sweeps shifted horizontally to fall onto a master curve which is well-fit by a single relaxation Maxwell model. Inset: Arrhenius plot of horizontal shift factor a_T with reference temperature of 45°C.

kPa). Notably, the crossover points between G' and G" vary with transition metal ion. This matches the expected behavior in coordination gels, as the viscoelastic behavior is dependent on ligand exchange kinetics. The characteristic relaxation time τ was measured as the inverse of the frequency at which G" is at a maximum. The gels differ in τ by over two orders of magnitude, in a manner that follows measured water exchange kinetics.

To further interrogate the thermodynamics of the coordination networks, we measured the frequency-dependent rheological properties at a range of temperature T = 15-45℃. We find that the viscoelastic moduli G' and G" follow time-temperature superposition and collapse onto a master curve by applying horizontal shift factors a_T. (Figure 3a and b) Furthermore, this master curve (T_{ref} = 45℃) is well fit by a single-relaxation Maxwell model, with $G'_{plateau}$ = 21.9 kPa and τ = 2.95 s. This suggests that the viscoelasticity is primarily determined by the crosslinks, with minimal effect of chain entanglement in this dilute, highly swollen network. A plot of $\ln(a_T)$ versus inverse absolute temperature (inset in Figure 2b) follows a linear relationship over the range of temperatures tested. This shows that the hydrogels exhibit Arrhenius behavior as described by the equation

$$\ln(a_T) = \frac{E_a}{R}\left(\frac{1}{T} - \frac{1}{T_{ref}}\right) \qquad (1)$$

The slope of the linear fit allows us to determine an activation energy of viscoelasticity of 34 kT in this system, which is approximately ½ of the total energy of complex formation ($\Delta G_{HOPO\text{-}Al(III)}$ = 78 kT). This value is equal or higher than strong non-covalent interactions including biotin-avidin (35 kT)[28], Upy quadruple H-bonding groups (18 kT in chloroform),[29] and gold-thiol bonds (35 kT).[30] Finally, the amount of elastically effective crosslinks in this hydrogel is determined to be 72% by comparison of the observed plateau modulus to the theoretical plateau modulus in this system, as described by

$$G = \rho RT$$

where ρ is equal to the maximum theoretical crosslink density.

This detailed rheological characterization of HOPO coordination networks highlights several promising features for energy dissipative materials:

(1) individual crosslinks have a high binding energy
(2) effective bond lifetimes are tunable by changing metal ion
(3) the dynamic nature of the coordination bonds allows network recovery and self-healing

III. Characterization of interpenetrating network hydrogels

However, the tetraPEG architecture limits the large strain amplitude mechanical properties of these materials. In order to fully realize the potential of coordination bonds, we incorporated this coordination network with a covalent scaffold to form an interpenetrating network, as depicted in Figure 1. We envisioned the two components performing cooperatively, with the more highly crosslinked coordination network rupturing sacrificially, and the loosely crosslinked covalent network providing an elastic restoring force after deformation. The covalent network is made from an aqueous solution of hydroxyethylacrylamide with 0.001 equivalents methylene bisacrylamide crosslinker. Network formation is initiated by an ammonium persulfate/tetramethylenediamine redox pair in sealed syringe bodies or Teflon molds for 24 hours at 40℃ to achieve the desired geometry. This gel was found to be miscible with unfunctionalized tetraPEG at up to 20 wt-%, but the radical scavenging nature of the HOPO moieties inhibited polymerization of the network in the presence of the functionalized tetraPEG. To ensure consistent degree of polymerization, the functionalized tetraPEG with *mono*-coordinated metal was introduced by diffusion into the lyophilized covalent network, followed by addition of base to trigger crosslinking. Each step was confirmed to be complete after 24 hours at 40℃ both by mechanical and spectroscopic measurements. The final interpenetrating network hydrogels consisted of 23 wt-% covalent network and 10 wt-% coordination network.

8.2).

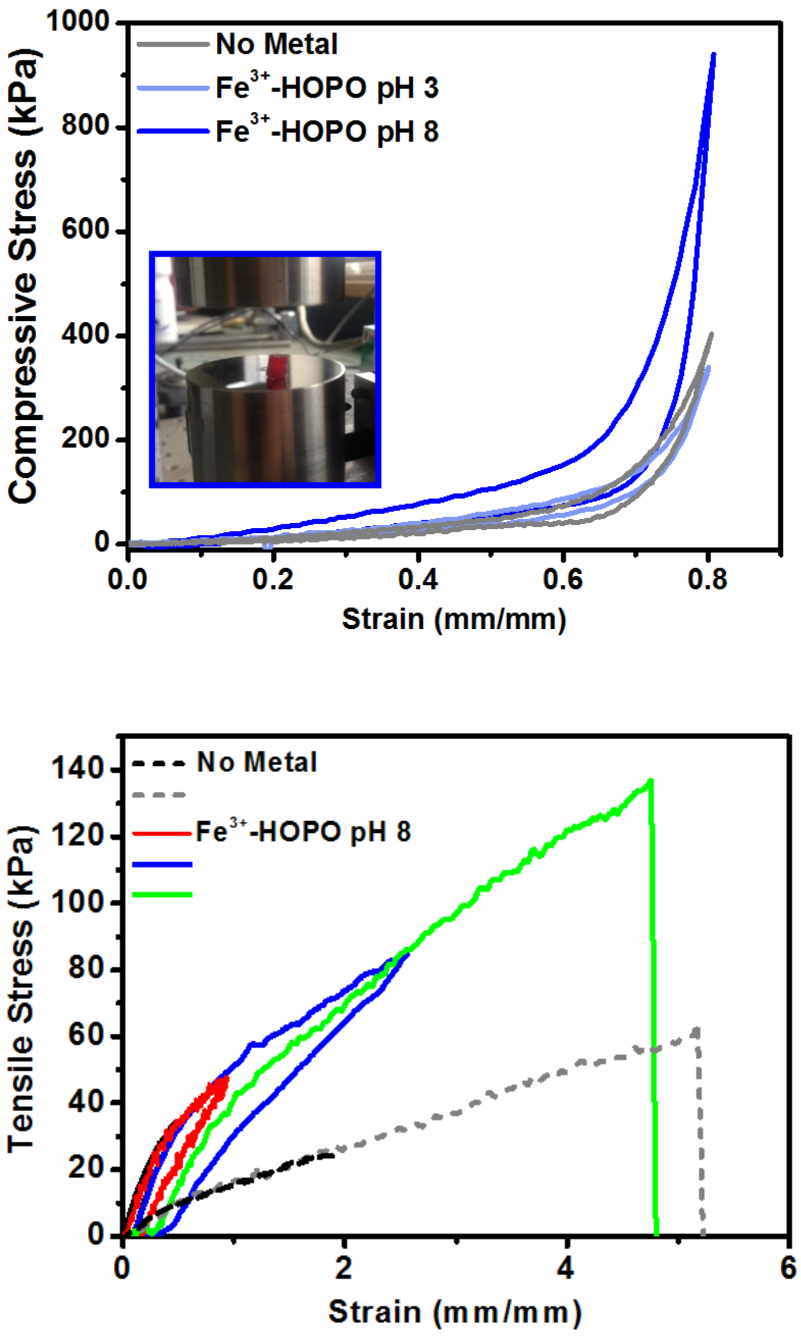

Figure 4: Compressive stress/strain curves for interpenetrating network without Fe^{3+} added (grey), with Fe^{3+} at low pH (light blue), and at high pH (dark blue). (b) Tensile stress/strain curves upon cyclic loading to higher extensions. Dotted lines are the interpenetrating network without metal, and the solid lines are with Fe^{3+} added (pH 8.2).

The coordination-covalent IPNs were tested both in compression and tension. Compression samples were molded in syringes, whereas tensile samples were stamped with a dogbone die punch. Figure 4 shows the results of compression tests on Fe^{3+}-HOPO IPNs carried out to 80% strain at a constant compression and unloading speed corresponding to an initial strain rate of 4 mm/mm min^{-1}. The curves for the IPN without Fe^{3+} added and with Fe^{3+} at pH 3 are similar and show predominantly elastic behavior. Upon raising the pH to 8.2 to trigger coordination crosslinking, an increase in the modulus, stress at 80% strain, and hysteresis upon unloading can be seen, indicating a mechanical contribution to the hydrogel via the coordination network. Similar effects are notable in mechanical test in tension, as depicted in Figure 4b. (Appendix C.2)

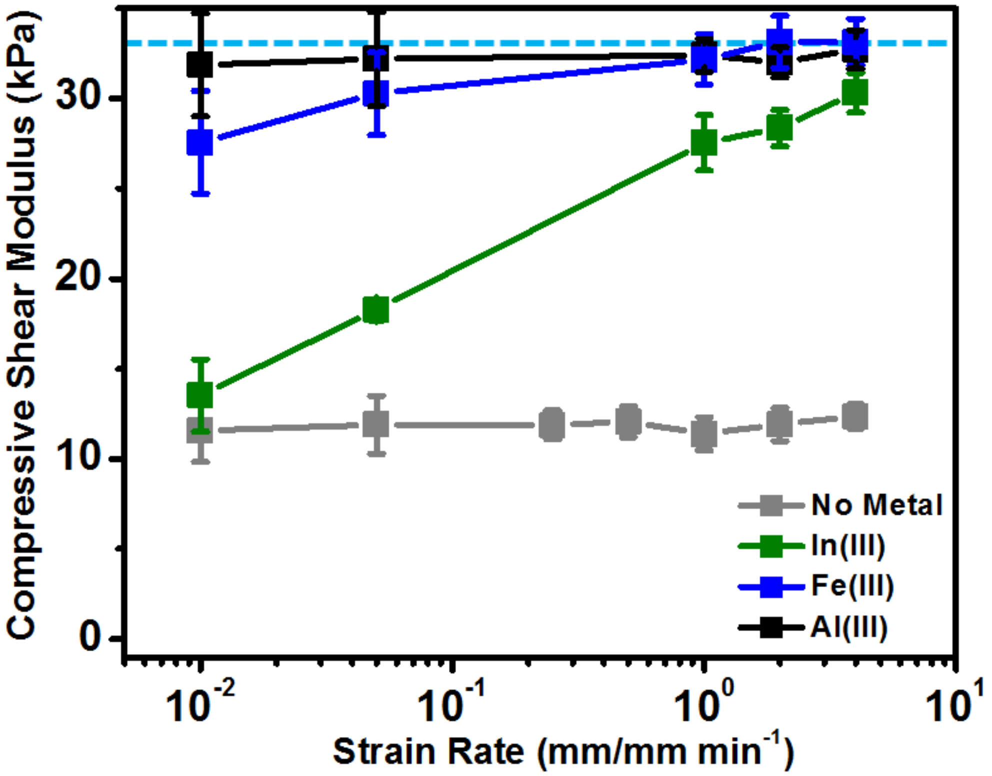

Figure 5: Initial compressive shear modulus as a function of strain rate for interpenetrating network hydrogels with no metal and In(III), Fe(III), Al(III) at pH 8.2. The blue dotted line represents the additive sum of the covalent acrylamide network and the shear plateau modulus of the coordination network.

To demonstrate the strain rate and metal-dependent reinforcement provided by the coordination network, IPN samples were made with Al^{3+}, Fe^{3+} and In^{3+} and measured at varying compression rates. The shear compressive modulus was found to be constant at low strains, well described by the statistical thermodynamic treatment of rubber elasticity,

$$G = \frac{\tau}{\lambda - \lambda^{-2}}$$

where τ is the compressive stress and λ is the extension ratio. Moduli were extracted from the linear fit of the τ versus λ-λ^{-2} plot for strains between 5-25% and summarized in Figure 5. Without metal, the initial compressive shear modulus is 11.8 ± 0.4 kPa and is unchanged within error for strain rates from 0.01 to 4 mm/mm min^{-1}. The addition of metals and base triggers formation of the coordination network. Upon compression, a clear strain rate dependence can be observed. IPNs with In^{3+}-HOPO coordination networks shown a minimally higher modulus than without metal at low strain rates (G = 16.1 ± 2.0 kPa), but trend towards the additive moduli of the coordination and covalent network as the strain rate increases to 4 mm/mm min^{-1} (G = 30.4 ± 1.4 kPa). Compression of IPNs incorporating the more kinetically inert metals, Fe^{3+} and Al^{3+}, exhibit moduli that are less dependent on strain rate over the range of accessible rates, though it should be noted that the Fe^{3+}-HOPO IPN hydrogels exhibit some softening at low strain rates.

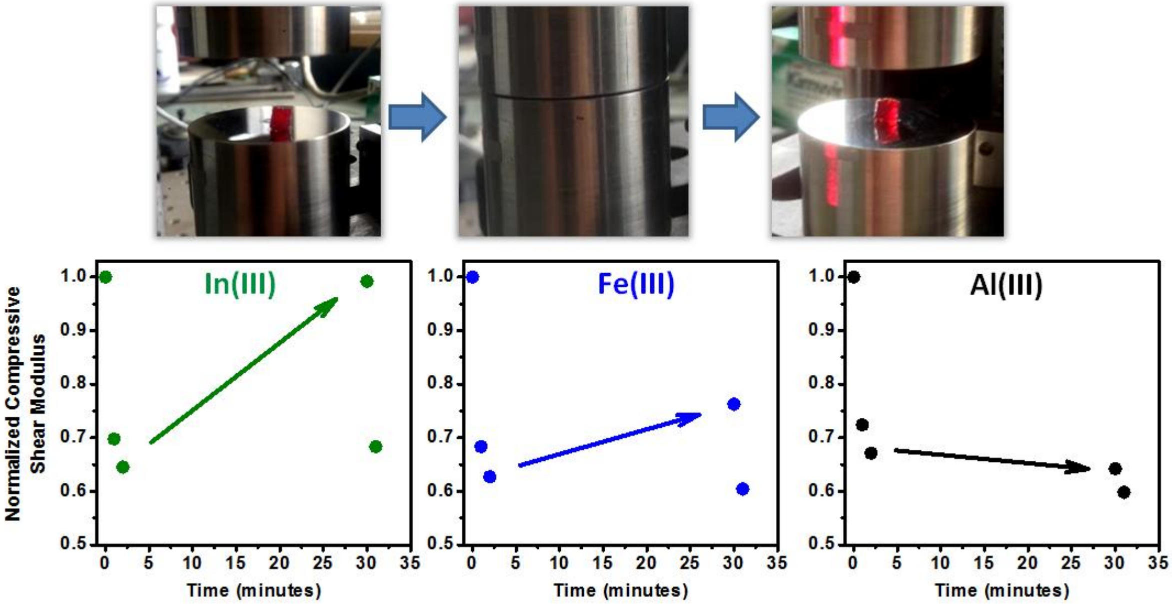

Figure 6: Measurement of initial compressive modulus upon repeated cycling to 80% compression, followed by 30 minutes recovery.

To this point, we have demonstrated that incorporation of the coordination network leads to strain-rate and metal-dependent changes in mechanical response. We can take advantage of this control to create IPNs with tunable recovery dynamics. Figure 6 shows the extracted initial moduli from consecutive compression cycles to 80% strain, followed by a 30 min recovery period. All hydrogels show lower initial moduli, signifying rupture of crosslinks, upon repeated cycling. IPN hydrogels with labile In^{3+} crosslinking heal rapidly, recovering to 99% of their initial modulus after 30 minutes rest. Fe^{3+} IPNs show partial recovery after 30 minutes, while Al^{3+} hydrogels remain damaged. Cyclic compression to 80% strain shows no damage in the covalent network alone.

IV. Conclusions

In summary, we have taken advantage of high-affinity coordination crosslinks to introduce rate-dependent, recoverable reinforcement in an interpenetrating network hydrogel. Pure coordination networks exhibit a high activation energy of flow and allow for the direct relation of coordination chemistry to bulk mechanical properties. The effective bond lifetimes of these networks is dependent upon complex dissociation and can be varied over 2 orders of magnitude by using several different hard, trivalent metal ions with varying kinetic lability. To address the brittle, dynamic nature of this system, coordination networks were incorporated into a loosely crosslinked covalent scaffold. The mechanical properties of these IPN hydrogels blend the properties of the covalent and the coordination networks. The coordination networks provide stiffness and energy dissipation at strain rates above their characteristic relaxation time, and minimal reinforcement at slow rates. Labile In^{3+}-coordinate hydrogels are damaged by repeated compressive cycles, but recover over the course of 30 minutes. IPN hydrogels with Fe^{3+} and Al^{3+} show slower recovery dynamics. This work highlights that the incorporation of a small amount of high-affinity coordination complexes can impart significant changes in mechanical properties in IPN hydrogels.

V. Experimental

Materials

All reagents were purchased from commercial sources and used without further purification unless otherwise stated. 4-arm PEG-SAS active ester (M_w: 10,000 Da) was purchased from Laysan Bio (Arab, Alabama) and used as received. Triethylamine was dried by distillation and stored over molecular sieves. Hydroxyethylacrylamide was passed over a plug of basic alumina to remove the inhibitor before polymerization.

Instrumentation

^{1}H and ^{13}C NMR spectra were recorded using a Varian 600 MHz spectrometer with the solvent signal as internal reference. ESI mass spectrometry was performed on a Micromass QTOF2 quadrupole/time-of-flight tandem mass spectrometer. UV-Vis spectra were recorded on an Agilent 8453 spectrophotometer using quartz cuvettes with 1cm path length and blanked against the relevant buffer solution.

Synthesis

1-(2'-aminoethyl)-2-methyl-3-hydroxy-4-pyridinone dihydrochloride (HOPO-amine): Synthesized following the procedure of Dobbin *et al*.[27] The desired compound was isolated as an off-white powder in 3 steps from maltol. (24% overall yield): ^{1}H NMR (600 MHz, D_2O) δ 2.49 (s, 3H), 3.39 (t, 2H), 4.57 (t, 2H), 7.02 (d, 1H), 7.96 (d, 1H). ^{13}C NMR (125 MHz, D_2O) δ 12.3, 38.1, 52.6, 111.6, 138.9, 142.2, 143.2, 160.0.

PEG-(HOPO)$_4$:

A 25 mL Schlenk flask was charged with a suspension of HOPO-amine (106 mg, 0.44 mmol) and 4-arm PEG-SAS (1 gram, 0.4 mmol end groups) in dry dimethylformamide (DMF) (7 mL) and purged with argon for 10 min. Dry triethylamine (140 µL, 0.92 mmol) was added dropwise through a syringe. The suspension was stirred at room temperature for 16 hours under an inert atmosphere. The reaction mixture was concentrated under vacuum, and diluted with 10 mL of 0.1 M HCl. This solution was directly transferred to dialysis tubing (MWCO: 3500 Da) and dialyzed against 0.001 M HCl for 2 days with frequent buffer changes. The solution was subsequently dialyzed against deoxygenated milliQ water in a sealed dialysis vessel for 8 hours with frequent buffer changes. The resulting solution was lyophilized to yield the desired product as a fluffy white powder. (930 mg, 94% yield, 96% funtionalization). ^{1}H NMR: (600 MHz, $CDCl_3$) δ 2.52 (s, 12H), 3.40-3.74 (br, 940H), 4.30 (br, 8H), 6.75 (s, 4H), 6.92 (s, 4H), 7.65 (s, 4H), 7.81 (s, 4H).

HOPO-metal coordination hydrogels:

Coordination hydrogels were formed following a slightly modified version of the procedure established by Menyo et al.[23] Briefly, a 100 μL 10% w/v hydrogel was made by dissolving 10 mg of the PEG-HOPO 4-arm crosslinker in (50 μL) of unbuffered Milli-Q water. To this solution was added 10 μL of a 0.01 mM $FeCl_3•6H_2O$ solution to achieve a chelator:M(III) ratio of 3:1. This solution as used for subsequent processing to form interpenetrating network hydrogels. Finally, gelation was triggered by addition of a stoichiometric equivalent of NaOH (30 uL) and 100 mM tris buffer (10 μL) to achieve the desired pH. Hydrogel pH was verified by determination with a pH probe electrode.

Hydroxyethylacrylamide covalent hydrogels:

A solution of hydroxyethylacrylamide (230 mg, 2 mmol), methylene bisacrylamide (0.154 mg, 0.001 mmol), and ammonium persulfate (1 mg, 0.004 mmol) in milliQ water (total solution volume: 990 μL) was sparged with argon in a septa-capped vial for 10 minutes. A small amount of 8 vol-% tetramethylethylenediamine stock solution (10 μL) was added via syringe at room temperature. This solution was allowed to mix for 30 sec, then transferred into a 1 mL syringe bodies for compression samples or between two glass plates with a 0.5 mm thick Teflon spacer for tensile samples. Gelation proceeded for 16 hours at

40℃ in an oven under nitrogen atmosphere. After polymerization, samples were washed extensively in deionized water to remove residue monomer, and dried by lyophilization.

Interpenetrating network hydrogels:

Lyophilized hydroxyethylacrylamide hydrogels were re-swollen with a 20 wt-% solution of PEG-$HOPO_4$ as described in the coordination hydrogel section above. Diffusion was tracked visually and through mechanical testing, and equilibration was found to be complete after 24 hours at 40℃. As described above, coordination network gelation was triggered by addition of a tris buffer solution with a stoichiometric amount of NaOH. Swelling and equilibration of this network was found to be complete after 24 hours at 40℃.

Rheology

Rheological experiments were performed on an AR-G2 stress-controlled rheometer (TA Instruments) with parallel plate geometry (20 mm diameter rotating top plate, Peltier temperature-controlled lower-plate geometry) at 30℃ unless otherwise noted. The testing geometry was fitted with a custom-built humidity chamber to prevent desiccation during testing. Gel equilibration was monitored via initial small-amplitude time sweeps (1% strain, 0.15 rad/s) to ensure gel equilibration, and further rheological testing proceeded only after a stable G' value had been achieved (up to 10 minutes for highly elastic hydrogels). Strain sweep experiments (0.2 rad/s) determined the linear viscoelastic region to extend to 30-50% strain for all coordination hydrogels tested. Oscillatory shear testing of gels as a function of frequency was performed with a strain amplitude of $\gamma_o = 5\%$. Time-temperature superposition measurements of linear viscoelasticity were performed at temperatures from 15℃ to 45℃. Characteristic relaxation time, τ, was determined as the inverse of the frequency at which the loss modulus (G") was a maximum. Data points represent the average of testing on three separate gels measured in duplicate.

Mechanical Testing

Compression testing was carried out on interpenetrating network hydrogel samples (diameter: 3.9 mm, thickness: 3.0 mm) on a custom-built tensile/compression tester equipped with a 50N load cell. Samples were coated with a thin layer of mineral oil to prevent desiccation and ensure sliding at the sample/plate interface. Hydrogels were compressed between two freshly polished, mirror-smooth steel plates to the noted ultimate compression at the noted strain rate, and immediately unloaded at the same strain rate. Freshly prepared samples were used except as noted for test of damage and recovery upon cyclic loading. Initial compressive moduli were determined by the slope of the τ versus $\lambda - \lambda^{-2}$ plot between 5-25% compressive strain. Reported initial compressive moduli represent the average and standard deviation of 3 separate hydrogels for each condition.

Tensile testing was performed on the same custom-built instrument. Dogbones with a gage width of 2mm and a gage length of 8 mm were made by stamping IPN hydrogels with a die punch. Tensile clamps were coated with sandpaper-covered foam to prevent sample slipping or tearing at the clamp interface.

VI. References

(1) Degtyar, E.; Harrington, M. J.; Politi, Y.; Fratzl, P. *Angew. Chemie (International Ed.* **2014**, *53*, 12026–12044.

(2) Lichtenegger, H.; Birkedal, H.; Casa, D.; Cross, J.; Heald, S.; Waite, J.; Stucky, G. *Chem. Mater.* **2005**, 2927–2931.

(3) Broomell, C.; Chase, S.; Laue, T.; Waite, J. *Biomacromolecules* **2008**, 1669–1677.

(4) Lichtenegger, H.; Schöberl, T.; Bartl, M. *Science (80-.).* **2002**, *298*, 389–392.

(5) Broomell, C. C.; Zok, F. W.; Waite, J. H. *Acta Biomater.* **2008**, *4*, 2045–2051.

(6) Holten-Andersen, N.; Zhao, H.; Waite, J. H. *Biochemistry* **2009**, *48*, 2752–2759.

(7) Holten-Andersen, N.; Fantner, G. E.; Hohlbauch, S.; Waite, J. H.; Zok, F. W. *Nat. Mater.* **2007**, *6*, 669–672.

(8) Gosline, J.; Lillie, M.; Carrington, E.; Guerette, P.; Ortlepp, C.; Savage, K. *Philos. Trans. R. Soc. Lond. B. Biol. Sci.* **2002**, *357*, 121–132.

(9) Vaccaro, E.; Waite, J. *Biomacromolecules* **2001**, 906–911.

(10) Harrington, M. J.; Waite, J. H. *J. Exp. Biol.* **2007**, *210*, 4307–4318.

(11) Ashton, N. N.; Stewart, R. J. *Soft Matter* **2015**.

(12) Krogsgaard, M.; Behrens, M. a; Pedersen, J. S.; Birkedal, H. *Biomacromolecules* **2013**, *14*, 297–301.

(13) Krogsgaard, M.; Hansen, M. R.; Birkedal, H. *J. Mater. Chem. B* **2014**, *2*, 8292–8297.

(14) Barrett, D. G.; Fullenkamp, D. E.; He, L.; Holten-Andersen, N.; Lee, K. Y. C.; Messersmith, P. B. *Adv. Funct. Mater.* **2012**, 1111–1119.

(15) Fullenkamp, D. E.; He, L.; Barrett, D. G.; Burghardt, W. R.; Messersmith, P. B. *Macromolecules* **2013**, *46*, 1167–1174.

(16) Holten-Andersen, N.; Jaishankar, A.; Harrington, M. J.; Fullenkamp, D. E.; DiMarco, G.; He, L.; McKinley, G. H.; Messersmith, P. B.; Lee, K. Y. C. *J. Mater. Chem. B* **2014**, *2*, 2467.

(17) Yount, W. C.; Loveless, D. M.; Craig, S. L. *J. Am. Chem. Soc.* **2005**, *127*, 14488–14496.

(18) Yount, W.; Juwarker, H.; Craig, S. *J. Am. Chem. Soc.* **2003**, *4*, 15302–15303.

(19) Martell, A.; Smith, R. *Critical Stability Constants*; Plenum Press: New York, 1977.

(20) Wei, Z.; He, J.; Liang, T.; Oh, H.; Athas, J.; Tong, Z.; Wang, C.; Nie, Z. *Polym. Chem.* **2013**, *4*, 4601.

(21) Pan, Y.; Gao, Y.; Shi, J.; Wang, L.; Xu, B. *J. Mater. Chem.* **2011**, *21*, 6804.

(22) Sun, J.-Y.; Zhao, X.; Illeperuma, W. R. K.; Chaudhuri, O.; Oh, K. H.; Mooney, D. J.; Vlassak, J. J.; Suo, Z. *Nature* **2012**, *489*, 133–136.

(23) Menyo, M.; Hawker, C.; Waite, J. *Soft Matter* **2013**, *9*, 10314–10323.

(24) Helm, L.; Merbach, a. E. *Coord. Chem. Rev.* **1999**, *187*, 151–181.

(25) Clevette, D.; Lyster, D.; Nelson, W. *Inorg. …* **1990**, 667–672.

(26) Chaves, S.; Gil, M.; Marques, S.; Gano, L.; Santos, M. A. *J. Inorg. Biochem.* **2003**, *97*, 161–172.

(27) Dobbin, P. S.; Hider, R. C.; Hall, a D.; Taylor, P. D.; Sarpong, P.; Porter, J. B.; Xiao, G.; van der Helm, D. *J. Med. Chem.* **1993**, *36*, 2448–2458.

(28) Green, N. *Biochem. J* **1966**, 774–780.

(29) Söntjens, S.; Sijbesma, R.; van Genderen, M.; Meijer, E. *J. Am. Chem. Soc.* **2000**, 9001–9007.

(30) Utzig, T.; Raman, S.; Valtiner, M. *Langmuir* **2015**.

5 Light as an external stimulus to allow spatiotemporal control over catechol reactivity

Reproduced in part with permission from: Fors, B.P., Poelma, J.E., Menyo, M.S., Robb, M.J., Spokoyny, D.M., Waite, J.H., and Hawker, C.J. (2013). Fabrication of Unique Chemical Patterns and Concentration Gradients with Visible Light. J. Am. Chem. Soc. 135 (38), 14106-14109. Copyright (2013) American Chemical Society.

I Introduction

The ability to exhibit spatial control over the arrangement of organic, inorganic and biological components at surfaces and interfaces is vital to continued research progress in areas such as biological assays, antifouling materials, stimuli-responsive surfaces, and catalysis.[1–4] Top-down lithographic techniques have been widely used to create single component patterns.[5–7] This strategy often requires harsh conditions, and generally relies on destructive techniques, complicating or eliminating the potential for subsequent patterning steps on the functionalized substrate. Microcontact printing (μCP) has also been widely employed, however, the synthesis of patterned stamps requires lengthy microfabrication steps.[8,9]

The use of photomediated reactions is a promising avenue towards the creation of arbitrarily patterned substrates.[10–13] Light is a convenient external trigger, as it can be finely manipulated by controlling area, time, and dosage. Furthermore, many photomediated processes can be carried out under environmental conditions, allowing forays into life sciences.[14] While these methods are successful for simple patterns, the synthesis of complex, multifunctional patterns remains a challenge, often necessitating complicated, multistep procedures that require harsh chemical or photo-etching steps. These factors limit the scope and permutations of patternable components.

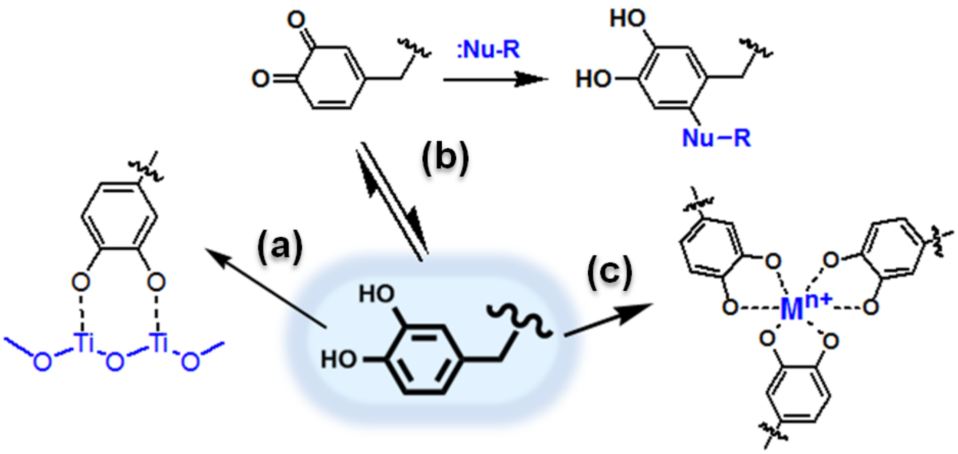

Figure 1: Schematic showing the major modes of reactivity of catechols.

To address this issue, I drew inspiration from the versatile adhesive capabilities of the Blue mussel (*M. edulis),* a marine organism capable of strong attachment to surfaces such as glass, Teflon and metals under turbulent aqueous conditions.[15] The attachment apparatus, or byssus, consists of a number of threads tipped in plaques made up of adhesive proteins with extraordinarily high (up to 30%) content of the modified amino acid 3,4-dihydroxyphenylalanine (Dopa). Though incapable of capturing the complex subtleties in structure and processing of the mussel byssus, reductionist approaches have been successful in the creation of synthetic glues with wide-ranging adhesion.[16,17] The performance of these synthetic adhesives relies on the binding chemistry of the catechol moiety. As described in the previous chapter, catechols and analogous chelating moieties form robust, pH-responsive complexes with a variety of metal ions,[18,19] as well as with boronic acids,[20–22] and attach strongly to metal oxide surfaces.[23,24] (Figure 1) They are capable of covalent crosslinking with nucleophiles such as amines, thiols and imidazoles, allowing the attachment of synthetic organics or proteins and peptides.[25–28] The growth of silver, gold and titania nanoparticles can be templated by catechols via binding and/or redox chemistry.[29]

In 2007, Lee *et al* recognized that a basic solution of dopamine readily polymerizes and coats the surface of a variety of substrates.[30] This coating, dubbed “polydopamine,” can be formed on substrates ranging in surface energies; from noble metals, to metal oxides, to polymers such as polyethylene and polytetrafluoroethylene. This coating has been shown to maintain some degree of catechol functionality, as well as a complex mixture of oxidation products (dopaquinones, dihydroxyindolines, and indoledione species).[31,32]

Many research efforts have employed this versatile chemistry to pattern and functionalize surfaces using traditional lithographic techniques. Sun *et al* showed that microcontact printed polydopamine patterns could be used to exert spatial control over cell attachment.[33] In another study, electrodeposited polydopamine lines were reacted with amino-functionalized ssDNA to allow DNA templating.[34] Inkjet printing of polydopamine nanoparticles was shown to provide a reactive surface for electroless copper plating[35].

Barner-Kowollik *et al* used catechols to attach photo-reactive species for patterning on gold, PET and Si substrates.[36] However, the conspicuous and facile reactivity, and the complexity of species within polydopamine make the construction of well-controlled catechol-based patterns a challenge using these methods.

Traditionally, acetonide or benzyl protecting groups are used to limit undesired reactivity in catecholic species. These functional groups are stable to a wide variety of conditions, but deprotection requires harsh treatment with concentration acid solutions. Silyl ethers have been used, but again, deprotection has been achieved using a F^- ion source and organic solvent.[37,38] Heo *et al* demonstrated that triethylsilyl ether protected catechols can be cleaved readily in pH 3 HCl solution.[39] Furthermore, they were able to show patterned adhesion of silica beads by microcontact printing. These benign conditions are amenable to further patterning steps.

In this chapter, I use light as a stimulus to create catechol-based patterns for surface functionalization. The uniquely versatile reactivity and binding capabilities of the catechol moiety allow the creation of spatially defined microarrays containing organic, inorganic and biological components. In the first part of this chapter, I will describe the pairing of a light-mediated attachment strategy with a facile, acid-labile deprotection catechol chemistry to allow complex patterning and activation of species including catechols. The second part focuses on the patterning of photocaged catechol species, which allows the creation of arbitrary patterns via irradiation with light. Using this photo-deprotection strategy, I will demonstrate that the coordination, oxidation and chelation-based prongs of reactivity can be controlled to yield versatile patterning.

II ATRA-based patterning of alkenes and protected catechols

1. Introduction

Fors *et al* recently pioneered a photomediated strategy for the polymerization of methacrylate monomers in solution[40] and on silica substrates.[41] The short excited-state lifetime of the Ir(ppy)$_3$ photocatalyst enables spatiotemporal control over reactivity and the visible light absorbance spectrum allows low energy irradiation to be used. Stephenson *et al* demonstrated that similar iridium catalysts mediated atom-transfer radical addition (ATRA) reactions mediated by visible light.[42,43]

We hypothesized that the combination of these two chemistries would enable the photopatterning of a diverse range of molecules containing terminal alkene substituents starting from an alkyl bromide functionalized surface (Figure 2a). This would allow the creation of a variety of functional surfaces depending on the nature of light exposure. Upon irradiation through a binary photomask, surface modification would occur only in irradiated regions (Figure 2b). Non-uniform light intensity would allow the creation of complex gradients where the chemical concentration on the surface would be proportional to the dosage of incident light (Figure 2c).[44] Finally, the non-destructive nature of the patterning procedure would result in residual, reactive alkyl bromide moieties in non-irradiated regions, allowing sequential patterning of diverse components. The combination of these features and the benign nature of the irradiating light, would allow the patterning of multifunctional surfaces of graded chemical compositions.

The modularity of this system should allow the patterning of a diverse library of alkenes, however, the facile reactivity of catecholic functionalities with radical species was a concern. In order to address this issue, we utilized a triethylsilyl-protected species which can be easily deprotected upon treatment in dilute acidic solution.

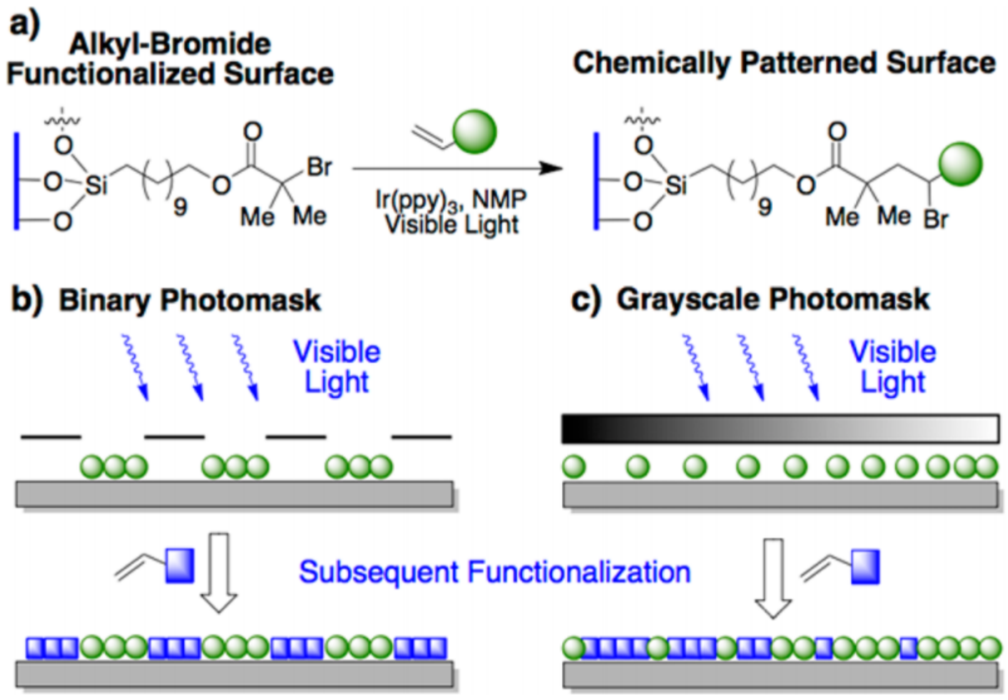

Figure 2: Patterning and backfilling using ATRA chemistry for surface functionalization.

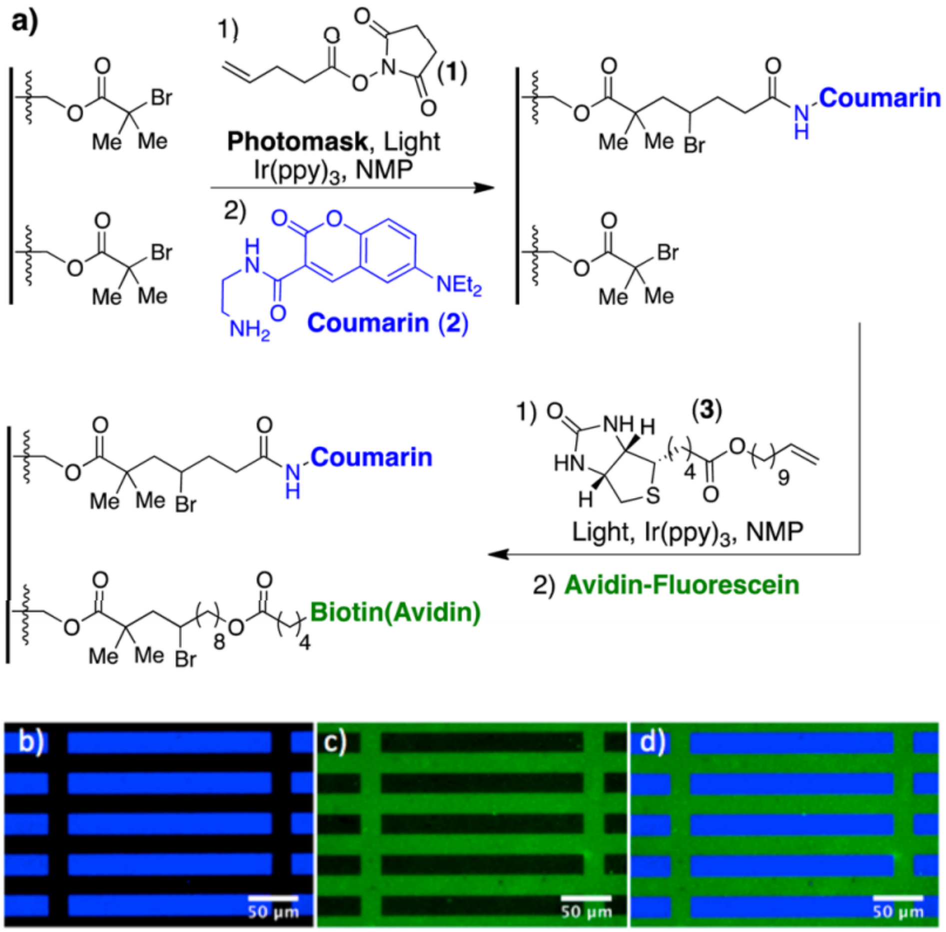

Figure 3: Fabrication of distinct, orthogonal chemical patterns created by irradiation through a binary photomask.

2. Results and discussion

We first looked to use a diagnostic model system which could interrogate the scope of this ATRA patterning chemistry. To this end, we investigated the patterning of a reactive N-hydroxysuccinimide (NHS) ester synthesized from 4-pentenoic acid (1), which allows subsequent functionalization with amino-functional molecules. The starting substrate for all experiments described in this section is a silicon oxide wafer that has been functionalized with an alkyl bromide via silanziation chemistry. On this substrate was deposited a solution of the alkene-functional activated ester, **1,** and the Ir(ppy)$_3$ photocatalyst in N-methylpyrrolidinone (NMP). This substrate was covered with a binary photomask (20 x 200 μm rectangles) and irradiated with a 50 W fluorescent lamp for 30 min in an inert atmosphere (Figure 3a). The substrate was then rinsed thoroughly in the dark to remove residual, unreacted alkene, and to mitigate any ambient light functionalization. These patterned substrates were then treated with amino-functional coumarin (2), fluorescein, or rhodamine dyes and visualized via a fluorescent microscope outfitted with a suitable filter cube. Figure 3b clearly shows that functionalization occurred only where the light reached the substrate and reveals that good spatial resolution can be obtained using this photomediated ATRA reaction. A separate mask was used to pattern features down to about a micron, nearing the optical resolution limit for this technique. (Figure 4)

The nondestructive nature of this patterning chemistry allows the preservation of reactive alkyl bromide sites in the non-irradiated regions. To demonstrate that these chain ends were still active, a secondary patterning step was carried out. The substrate was exposed to an alkene-functional biotin molecule and irradiated in the absence of photomask. The wafer was incubated with a commercial FITC-labeled avidin. Powerfully, this treatment resulted in fluorescence in only the previously unexposed regions (Figure 3c). This results demonstrates that the initial patterning step was carried out to high yield, and that the unexposed alkyl bromides are conserved to a high degree.

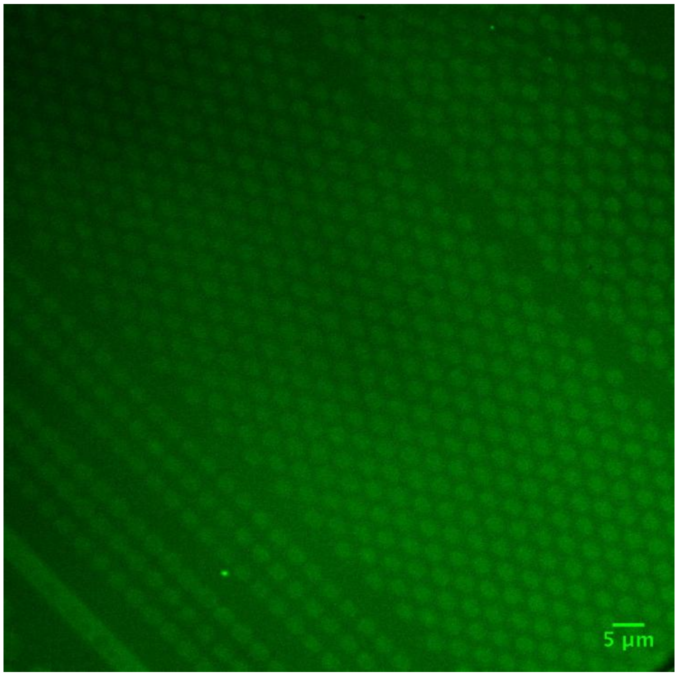

Figure 4: Features can be patterned with a resolution of approximately 1 micron.

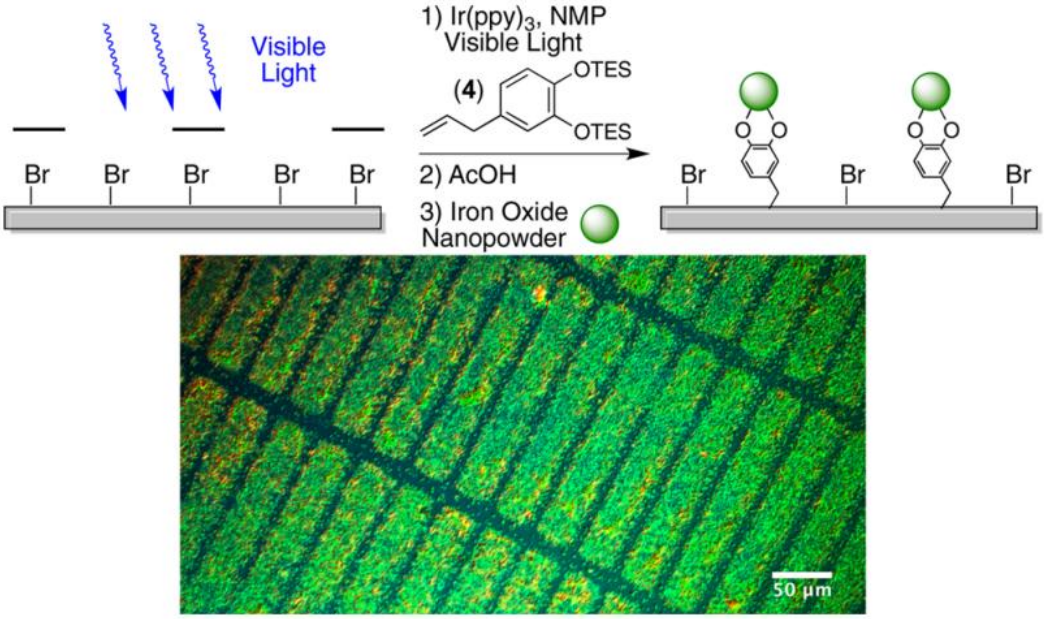

Figure 5: Selective adsorption of iron oxide nanoparticles on substrates patterned with catechol species.

After demonstrating the viability of this ATRA chemistry for the patterning and backfilling of activated ester and biotin alkenes, we moved to show that alkenes with catecholic moieties could be patterned. An identical procedure was used to that described above, replacing the activated ester alkene (1) with a silyl-protected catechol (4). The silyl ethers were cleaved by soaking in a 0.01 M HCl solution for 30 minutes, as described in a previous publication.[39] Following deprotection, the substrate was immersed in an ethanolic suspension of iron oxide nanoparticles. After rinsing, the surface was visualized with polarized optical microscopy to reveal templated assembly of nanoparticles in the patterned regions. (Figure 5)

III. Using photolabile protecting groups to activate catechols

1. Introduction

The previous section demonstrates the use of a novel photomediated technique to selectively pattern protected catechol species, which can then be activated by treatment in a dilute acidic solution. This allows fine control over patterns and gradients, but is not conducive to sequential, selective activation of patterned species. In this section, I build upon the work described earlier, using a photomediated deprotection strategy to selectively decage areas of surface-bound catechols. Furthermore, I broaden the scope of reactive molecules, demonstrating that organic, metallic, and metal oxide particles can be attached by exerting control over the reactive state of unprotected catechols.

Ortho-nitrobenzyl (*o*-NB) alcohol derivatives are a well-established photocaging chemistry[45,46] with vast potential in materials science.[47] Upon irradiation with UV light, an *o*-nitrobenzyl alcohol derivative undergoes photoisomerization to the corresponding onitrosobenzylaldehyde. (Scheme 1) First demonstrated for carboxylic acids, the chemistry was then expanded to amines[48] and phenolic compounds.[49]

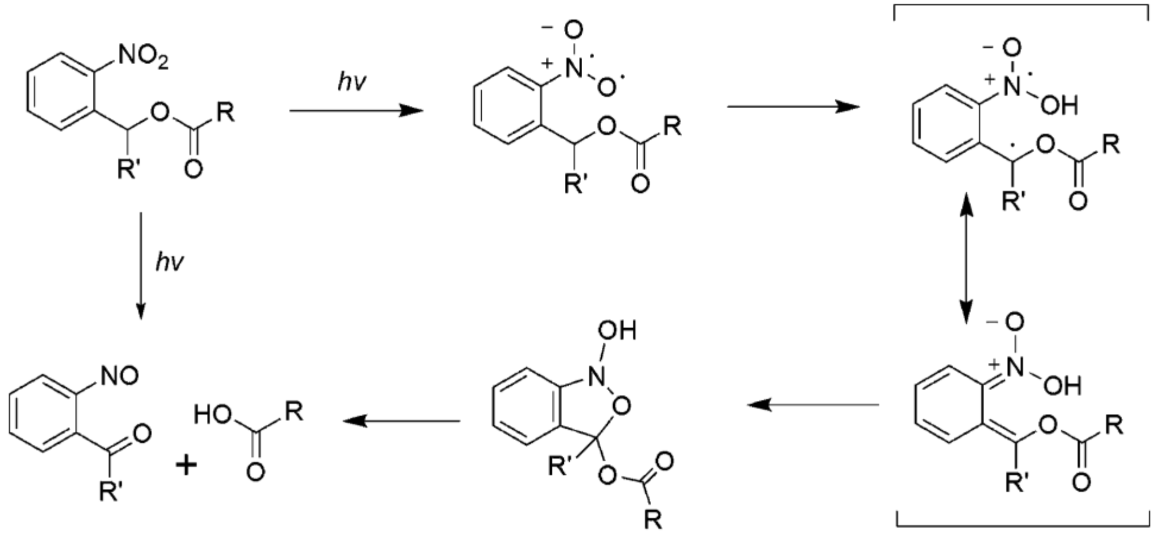

Scheme 1: Decaging of *o*-nitrobenzyl-protected carboxylic acids

Allen *et al* used *o*-NB protecting groups to selectively activate catecholic species within metal-organic frameworks.[50] Nishidi *et al* demonstrated that *o*-NB photocaging chemistry could be used to deprotect catechol species along the backbone of acrylamides.[51] In this work, basic polymer solutions were irradiated under a mercury light. Deprotection was accompanied by rapid auto-oxidation under these conditions, yielding adhesive hydrogels. This is a compelling demonstration of the activation of catechols, however, this work does not take advantage of the spatiotemporal control offered by the use of light as a stimulus.

I have expanded upon this work, using *o*-NB chemistry to demonstrate spatially resolved decaging of surface-immobilized catechol species. The versatile reactivity allows the micron-scale arrangement of components with potential use for catalysis, cell manipulation, sensing, and other applications.

2. Results and discussion

Model compound **1** was synthesized to demonstrate that *o*-NB protected catechols could be deprotected without degradation. (Scheme 2) A methanolic solution of **1** was irradiated under a mercury lamp at 365 nm (4.6 mW/cm) in an NMR tube, and the kinetics of deprotection were monitored via NMR. (Figure 6). In 1 mM solutions, 95% deprotection was observed after 2 hours, with quantitative conversion after 3 hours. The decrease in reaction kinetics with time is not surprising, as the liberated *o*-nitrosobenzaldehyde has a similar chromophore to the protected species, therefore decreases the effective light intensity reaching the target molecule as conversion progresses. It should also be noted that the addition of an aldehyde scavenger, semicarbazide hydrochloride, was found to be essential to prevent dimerization of the liberated aldehyde species and drive the deprotection to quantitative yield. On surfaces and in flow cells, these high molar absorptivity byproducts can be washed into the bulk, and deprotection is expected to proceed rapidly.

Two methods were used to attach photocaged catechols to surfaces: direct silanization, and post-functionalization of wafers reacted using the ATRA chemistry described in the previous section.

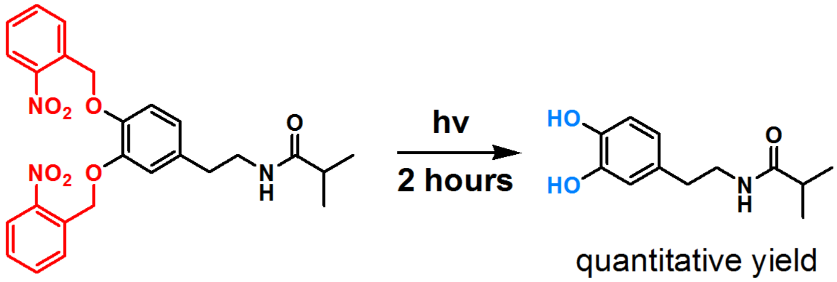

Scheme 2: Deprotection of o-NB protected catechol model system by irradiation with mercury lamp with 365 nm cutoff (4.6 mW/cm^2).

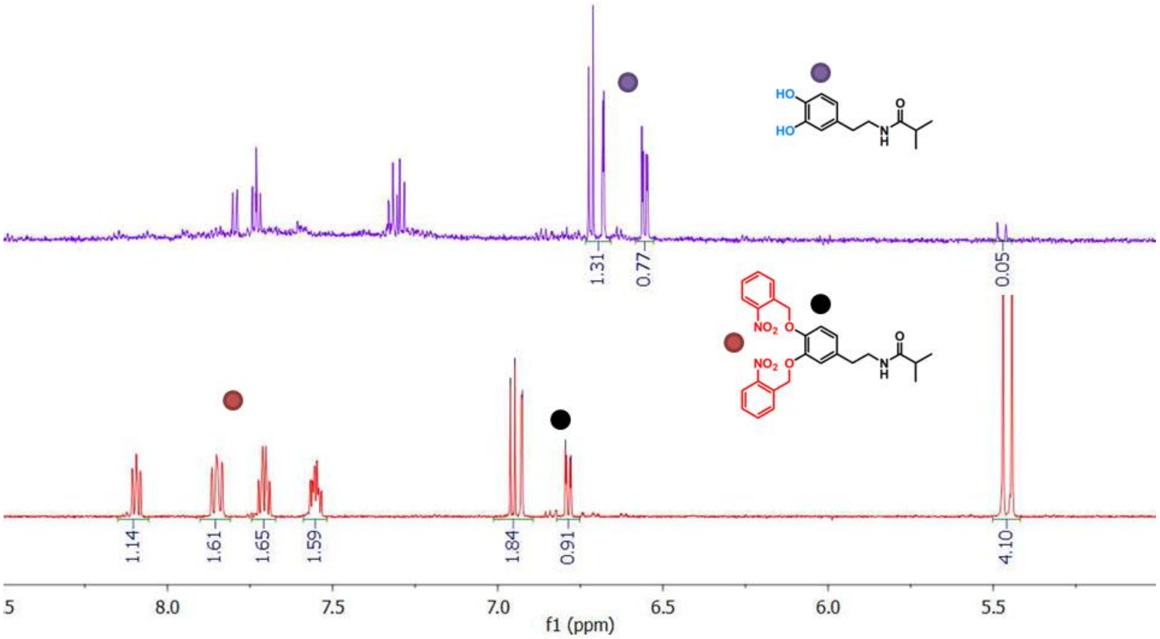

Figure 6: NMR spectra of aromatic region of o-NB protected model compound (bottom), and after 3 hours irradiation (top).

Strategy 1: Trichlorosilane

In the first method, a trichlorosilane-functional, potocaged catechol was synthesized via hydrosilation of o-NB protected eugenol. (Scheme 4). This molecule was attached to Piranha-cleaned glass and quartz slides via a silanization reaction. Functionalization was monitored using contact angle measurements, with the contact angle shifting from <10° for the bare quartz, to 72±2° after silanization in toluene for 16 hours. X-ray photoelectron spectroscopy (XPS) was used to confirm attachment. *In situ* deprotection was investigated with UV-visible spectroscopy. A slow scan speed was necessary to achieve adequate resolution due to the low absorbance of the near monolayer film. Figure 7a shows the characteristic solution spectra from an *o*-NB protected precursor and a silyl-protected catecholic precursor to the silanizing reagent. Characteristic is the much increased molar absorptivity of the o-NB derivative (18,250 M^{-1} cm^{-1}) verus the silyl-protected derivative (2500 M^{-1} cm^{-1}), as well as a shift in λ_{max} from 268nm to 280nm. Figure 7b shows the evolution in absorbance of a *o*-NB catechol silanized quartz slide as a function of irradiation time (4.6 mW/cm^2 UV lamp described in Experimental). Notable is a monotonic decrease in peak absorbance accompanied by a redshift in λ_{max} characteristic of conversion of loss of o-NB functionality. The reaction was essentially complete after 30 minutes. After irradiation, contact angle shifted to 52±2°, as nonpolar nitrobenzyl functionality was cleaved and replaced with phenols.

Caged and decaged samples were monitored via X-ray photoelectron spectroscopy to confirm deprotection, as shown in Figure 8. Before irradiation, samples showed a strong nitrogen 1s peak at a binding energy of 406 eV, characteristic of nitro functionality. After 30 minutes, the peak at 406 showed complete attenuation, replaced by a small peak at 400 eV, attributed to adventitious environmental nitrogen species.

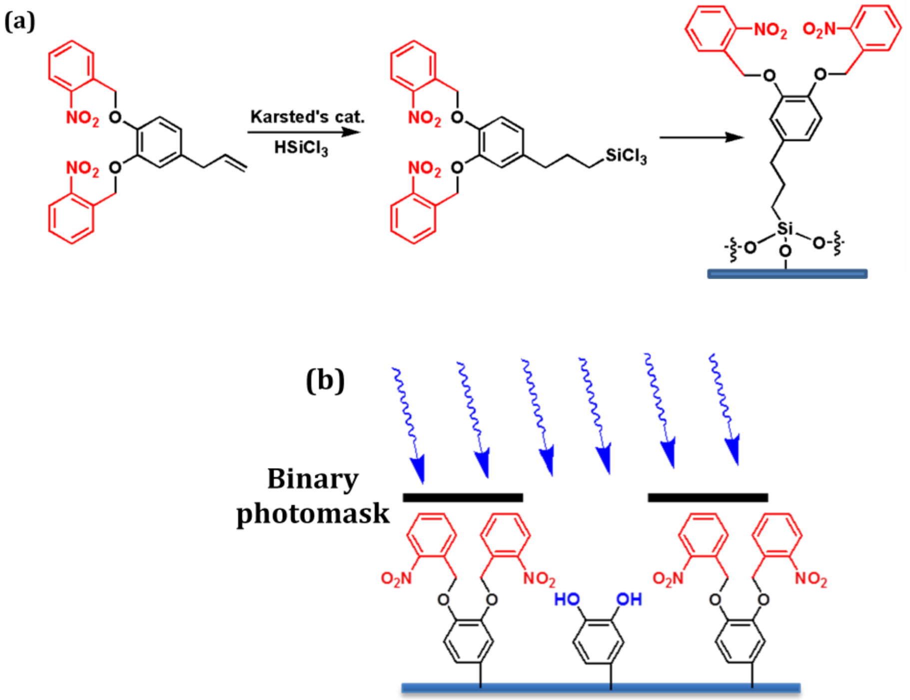

Scheme 3: (a) Synthesis and surface immobilization of o-NB protected trichlorosilane-fucntional eugenol. (b) Cartoon showing deprotection in irradiaded regions.

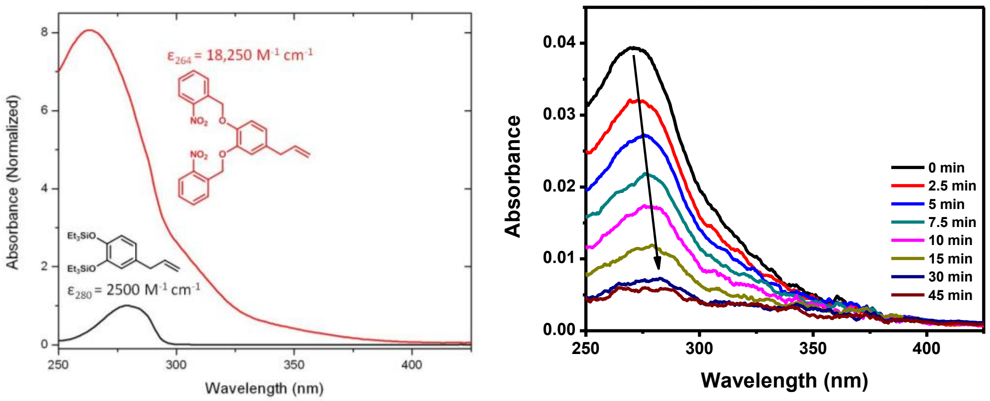

Figure 7: (a) UV-vis absorption spectra of o-NB protected eugenol and silyl-protected eugenol, showing key difference in λ_{max} (272 vs. 280 nm), as well as molar absorptivity. (b) Absorption spectra of o-NB eugenol immobilized on quartz slide during irradiation.

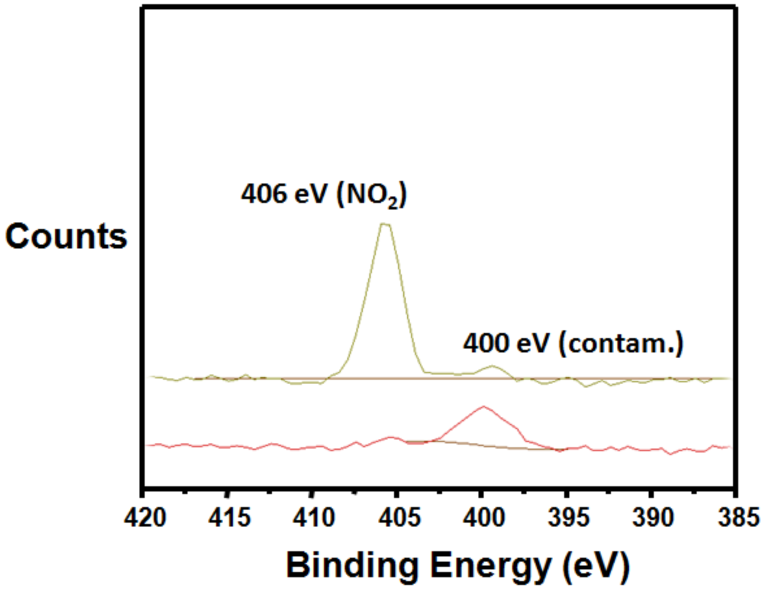

Figure 8: X-ray photoelectron spectra of the N 1s region before (yellow) and after (red) 30 minutes irradiation.

Strategy 2: Atom transfer radical addition

The second method was based on the ATRA chemistry demonstrated in the previous section. This approach was adopted to provide greater versatility and tether length to the system, to allow more robust attachment of nanoparticles with small radii of curvature, to maximize stronger, multifunctional attachment. As opposed to the patterned irradiation during functionalization demonstrated earlier, in this case, +-NB protected catechols were functionalized uniformly on the substrate, and activated in a patterning step using irradiation through a patterned photomask. Alkyl bromide-functionalized silica substrates were reacted with NHS-alkene (**1**), followed by subsequent functionalization with *o*-NB protected dopamine (Figure 9) in dry solvent. A grazing angle attenuated total reflectance attachment (Harrick GATR) was used to characterize each step of the functionalization and deprotection, on Si surfaces (Figure 9). The black trace shows the Si-background subtracted spectrum of the alkyl bromide functionalized initiator layer, with characteristic carbonyl ester stretch at 1745 cm^{-1}. Subsequent functionalization with the NHS-alkene is confirmed by the appearance of distinctive peaks at 1815 and 1786 cm^{-1}. After functionalization with o-NB dopamine, these carbonyl stretches subsided and were replaced by an aromatic C-C stretch at 1512 cm^{-1} and an symmetrical NO_2 stretching vibration at 1335 cm^{-1} that attenuates after 30 minutes blanket irradiation. As the alkyl bromide substrates are nonpolar, no significant difference in water contact angle could be tracked during the functionalization process.

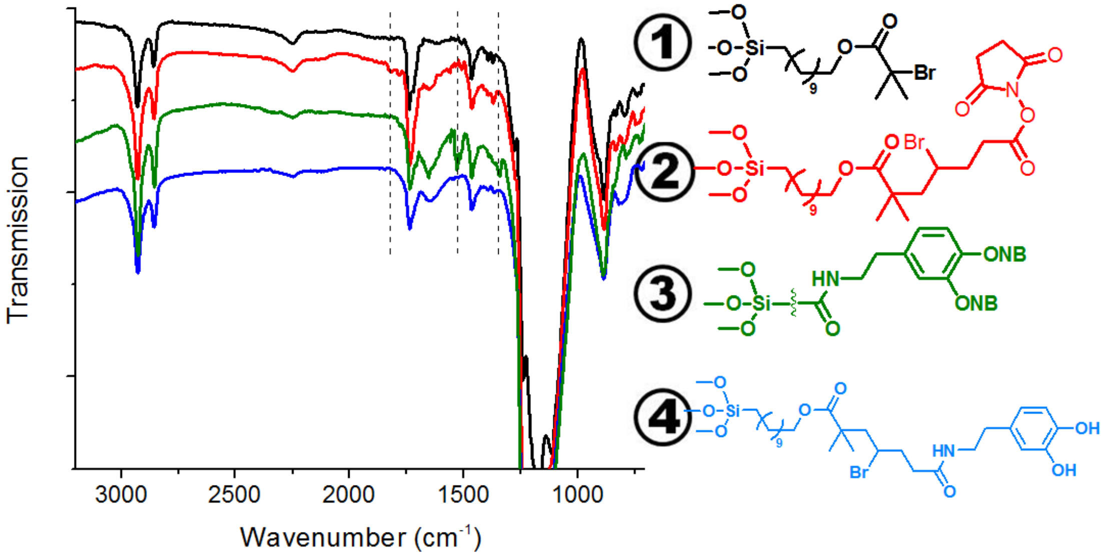

Figure 9: Attenuated total reflectance-infrared spectroscopy (ATR-IR) characterization of silicon wafers after functionalization with alkyl bromide iniator (1), reaction with NHS-alkene (2), reaction with o-NB dopamine (3), and deprotection using UV irradiation.

The methods described above demonstrate that o-NB protected monolayers can be created via a variety of approaches. For the sake of continuity, the results described below have all been carried out on substrates prepared using the second photomediated method described, building upon the ATRA chemistry described in the first section of this chapter. Substrates were irradiated through a binary photomask with clear 20x200 μm rectangles for 30 minutes sandwiched between a methanolic solution of semicarbazide hydrochloride. Samples were rinsed extensively with methanol and dried thoroughly before functionalization.

Initial binding studies investigated the adsorption of commercial titanium dioxide nanoparticles (Sigma-Aldrich, Titanium(IV) oxide, anatase, diameter <25 nm). These have been demonstrated previously to bind coordinatively and with high affinity to catechol species in solution. (Chapter 2). Substrates were stacked on edge in a dilute, acidic nanoparticle solution for 30 minutes with mild shaking, followed by sonication in acidic solution for 15 minutes to remove settled nanoparticles. Samples were visualized through a variety of optical techniques. Figures 10a and b show micrographs of patterned particles, confirming selective adsorption in irradiated regions.

The susceptibility to oxidation opens several pathways to surface functionalization. Catechols serve as reducing agents for metal salts such as Ag^+ and Cu^{2+}. This reduced metal subsequently serves as a template to catalyze further metal reduction. This strategy was employed to selectively pattern silver nanoparticles in irradiated regions. Patterned rectangles are evident via optical microscopy. Figure 11. Secondary ion mass spectroscopy (SIMS) shows enrichment of silver in irradiated regions. Scanning electron microscopy confirms the formation of nanoparticles (*diameter: 20-40 nm).*

Similarly, irradiated substrates were soaked in a $Cu^{2=}$ solution with and without the addition of an external reducing agent. In the presence of 0.1 M hydrazine hydrate, a copper layer blanketed the surface. In the absence of hydrazine, decaged catechols template adsorption and reduction in irradiation regions. (Appendix D.1)

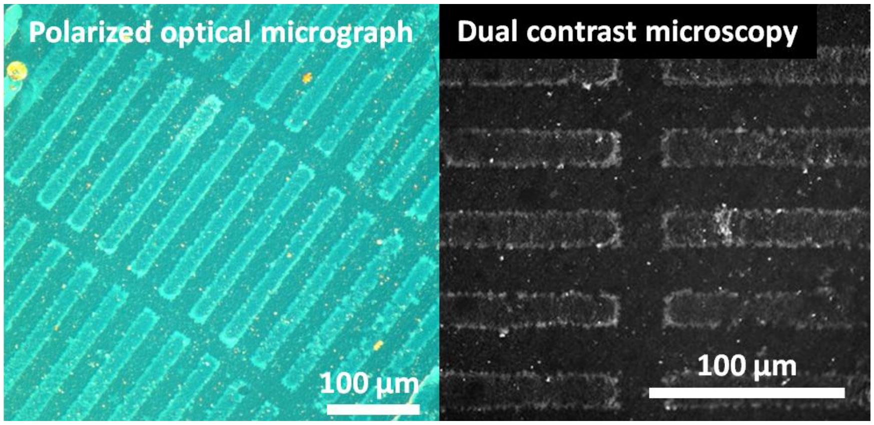

Figure 10: (a) Reflected light optical micrograph and through a cross-polarization filter and (b) dual contrast micrograph showing TiO_2 adsorption in deptrotected regions.

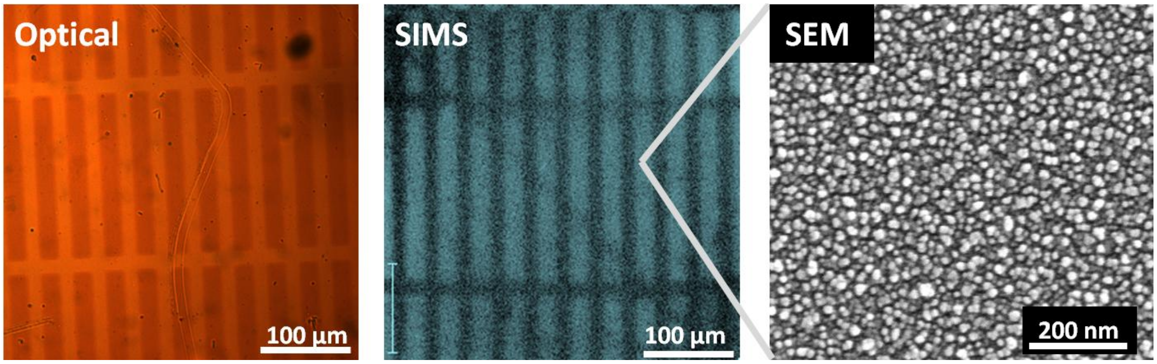

Figure 11: (a) Optical micrograph showing silver precipitation in irradiated regions. (b) Secondary ion mass spectroscopy image of silver localization. (c) Scanning electron micrograph of 20-30 nm diameter silver nanoparticles formed in deptrotected regions.

The versatile reactivity of quinones enables patterning with a variety of nucleophilic species. Patterned, deprotected substrates were treated with a solution of sodium periodate to oxidize catechols to quinones, followed by treatment with nucleophiles. To demonstrate this capability, hydrophilic and hydrophobic species were immobilized. An amino-functional poly(ethylene glycol) was reacted at 50°C for 16 hours. The substrate was sonicated extensively in chloroform to remove adsorbed, unreacted species. A faint pattern in the irradiated regions was seen via reflected polarized light microscopy. The attached PEG leads to a drastic different in hydrophilicity between the patterned and unpatterned regions, which is clearly visualized by the creation of a breath figure, as shown in Figure 12. Heights of adsorbed polymers were determined to be 1.9 +/- 0.4 nm by stylus profilometry in the dry state.

Deprotected, oxidized patterns were treated with 1H,1H, 2H, 2H-perfluorooctanethiol to demonstrate that quinones could be reacted with a different nucleophile bearing hydrophobic functionality. In this case, the breath figure shows an inverse wetting, as the patterned fluorinated regions are more hydrophobic than the unpatterned regions. Attachment was verified via XPS, as a F 1s signal is evident in the patterned species at a binding energy of 689 eV. (Figure 13).

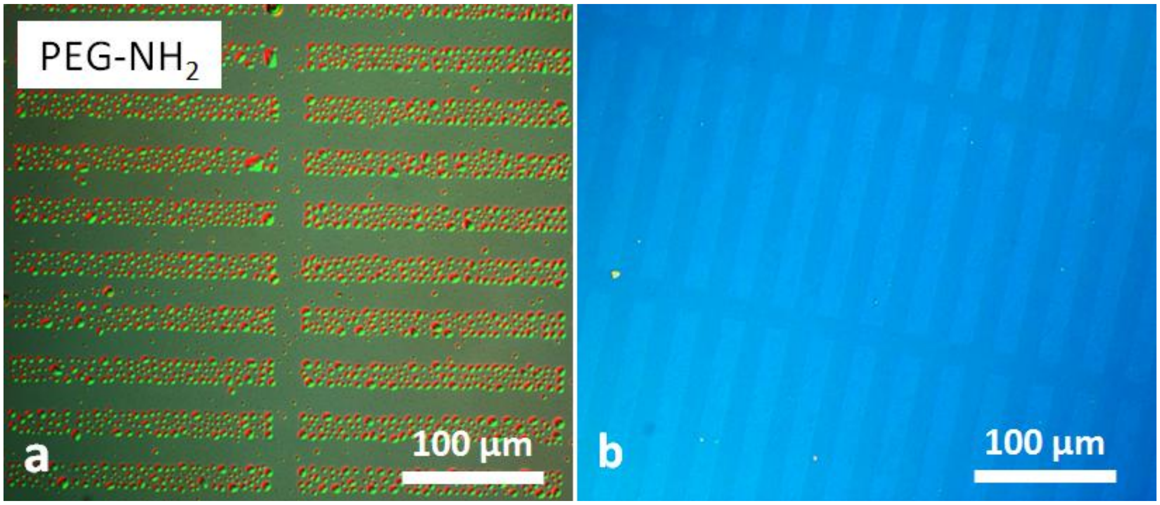

Figure 12: (a) Polarized optical micrograph taken of breath figure formed after immobilization of PEG-NH$_2$ to deprotected and oxidized catechols. (b) Polarized optical micrograph showing height difference upon functionalized.

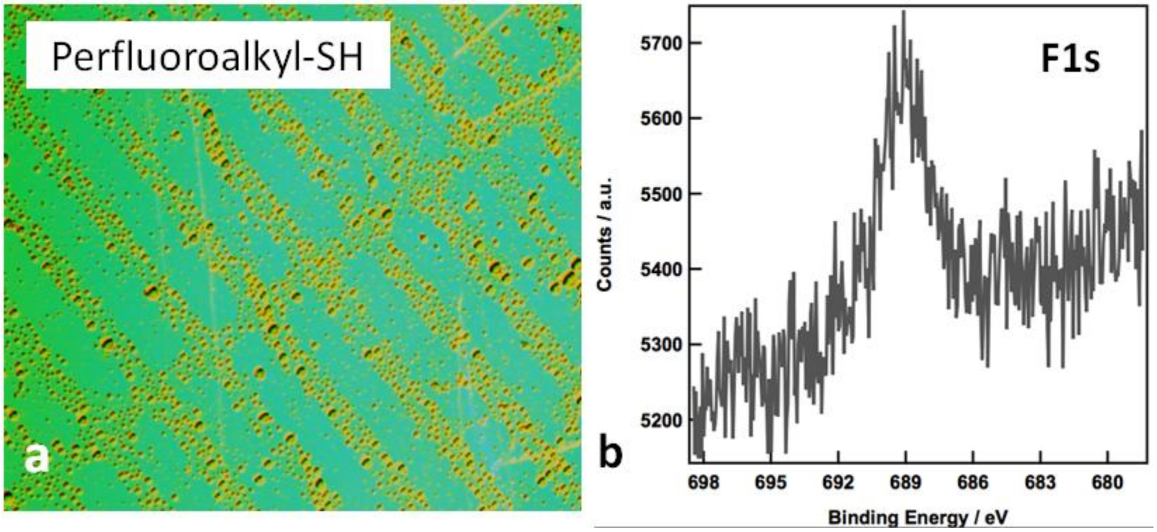

Figure 13: (a) Polarized optical micrograph taken of breath figure formed after immobilization of perfluoroalkane-SH to deprotected and oxidized catechols. (b) High resolution XPS of F 1s region, showing fluorine signal after attachment.

Finally, the coordination capability of catechols can also be demonstrated by patterning with substituents which exhibit increased or quenched fluorescence upon coordination with catechols. In the former case, the deprotected substrate is treated with a pH 10 solution of 1:2 $EuCl_3$:2-thenoyltrifluoroacetone. (Figure 11) These components form a ternary complex with catechol that shows a characteristic emission at 612 nm in solution, corresponding to the $^5D_0$ to $^7F_2$ transition.[52] Using appropriate filters in a confocal fluorescence microscope, this patterned fluorescence can be observed after soaking and rinsing the substrate. Catechols are known to strongly quench the fluorescence of quantum dots and ZnO species. CdSe@ZnS quantum dots capped with hexadecanethiol with peak absorption of 560 nm and a peak emission of 575 nm were purchased from OceanNanoTech LLC. A solution of quantum dots in hexane was spin coated onto the substrate and dried. Patterned regions show quenched flouresence, while protected regions fluoresce strongly, as shown in Figure 12.

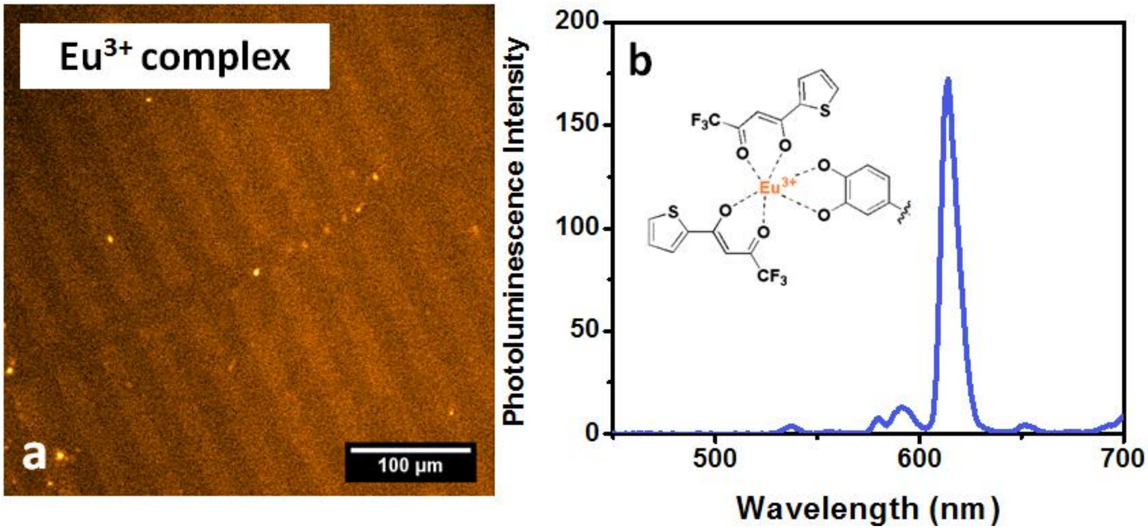

Figure 14: Fluorescence in ternary catechol-Eu^{3+}-2-thenoyltrifluoroacetone complexes.

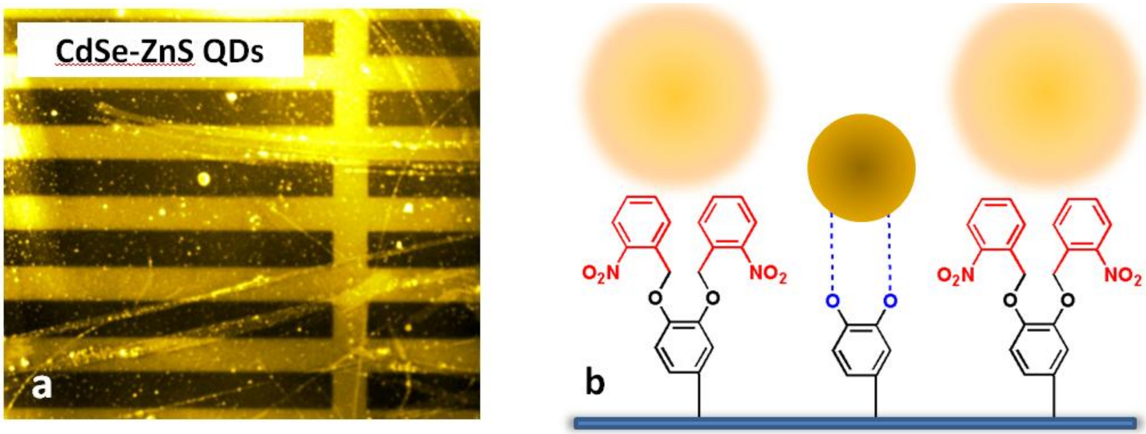

Figure 15: Quenched fluorescence of CdSe@ZnS quantum dots in regions of deprotected catechols.

IV. Conclusions

In this chapter, two photo-mediated approaches to patterned catechol arrays are demonstrated. In the first, Ir(ppy)$_3$ is used to catalyze the reaction of a variety of terminal alkenes with surface-immobilized alkyl bromide intiators. This concept was demonstrated using an NHS-alkene, visualized by reaction with amino-functional fluorescent dyes. This strategy is both non-destructive and relatively benign, allowing backfilling of unreacted initiators and a broad substrate scope. I show that triethylsilyl-protected eugenol can be patterned and deprotected by treatment in dilute acidic solution, and that this surface functionalization allows the template adsorption of iron oxide nanoparticles.

To further demonstrate the chemical versatility of catechol species, I describe a second light-mediated patterned strategy in which protected catechols are decaged by irradiation with light. This facile photodeprotection strategy is a viable strategy to exhibit spatiotemporal control over catecholic reactivity. Immobilization and deprotection is characterized via a variety of surface spectroscopic techniques. Deprotected regions selectively bind inorganic nanoparticles, precipitate noble metals, react with nucleophilic species, and coordinate to metal salts.

V. Experimental

Materials and Methods

All reagents were purchased from commercial sources and used without further purification unless otherwise stated. Triethylamine was dried by distillation and stored over molecular sieves. ATRA patterned steps were carried out in a nitrogen filled dry-box. N-methylpyrrolidone (NMP) was degassed by freeze-pump-thaw prior to being taken into the glovebox.

Instrumentation

^{1}H and ^{13}C NMR spectra were recorded using a Varian 600 MHz spectrometer with the solvent signal as internal reference. A HDX Double-Brite Pro Grade 26-Watt Fluorescent Work Light, which was purchased from The Home Depot, was used as the light source. Bulk FT-IR spectra were obtained using a Thermo-Nicholet Avatar-330 IR spectrometer with a single-bounce attenuated total reflection attachment (ATR) (diamond crystal). Grazing-angle FT-IR spectra were obtained using a Harrick VariGATR attachment, with an incident angle of 65°. Fluorescence micrographs were obtained with an Olympus BX51 microscope equipped with a Retiga 2000R camera from Qimaging. Optical micrographs were captured with a Nikon Elipse E600 microscope. Photomasks S3 containing transparent rectangles measuring 2.5 mm X 250 mm and 20 mm X 200 mm were purchased from Photronics, Inc. A HEBS5N grayscale lithography calibration mask was obtained from Canyon Materials, Inc. The grayscale mask contained regions of different features including prisms of variable slope, squares of varying optical density, tapered structures, refractive lenslet (positive and negative), refractive microlenses (positive and negative) and linear gradients. X-ray photoelectron spectroscopy (XPS) measurements were performed on an Axis UltraXPS system (Kratos) with monochromatic AI KR X-ray source (1486.6 eV) operating at 225 W under 7 x 10^{-9} Torr vacuum, and pass energy of 80 eV. The energy resolution was set at 0.1 eV with a dwell time of 100 ms. The spectra were analyzed using CasaXPS v.2.3.12 software. Scanning electron microscope (SEM) images were acquired using an FEI XL30 Sirion FEG digital electron scanning microscope.Secondary ion mass spectroscopic (SIMS) measurements were acquired with a Physical Electronics 6650 Quadropole instrument.PEG brush attachment was quantified with an AMBios XP-100 profilometer. Samples were scanned over a length of 100 μm with a force of 0.8 mg at a rate of 0.1 mm/sec.UV-visible spectroscopic measurements were acquired on a Shimadzu UV3600 UV-Nir-NIR spectrometer. Measurements were obtained in Absorption mode, with a resolution of 1 cm^{-1}, Very Slow scan rate, and a working range of 250-450 nm.

Chemical Synthesis

The synthesis of 4-pentenoic acid N-succinimidyl ester (NHS-ester), N-(2-Aminoethyl)-7-(diethylamino)-2-oxo-2H-chromene-3-carboxamide (amine-functionalized coumarin dye), alkene-functionalized biotin, triethylsilane-protected eugenol, amine-functionalized fluorescein dye, and 11-(Trichlorosilyl)undecyl 2-bromo-2-methylproanoate (alkyl bromide initiator) were synthesized as described.[53]

2-(3,4-bis(2-nitrobenzyloxy)phenyl)ethanamine hydrochloride (o-NB dopamine):

N-boc dopamine was synthesized following a literature procedure.[54] A 25 mL 3-neck round bottom flask, equipped with a magnetic stirbar and purged with argon, was charged with N-boc dopamine (200 mg, 0.789 mmol) and cesium chloride (1000 mg, 3.3 mmol) and dissolved in 7 mL acetone. *o*-nitrobenzyl bromide (375.3 mg, 1.73 mmol) was added dropwise through a syringe and the reaction mixture was stirred at room temperature for 2 hours. The residue was concentrated under vacuum and recrystallized from ether to yield the boc-protected version of the titular compound. Boc protection was removed by stirring in 4M HCl for 1 hour. The solution was concentrated filtered, and dried to yield the desired product. (298 mg, 82%). ^{1}H NMR (600 MHz, D_2O): δ 2.90 (t, 2H), 3.18 (t, 2H), 5.48 (d, 2H), 6.87-7.05 (m, 3H), 7.54 (m, 2H), 7.70 (m, 2H), 7.89 (m, 2H), 8.10 (m, 2H).

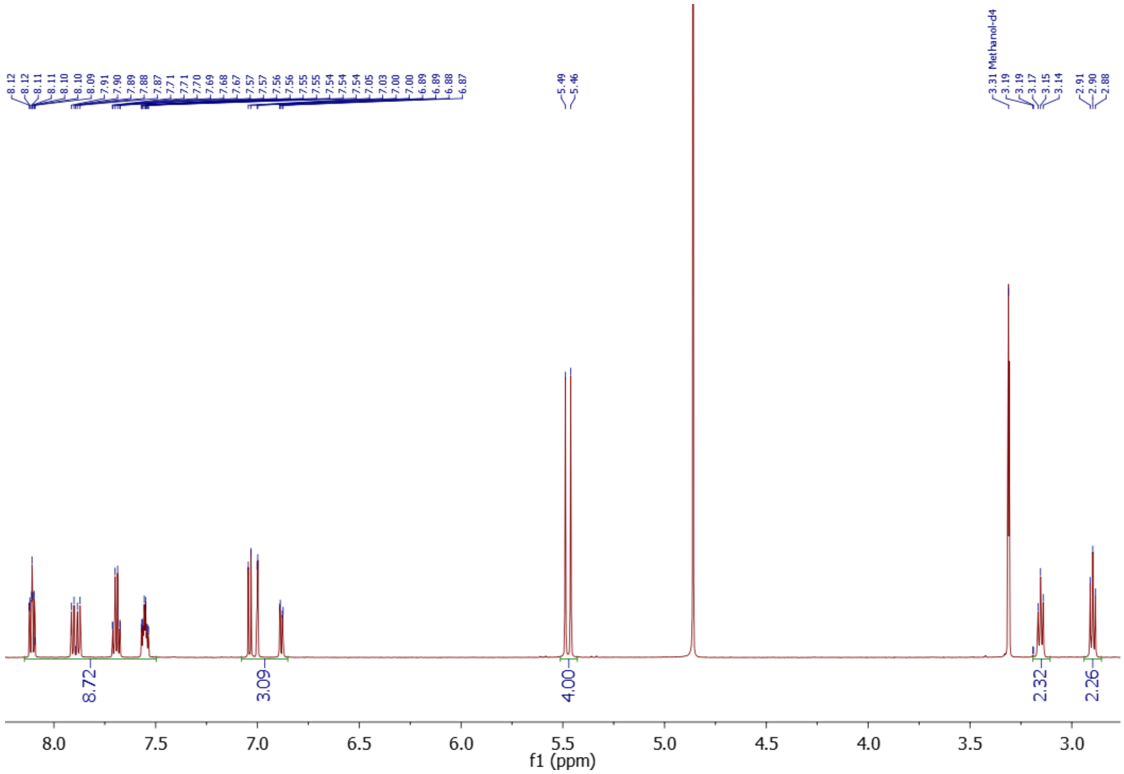

1-((2-(2-nitrobenzyloxy)-5-allylphenoxy)methyl)-2-nitrobenzene

A 10 mL Schlenk flask, equipped with a magnetic stir bar and a rubber septum, was evacuated and backfilled with argon and charged with triethylsilane-protected eugenol (500 mg, 1.315 mmol), Amberlyst acidic resin (280 mg, 1.315 mmol sites) in 3 mL acetone. The deprotection was monitored via TLC and the deprotection reaction was complete after 30 minutes. The resin was filtered and the solution concentrated. To this crude oil was added *o*-nitrobenzyl bromide (560 mg, 2.64 mmol) and potassium carbonate (500 mg) in 2 mL dry acetone. The reaction was stirred overnight under argon atmosphere. The residue was concentrated under vacuum and recrystallized from ether to yield a yellow solid. (271 mg, 49%). ^{1}H NMR (600 MHz, $CDCl_3$): δ 3.307 (d, 2H), 5.06 (m, 2H), 5.53 (d, 4H), 5.89 (m, 1H), 6.76-6.90 (m, 3H), 7.47 (m, 2H), 7.65 (m, 2H), 7.97 (m, 2H), 8.15 (m, 2H).

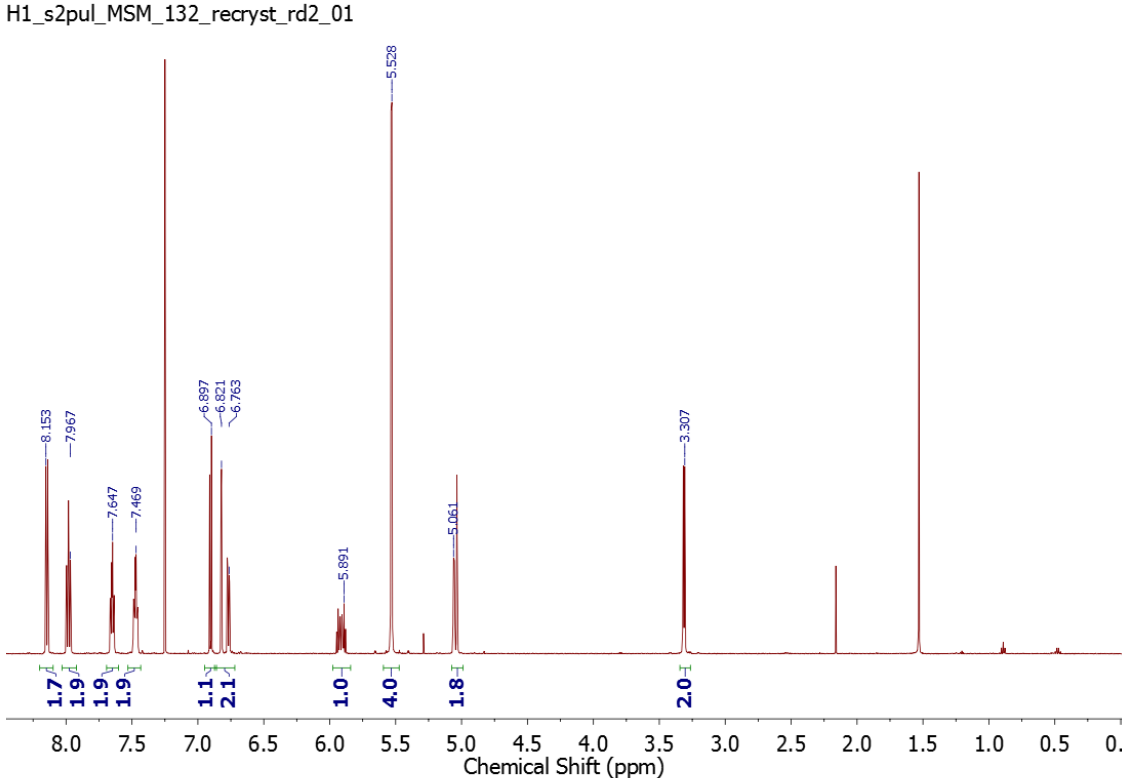

(3-(3,4-bis(2-nitrobenzyloxy)phenyl)propyl)trichlorosilane

A 10 mL schlenk flask, equipped with a magnetic stir bar and a rubber septum, was evacuated and backfilled with nitrogen and charged with 1-((2-(2-nitrobenzyloxy)-5-allylphenoxy)methyl)-2-nitrobenzene (72 mg, 0.169 mmol), trichlorosilane (171 µL, 1.69 mmol) and a solution of Karstedt's catalyst in xylene (2 µL, 2 wt% Pt in xylene). The solution was stirred at room temperature. Conversion was determined by ^{1}H NMR, and the reaction was found to go to completion in 2 hours. The reaction mixture was then concentrated under reduced pressure to give the title compound as a yellow solid. The compound was used directly without further purification. ^{1}H NMR (600 MHz, $CDCl_3$): δ 1.38 (d, 2H), 1.88 (quint, 2H), 2.71 (t, 2H), 5.58 (d, 4H), 6.76-6.90 (m, 3H), 7.47 (m, 2H), 7.65 (m, 2H), 7.97 (m, 2H), 8.15 (m, 2H).

Surface modification

Silicon substrates with 100 nm of oxide were purchased from Silicon Quest International. Quartz substrates were purchased from Ted Pella, Inc. Silicon substrates were purchased from Silicon Quest International. The substrates were diced into 1.5 cm x 1.5 cm squares (3cm x 3 cm for GATR and UV-vis measurements) and cleaned by sonication in acetone, followed by isopropyl alcohol, and finally deionized water. The wafers were then immersed in a piranha solution at 90℃ for 20 min. The substrates were then washed with copious amounts of deionized water, dried under a stream of nitrogen gas, and stored in a vacuum oven for 1 hour. After drying, the wafers were placed in petri dishes and covered with 30 ml of a solution containing the desired trichlorosilane in 250 ml of dry toluene (0.05% v/v) and 50 ml of dry triethylamine. The petri dishes were covered under a blanket of nitrogen and allowed to react overnight. Upon completion, the functionalized substrates were rinsed thoroughly with toluene followed by ethanol to remove the triethlyamine salts which precipitated during the reaction. The wafers were dried under vacuum and stored under ambient conditions.

Surface Irradiation

Patterning procedures for the ATRA chemistry are described.[53] Photodeprotection of *o*-nitrobenzyl-protected catechol substrates followed a similar procedure. A 50 mM solution of semicarbazide hydrochloride was pipette onto the functionalized substrate, which was then covered with a binary photomask containing 20 x 200 µm clear rectangles. The wafer was placed under an UV lamp (Black-Ray UV BenchLamp equipped with two Sylvania 15 W 350 Blacklight fluorescent tubes, λ = 365 nm, distance lamp-flask approx. 20 cm).

Surface Functionalization

After irradiation, silicon substrates were sonicated with methanol and water for 5 min. Wafers were placed in the appropriate solution. An example colloid functionalization is as such: a suspension of iron oxide nanopowder in ethanol, which was prepared by sonication of 20 mg of the nanopowder in 5 mL of EtOH for 1 hour. After 24 hours the substrate was removed from the suspension, washed 5 times with ethanol and visualized with optical microscopy. For nucleophile functionalization, the samples were first treated with a 50 mM aqueous solution of sodium periodate for 30 minutes to oxidize the exposed catechols. The resulting quinone-functional substrates were immersed in concentrated solutions of the desired nucleophile and heated at 60°C for 16 hours to ensure maximal functionalization. The substrates were then washed extensively by sonication in chloroform with several solvent changes for 1 hour.

VI. References

(1) Andruzzi, L.; Nickel, B.; Schwake, G.; Rädler, J. O.; Sohn, K. E.; Mates, T. E.; Kramer, E. J. *Surf. Sci.* **2007**, *601*, 4984–4992.

(2) Weinrich, D.; Jonkheijm, P.; Niemeyer, C. M.; Waldmann, H. *Angew. Chem. Int. Ed. Engl.* **2009**, *48*, 7744–7751.

(3) Kim, S. O.; Solak, H. H.; Stoykovich, M. P.; Ferrier, N. J.; Pablo, J. J. De; Nealey, P. F. **2003**, 411–414.

(4) Hannon, A. F.; Gotrik, K. W.; Ross, C. A.; Alexander-katz, A. **2013**.

(5) Ahn, S. J.; Kaholek, M.; Lee, W.-K.; LaMattina, B.; LaBean, T. H.; Zauscher, S. *Adv. Mater.* **2004**, *16*, 2141–2145.

(6) Ballav, N.; Schilp, S.; Zharnikov, M. *Angew. Chem. Int. Ed. Engl.* **2008**, *47*, 1421–1424.

(7) Khan, M. N.; Tjong, V.; Chilkoti, A.; Zharnikov, M. *Angew. Chem. Int. Ed. Engl.* **2012**, *51*, 10303–10306.

(8) Spruell, J. M.; Wolffs, M.; Leibfarth, F. a; Stahl, B. C.; Heo, J.; Connal, L. a; Hu, J.; Hawker, C. J. *J. Am. Chem. Soc.* **2011**, *133*, 16698–16706.

(9) Choi, S.; Newby, B. Z. **2003**, 7427–7435.

(10) Tasdelen, M. A.; Yagci, Y. *Angew. Chem. Int. Ed. Engl.* **2013**, *52*, 5930–5938.

(11) El Zubir, O.; Barlow, I.; Ul-Haq, E.; Tajuddin, H. a; Williams, N. H.; Leggett, G. J. *Langmuir* **2013**, *29*, 1083–1092.

(12) Orski, S. V; Poloukhtine, A. a; Arumugam, S.; Mao, L.; Popik, V. V; Locklin, J. *J. Am. Chem. Soc.* **2010**, *132*, 11024–11026.

(13) Gallant, N. D.; Lavery, K. a.; Amis, E. J.; Becker, M. L. *Adv. Mater.* **2007**, *19*, 965–969.

(14) Bao, C.; Zhu, L.; Lin, Q.; Tian, H. *Adv. Mater.* **2015**, 1–16.

(15) Waite, J. H. *Integr. Comp. Biol.* **2002**, *42*, 1172–1180.

(16) White, J.; Wilker, J. J. *Macromolecules* **2011**, *44*, 5085–5088.

(17) Chien, H.-W.; Kuo, W.-H.; Wang, M.-J.; Tsai, S.-W.; Tsai, W.-B. *Langmuir* **2012**, *28*, 5775–5782.

(18) Holten-Andersen, N.; Harrington, M. J.; Birkedal, H.; Lee, B. P.; Messersmith, P. B.; Lee, K. Y. C.; Waite, J. H. *Proc. Natl. Acad. Sci. U. S. A.* **2011**, *108*, 2651–2655.

(19) Menyo, M.; Hawker, C.; Waite, J. *Soft Matter* **2013**, *9*, 10314–10323.

(20) Springsteen, G.; Wang, B. *Tetrahedron* **2002**, *58*, 5291–5300.

(21) Pizer, R.; Babcock, L. *Inorg. Chem.* **1977**, *7*, 1677–1681.

(22) Okamoto, T.; Tanaka, A.; Watanabe, E.; Miyazaki, T.; Sugaya, T.; Iwatsuki, S.; Inamo, M.; Takagi, H. D.; Odani, A.; Ishihara, K. *Eur. J. Inorg. Chem.* **2014**, *2014*, 2389–2395.

(23) Yu, J.; Wei, W.; Menyo, M. S.; Masic, A.; Waite, J. H.; Israelachvili, J. N. *Biomacromolecules* **2013**, *14*, 1072–1077.

(24) Lee, H.; Scherer, N. F.; Messersmith, P. B. *Proc. Natl. Acad. Sci.* **2006**, *103*, 12999.

(25) Zhao, H.; Waite, J. H. *Biochemistry* **2005**, *44*, 15915–15923.

(26) Burzio, L.; Waite, J. *Biochemistry* **2000**, 11147–11153.

(27) Yu, M.; Hwang, J.; Deming, T. J. *J. Am. Chem. Soc.* **1999**, *121*, 5825–5826.

(28) Liu, B.; Burdine, L.; Kodadek, T. *JACS* **2008**, *128*, 15228–15235.

(29) Lee, Y.; Lee, S. H.; Kim, J. S.; Maruyama, A.; Chen, X.; Park, T. G. *J. Control. Release* **2011**, *155*, 3–10.

(30) Lee, H.; Dellatore, S. M.; Miller, W. M.; Messersmith, P. B. *Science* **2007**, *318*, 426–430.

(31) Scheidt, H. A.; Filip, C.; Turcu, R.; Bende, A.; Beck, S. **2013**.

(32) Dreyer, D. R.; Miller, D. J.; Freeman, B. D.; Paul, D. R.; Bielawski, C. W. *Chem. Sci.* **2013**, *4*, 3796.

(33) Sun, K.; Xie, Y.; Ye, D.; Zhao, Y.; Cui, Y.; Long, F.; Zhang, W.; Jiang, X. *Langmuir* **2012**, *28*, 2131–2136.

(34) Loget, G.; Wood, J.; Cho, K. *Anal. ...* **2013**.

(35) Liu, L.; Bromberg, V.; Singler, T. J. **2014**.

(36) Preuss, C. M.; Tischer, T.; Rodriguez-Emmenegger, C.; Zieger, M. M.; Bruns, M.; Goldmann, A. S.; Barner-Kowollik, C. *J. Mater. Chem. B* **2014**, *2*, 36.

(37) Gomes, J.; Grunau, A.; Lawrence, A. K.; Eberl, L.; Gademann, K. *Chem. Commun. (Camb).* **2013**, *49*, 155–157.

(38) Nishida, J.; Kobayashi, M.; Takahara, A. *J. Polym. Sci. Part A Polym. Chem.* **2013**, *51*, 1058–1065.

(39) Heo, J.; Kang, T.; Jang, S. G.; Hwang, D. S.; Spruell, J. M.; Killops, K. L.; Waite, J. H.; Hawker, C. J. *J. Am. Chem. Soc.* **2012**, *134*, 20139–20145.

(40) Fors, B. P.; Hawker, C. J. *Angew. Chem. Int. Ed. Engl.* **2012**, *51*, 8850–8853.

(41) Poelma, J. E.; Fors, B. P.; Meyers, G. F.; Kramer, J. W.; Hawker, C. J. *Angew. Chem. Int. Ed. Engl.* **2013**, *52*, 6844–6848.

(42) Wallentin, C.; Nguyen, J. D.; Finkbeiner, P.; Stephenson, C. R. J. **2012**.

(43) Nguyen, J. D.; Tucker, J. W.; Konieczynska, M. D.; Stephenson, C. R. J. **2011**, 4160–4163.

(44) Kley, E.; Thoma, F.; Zeitner, U.; Wittig, L.-C.; Aagedal, H. *Optoelectron. ...* **1998**, *3276*, 254–262.

(45) Barltrop, J.; Plant, J.; Schofield, P. *Chem. Commun.* **1966**, *22*, 822–823.

(46) Patchornik, A.; Amit, B.; Woodward, R. *J. Am. Chem. Soc.* **1964**, 6333–6335.

(47) Zhao, H.; Sterner, E. S.; Coughlin, E. B.; Theato, P. **2012**.

(48) Cameron, J.; Frechet, J. *J. Am. Chem. ...* **1991**, 4303–4313.

(49) Breitinger, H.; Wieboldt, R. *Biochemistry* **2000**, 5500–5508.

(50) Allen, C. a.; Cohen, S. M. *J. Mater. Chem.* **2012**, *22*, 10188.

(51) Nishida, J.; Kobayashi, M.; Takahara, A. **2013**, 8–11.

(52) Guo, J.; Ping, Y.; Ejima, H.; Alt, K.; Meissner, M.; Richardson, J. J.; Yan, Y.; Peter, K.; von Elverfeldt, D.; Hagemeyer, C. E.; Caruso, F. *Angew. Chem. Int. Ed. Engl.* **2014**, *53*, 5546–5551.

(53) Fors, B. P.; Poelma, J. E.; Menyo, M. S.; Robb, M. J.; Spokoyny, D. M.; Kramer, J. W.; Waite, J. H.; Hawker, C. J. *J. Am. Chem. Soc.* **2013**, *135*, 14106–14109.

(54) Liu, Z.; Hu, B.; Messersmith, P. *Tetrahedron Lett.* **2010**, *51*, 2403–2405.

6 Conclusions

I Summary

Marine organisms have inspired much research in the areas of wet adhesives, coatings and energy dispersive materials. Many reductionist approaches to mussel-inspired synthetic materials focus solely on incorporating catecholic moieties. Taken out of context, these synthetic materials generally exhibit inferior adsorption and adhesion, and suffer from uncontrolled reactivity and oxidation. These considerations limit the range, scope and performance of catecholic materials. The original motivation behind this project was to fuse a fundamental understanding of the native mussel foot proteins with a rational engineering approach – first identifying strategies that allow fine control over catechol reactivity, then building these design principles into synthetic systems.

II Local and global environment

The mussel foot proteins with the highest amount of Dopa (mfp-1 (18 mol-%), mfp-3 (20 mol-%), mfp-5 (30 mol-%)) also contain a large amount of basic residues. The surface adsorption and adhesion of one of these proteins, mfp-3fast, to TiO_2 surfaces was studied with surfaces forces apparatus and resonance Raman spectroscopy. The adhesion and degree of coordinative binding was found to be dependent on the deposition pH in the system. The non-monotonic trend in adhesion and adsorption as the pH increases was rationalized by the presence of two competing factors: a transition from bidentate hydrogen bonding to coordination bonding, and a increase in catechol oxidation at high pH.

To better understand the effect of positive charge on catechol behavior, a library of polyacrylamides with catecholic and charged cofunctionality was synthesized. The adsorption to TiO_2 was characterized via resonance Raman spectroscopy and found to depend on pH, as seen for the native proteins, but also on cofunctionality. This effect was explored more directly via metal binding studies. Cationic catecholic polyacrylamides show a greater propensity to form higher stoichiometry *tris* complexes than neutral polymers under the same global pH conditions. Efforts to study the effect of lysine-Dopa proximity via electrochemical and nuclear magnetic resonance spectroscopic means in a small peptide system failed to show the same dramatic trends as seen in the other two systems.

Overall, this work provides a promising foundation for continued studies into how both global and local factors alter the binding of catecholic macromolecules on metal hydroxide surfaces, but raises questions that must be addressed. One topic that requires further investigation is the clear separation of the competing effects of oxidation and coordination on adhesion. Evidence suggests the presence of a temporarily imposed low pH environment during protein secretion, which then equilibrates to sea water pH. Presumably, this strategy helps prevent oxidation, to promote coordinative binding as the pH increases. One strategy that has shown promising initial results is deposition at high pH using borate buffers.[1] Catechol-boronate complexes delay oxidation of unbound catechols, and may allow further surface equilibration without oxidation in solution. Furthermore, surfaces forces apparatus measurements of adhesion to TiO_2 are inseparably convoluted due to photocatalytic processes triggered by the high-intensity white light required.

III Catechol analogues for supramolecular metal coordination hydrogels

The previously described work on adsorption and metal binding led to the important observation that local cationic functionality results in lower catecholic proton affinity. Chemical modification strategies were used to directly synthesize electron-deficient catecholic moieties with lower phenolic pK_a values. These analogues, nitrocatechol and 3-hydroxy-4-pyridinone (HOPO), were shown to shift metal complex speciation and decrease the susceptibility to oxidation, while maintaining the bidentate, vicinal hydroxyl geometry vital for binding. In contrast to catechol-based complexes, HOPO complexes form oxidation-resistant *tris* complexes in physiological buffer conditions.

The enhanced performance of catecholic analogues in synthetic constructs was demonstrated through the creation of supramolecular hydrogels crosslinked by metal coordination bonds. Here, the mechanical properties of the hydrogels were found to be primarily dependent on the chemical character of the coordination complexes. HOPO hydrogels can be triggered by injection into high pH buffer solutions, and exhibit stable, tunable viscoelasticity. These gels dissolve over the course of days, releasing encapsulated payload. HOPO coordination networks were incorporated into covalent scaffolds to create interpenetrating networks. These hydrogels exhibit the strain-rate dependent mechanical properties characteristic of coordination hydrogels, but are able to recover after mechanical deformation.

Metal coordination bonds are interesting supramolecular crosslinkers due to their strength, recoverability, and tunable exchange kinetics. This work identifies HOPO as a superior analogue to catechols for the creation of coordination crosslinked materials due to its optimized speciation at biologically relevant pH values and decreased susceptibility to covalent crosslinking. These initial demonstrations should pave the way for wider incorporation of HOPO into supramolecular constructs where stable, dynamic coordination is desired.

At the same time, chelating moieties such as histidines have also been shown to be capable of strong, tunable metal binding in supramolecular hydrogels.[2] An underexplored advantage of HOPO moieties is that they maintain the vicinal hydroxyl moieties of the catechol and thus are expected to capable of the modes of adsorption exhibited by catechols. Studies of the adsorption of a electron-deficient catechols nitrocatechol and mimosine suggest that these are indeed capable of strong surface binding.[3,4] Furthermore, preliminary experiments of adsorption using quartz crystal microbalance and coordination using colloidal suspensions have provided initial evidence to support these findings.

IV Lighting the way to spatiotemporal control over catechols

Along with the versatile chemistry of catechols comes the caveat that it can be difficult to control this reactivity. This is most notably seen in the undesired oxidation of catechols under relatively benign conditions. Light is a powerful external stimulus for controlling reactivity. It is demonstrated that light can be used either to mediate the patterning of acid-labile silyl-ether protected catechols or to cleave photo-labile protecting groups.

An iridium-mediated atom transfer radical addition (ATRA) strategy was employed to selectively pattern triethylsilane-protected eugenol in irradiated regions. This chemistry is non-destructive and allows excellent spatial resolution (<1 micron). Protecting groups were cleaved with a mild acid wash, and the patterned catechol functionality was used to template the adsorption of iron oxide nanoparticles.

A photo-deprotection strategy was used to create diverse microarrays. Surface-immobilized, *ortho*-nitrobenzyl alcohol-protected catechol species were selectively decaged using ultraviolet radiation. The substrates were then selectively patterned in the irradiated regions. The diverse reactivity of catechols allowed the patterning of inorganic colloids, the templated precipitation of metallic elements, and, after oxidation, the reaction with a variety of organic, nucleophilic species.

Moving forward, there is much untapped potential in this system for sequential, multi-component patterning if two minor problems are addressed. The first issue was one of non-specific adsorption of hydrophobic components. For example, attempts at patterning the CdSe@ZnS quantum dots, as well as fluorescein isothiocyanate (FITC)-functionalized bovine serum albumin (BSA) resulted in blanket fouling of the substrates. Attempts were made to address this challenge through the use of a longer, hydrophilic catechol tether, to minimize fouling and increase chain mobility. Short poly(oligoethylene glycol) methacrylate brushes (<10 nm) were grown via an approach analogous to that described by Poelma et al.[5] While brush growth was successful, subsequent brush functionalization with NHS-alkene and reaction with an amino-functional *o*-NB protected dopamine species were inconclusive. This reaction involves many steps, resulting in a decreasing additive yield. To remedy this challenge, I suggest changing the alkyl bromide initiator monolayer from a hydrocarbon linker to a triethylene glycol species. This change will incorporate hydrophilic character into the initiator layer, negating the need to growth and functionalize hydrophilic brushes.

The second issue was stability of the patterned layers. Achieving well-defined patterns required striking a careful balance between rinsing away non-specifically adsorbed components and damaging the patterned array, especially in the case of large nanoparticles. This has been attributed to the relatively short spacer length between the substrate and the catechol, and the high curvature of nanoparticles. Initial attempts were made to remedy this again, by functionalizing polymer brushes with protected catechol species. If successful, efforts to address these challenges promise to assist in the creation of a modular system for the patterning of diverse substrates, with potential applications in catalysis, biology and materials science.

V References

(1) Kan, Y.; Danner, E. W.; Israelachvili, J. N.; Chen, Y.; Waite, J. H. *PLoS One* **2014**, *9*, e108869.

(2) Fullenkamp, D. E.; He, L.; Barrett, D. G.; Burghardt, W. R.; Messersmith, P. B. *Macromolecules* **2013**, *46*, 1167–1174.

(3) Amstad, E.; Gehring, A. U.; Fischer, H.; Nagaiyanallur, V. V.; Hähner, G.; Textor, M.; Reimhult, E. *J. Phys. Chem. C* **2011**, *115*, 683–691.

(4) Amstad, E.; Gillich, T.; Bilecka, I.; Textor, M.; Reimhult, E. *Nano Lett.* **2009**, *9*, 4042–4048.

(5) Poelma, J. E.; Fors, B. P.; Meyers, G. F.; Kramer, J. W.; Hawker, C. J. *Angew. Chem. Int. Ed. Engl.* **2013**, *52*, 6844–6848.

Appendix A – Supporting Info for Chapter 2: The effect of global and local chemical environment on the binding and adhesion of catecholic proteins, polymers and peptides

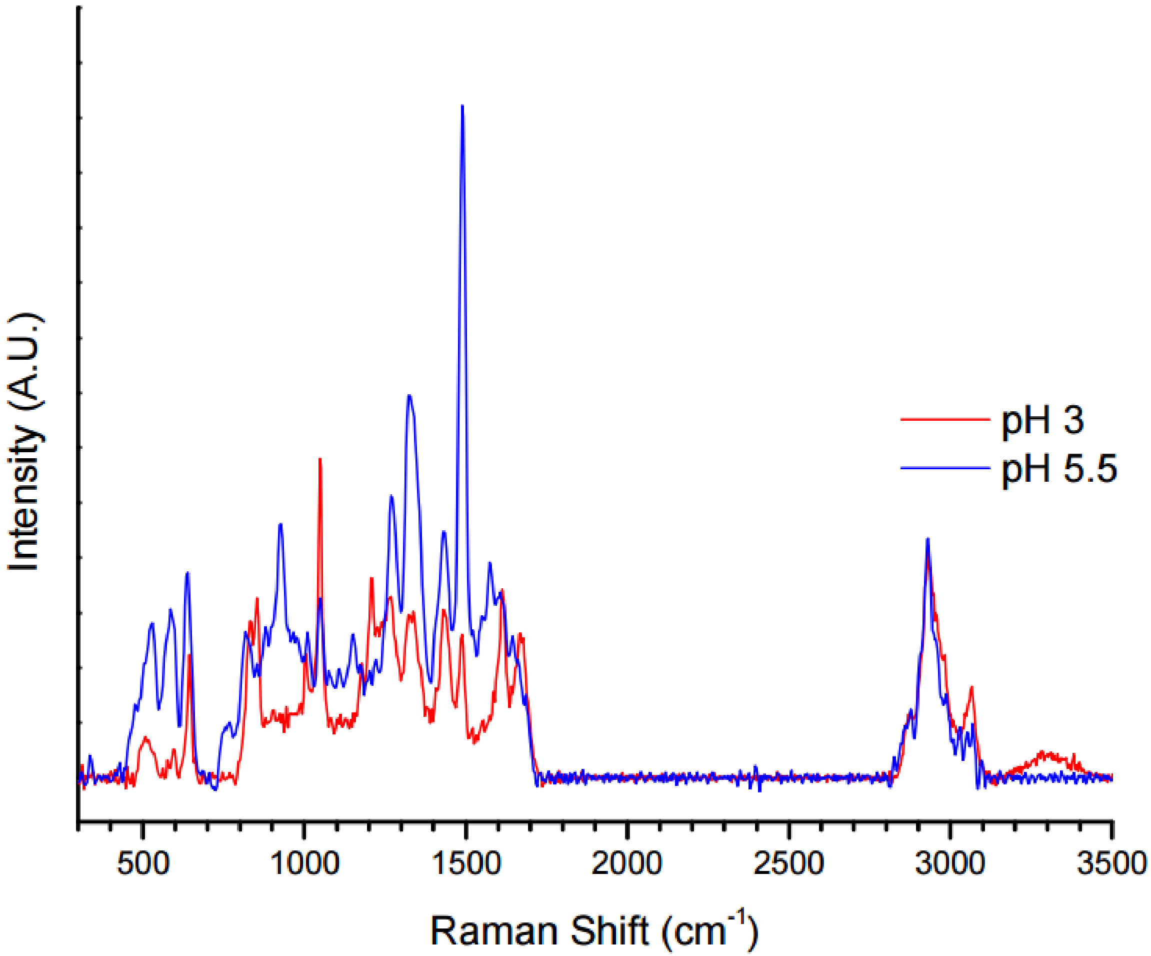

Figure A.1 Complete Raman spectra showing normalization to C-H region.

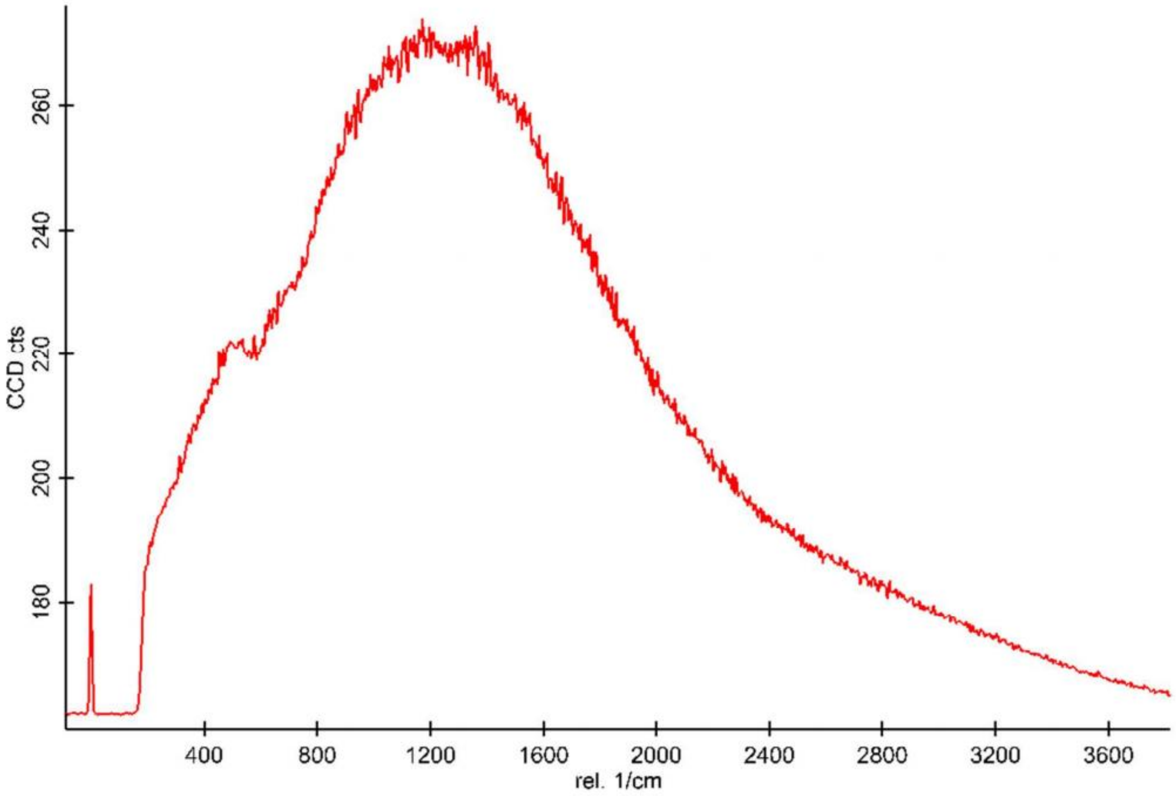

Figure A.2 Very strong fluorescence was observed for mfp-3 fast at pH 7.5, indicating possible oxidation processes.

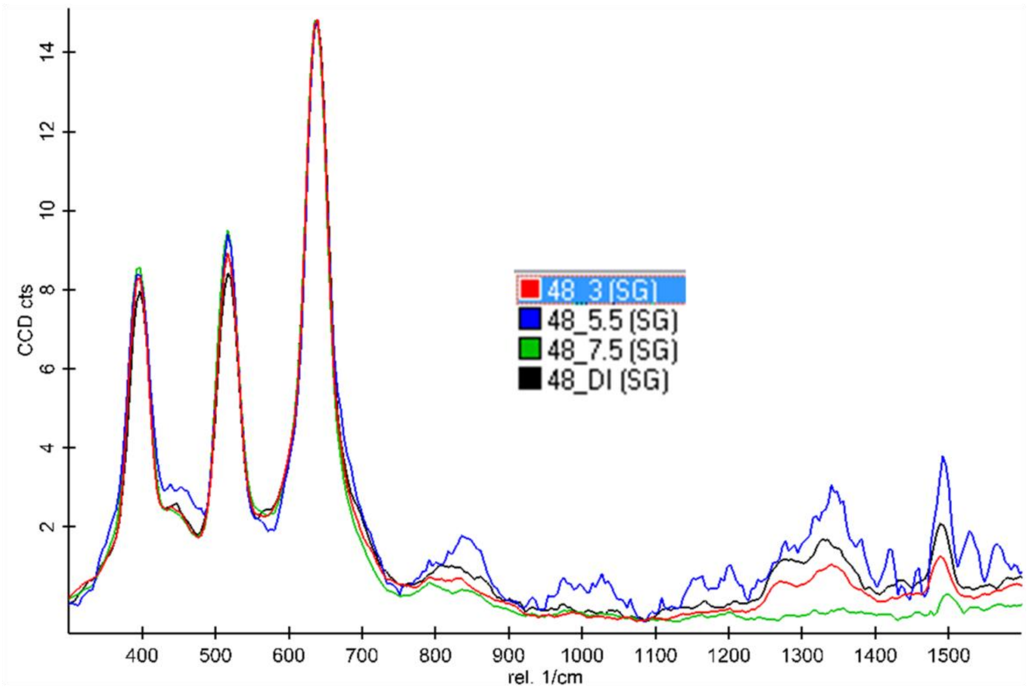

Figure A.3 Resonance Raman spectra of poly(dopamine acrylamide-co-(2-amino)ethylacrylamide-co-(2-Hydroxypropyl) acrylamide) P(DA-AEA-HPA)

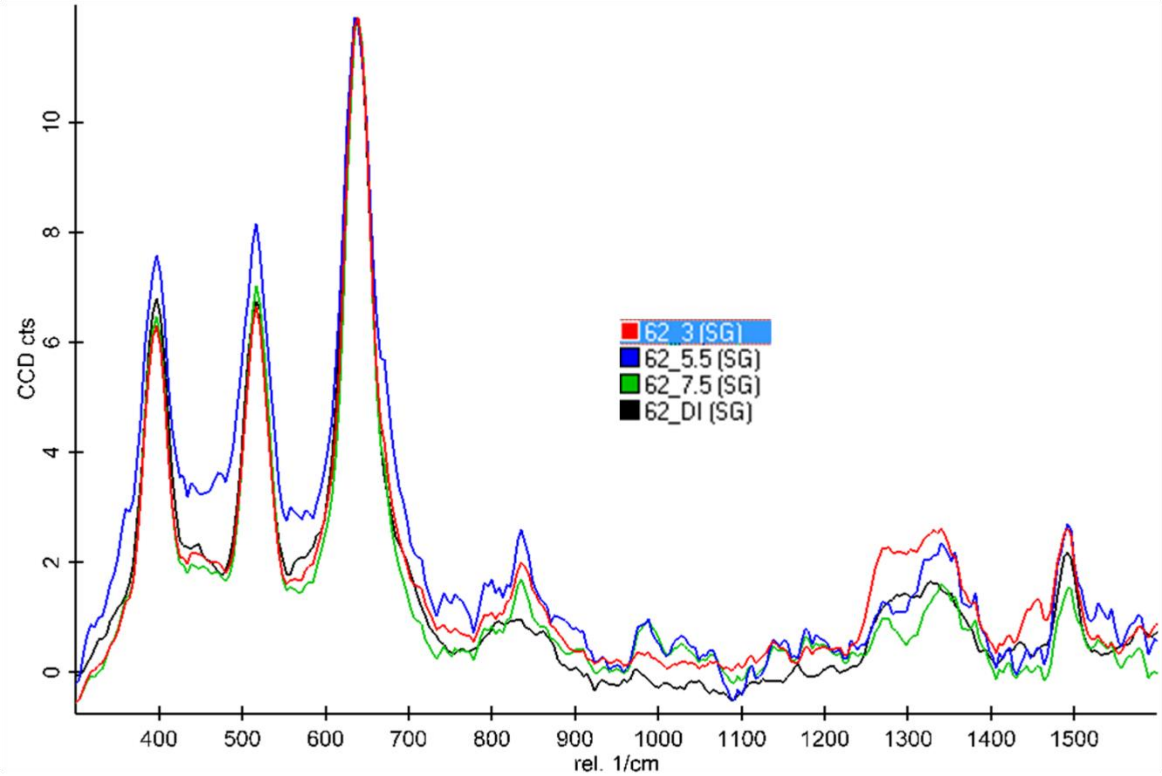

Figure A.4 Resonance Raman spectra of poly(dopamine acrylamide-co-(2-Hydroxypropyl) acrylamide)

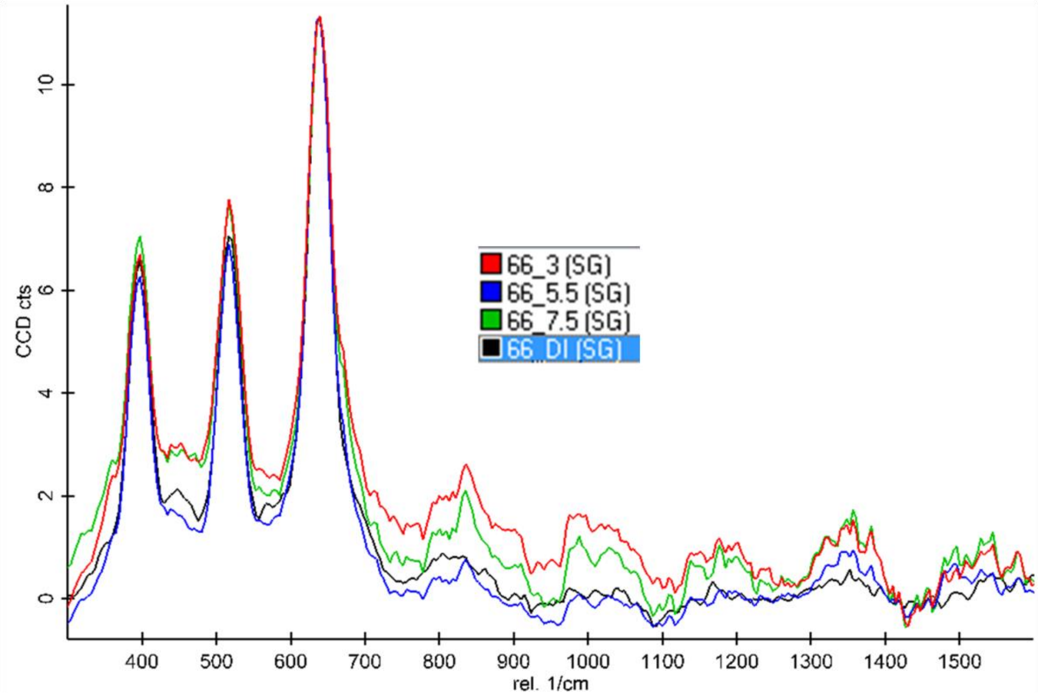

Figure A.5 Resonance Raman spectra of poly(dopamine acrylamide-co-(2-sodium sulfate) ethylacrylamide-co-(2-Hydroxypropyl) acrylamide) P(DA-SEA-HPA)

Appendix B – Supporting Info for Chapter 3: Catecholic analogues as metal chelation building blocks and their application in supramolecular hydrogels

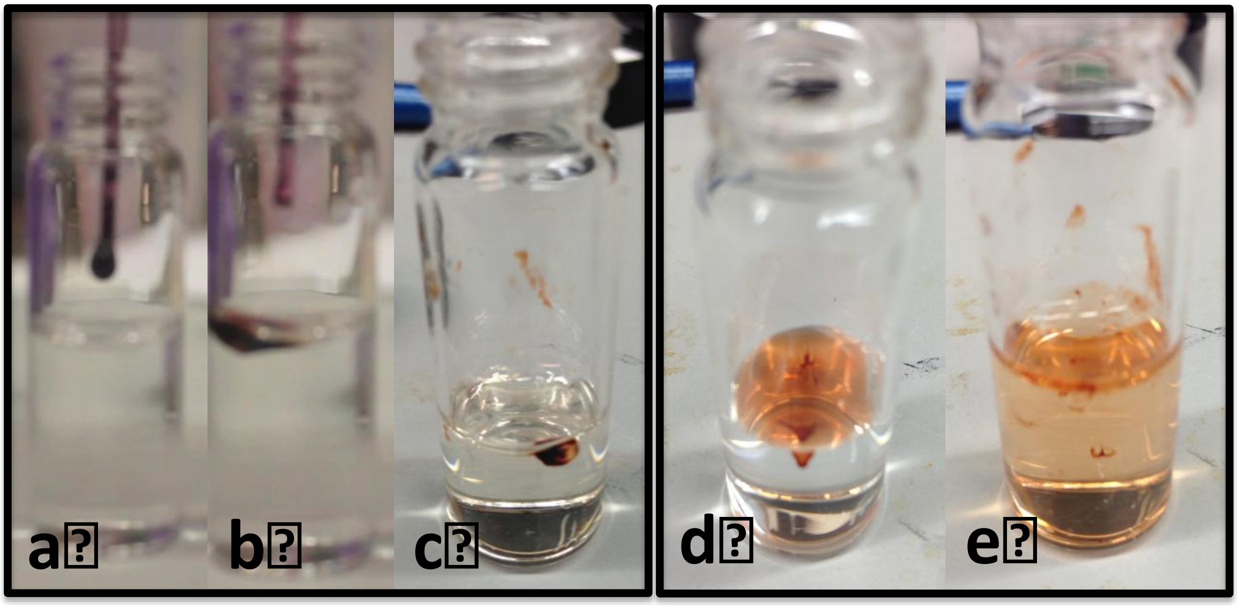

Figure B.1: (a-c) Gelation process for a HOPO-Fe(III) hydrogel. (a) A 10% w/v solution of Fe(III)-bound HOPO is dropped into pH 7.4 phosphate buffer solution. (b) Gelation is immediately apparent, leading to minimal leaking of the injection solution. (c) The gel remains a separate phase even after subjection to a vortex mixer. (d-e) Gelation process for a nitrocatechol-Fe(III) hydrogel into pH 9 buffer solution. (d) Upon dropping, immediate spreading of the injection solution is clearly evident. (e) Vortex mixing leads to complete dissolution into the bulk.

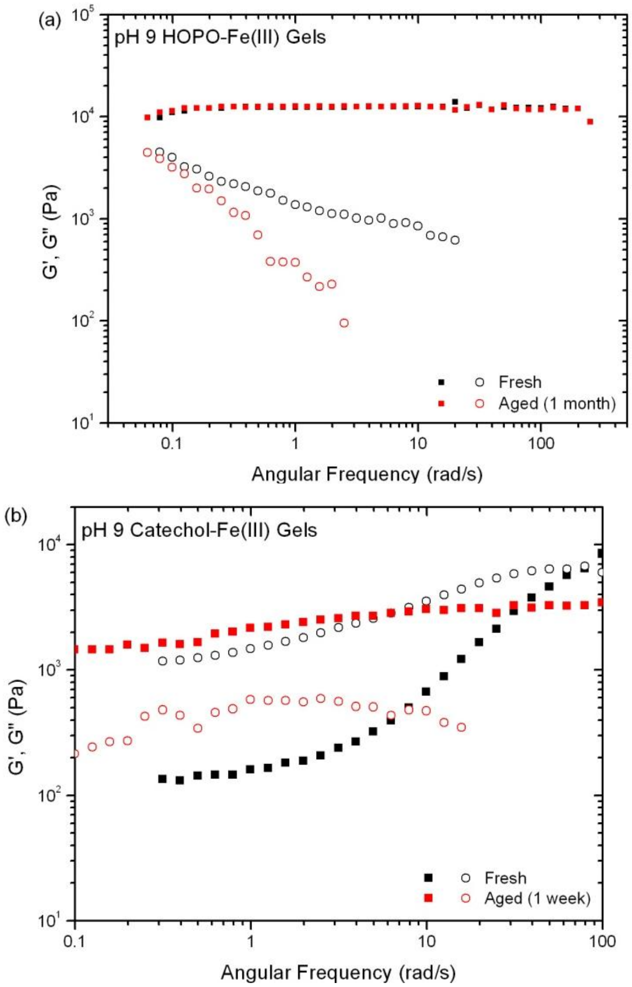

Figure B.2: Dynamic oscillatory rheology of (a) pH 9 HOPO-Fe(III) gels as synthesized (black) and after 1 month storage on benchtop (red) and (b) pH 9 catechol-Fe(III) gels as synthesized (black) and after 1 week storage on the benchtop (red). Notable is the dramatic shift in rheological behavior for the catechol-Fe(III) hydrogel, compared to minimal change, even after an extended time frame for the HOPO-Fe(III) hydrogel.

Appendix C – Supporting Info for Chapter 4: Strong, sacrificial metal coordination bonds enhance toughness and recovery in interpenetrating network hydrogels

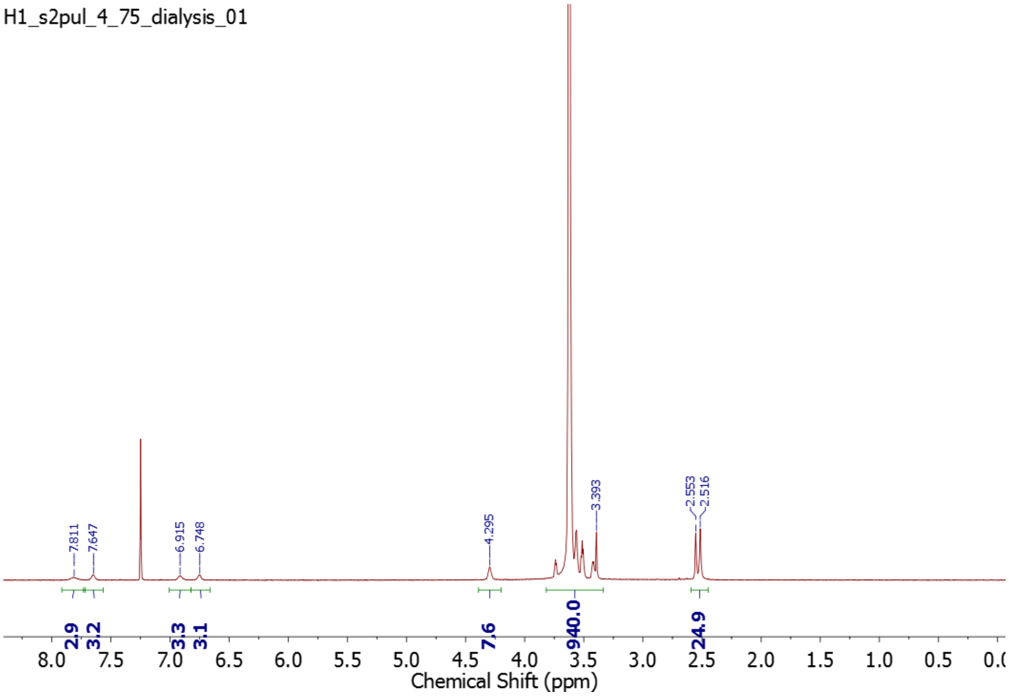

Appendix C.1: ^{1}H NMR of 4-arm PEG-HOPO in $CDCl_3$

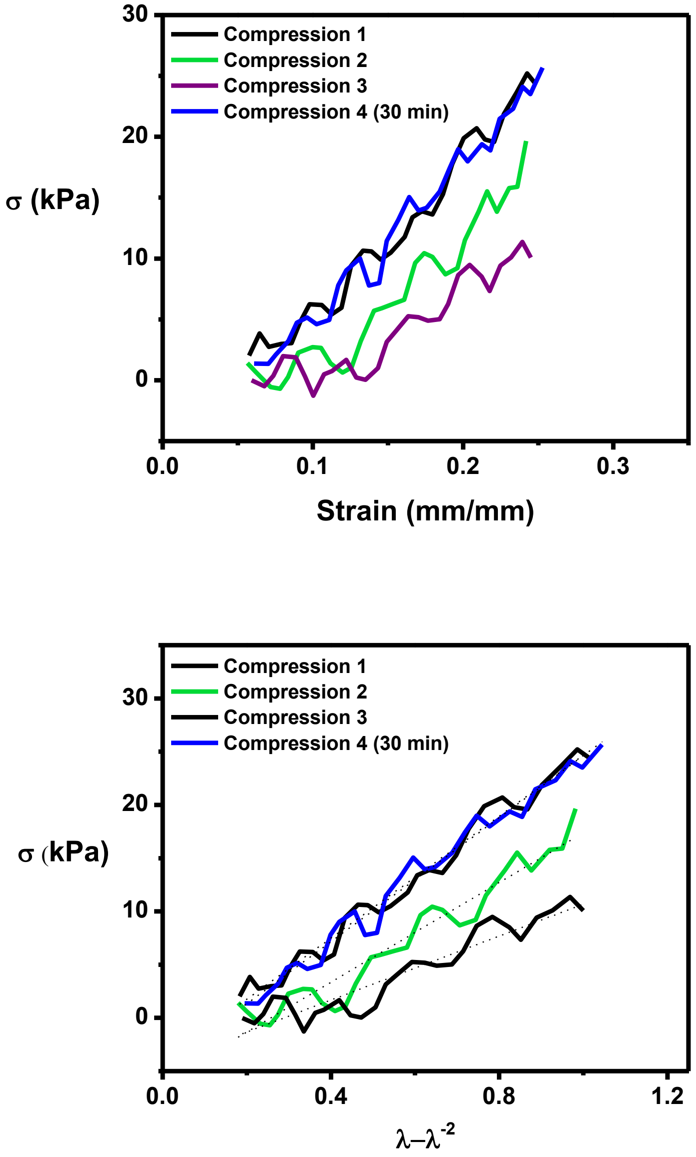

Figure C.2: σ versus γ and σ versus λ-λ^{-2} plot for repeated compression cycles of In(III) IPN hydrogel fitted with linear fits between 5-25% strain.

Appendix D – Supporting Info for Chapter 5: Light as an external stimulus to allow spatiotemporal control over catechol reactivity

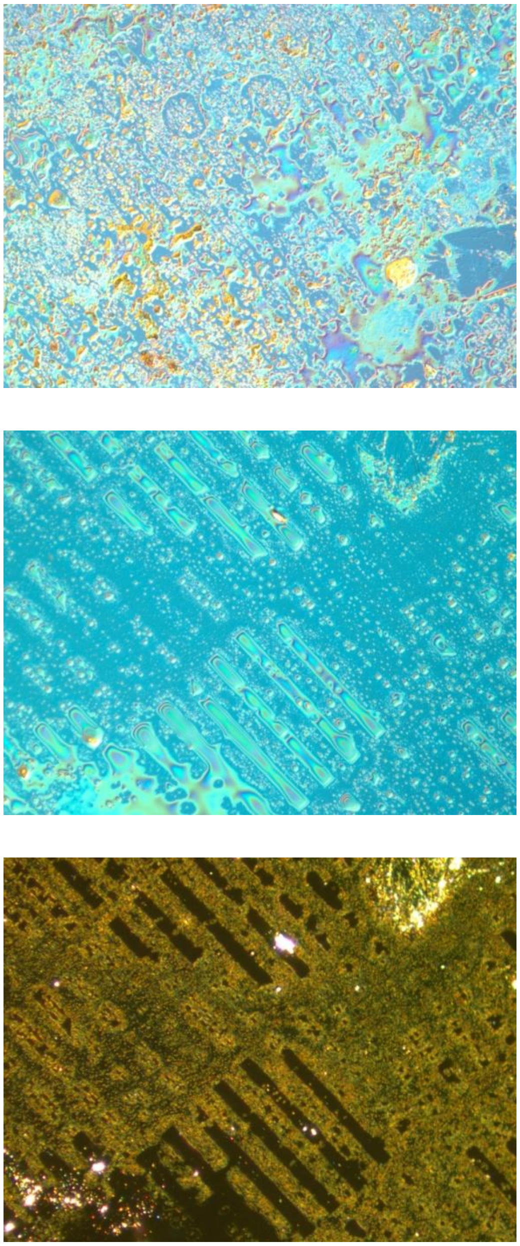

Figure D.1 Selective templating of Cu on patterned substrates. With hydrazine reducing agent (top), and without (middle). Dark-field of middle image (bottom).